

# Mesoscale two-sample testing for networks

Peter W. MacDonald

Department of Statistics and Actuarial Science  
University of Waterloo

Elizaveta Levina & Ji Zhu

Department of Statistics  
University of Michigan, Ann Arbor

October 22, 2024

## Abstract

Networks arise naturally in many scientific fields as a representation of pairwise connections. Statistical network analysis has most often considered a single large network, but it is common in a number of applications, for example, neuroimaging, to observe multiple networks on a shared node set. When these networks are grouped by case-control status or another categorical covariate, the classical statistical question of two-sample comparison arises. In this work, we address the problem of testing for statistically significant differences in a given arbitrary subset of connections. This general framework allows an analyst to focus on a single node, a specific region of interest, or compare whole networks. Our ability to conduct “mesoscale” testing on a meaningful group of edges is particularly relevant for applications such as neuroimaging and distinguishes our approach from prior work, which tends to focus either on a single node or the whole network. In this mesoscale setting, we develop statistically sound projection-based tests for two-sample comparison in both weighted and binary edge networks. Our approach can leverage all available network information, and learn informative projections which improve testing power when low-dimensional latent network structure is present.

**Keywords:** multiple networks, multiplex networks, latent space model, low rank matrix, random projection

## 1 Introduction

Recent advances in statistical computation and methodology have allowed researchers to analyze increasingly complex data structures. One such example is network data, which arise naturally in many scientific fields as a representation of pairwise connections (edges) among a collection of units (nodes). Classical statistical questions need to be answered anew for these complex structures, and in this work we develop methodology for one such classical question, two-sample testing for differences in the means. This problem is especially relevant in applications such as neuroimaging, where it is common to observe samples of networks

(each patient’s brain image corresponds to one network), often split into groups according to a case-control status or another categorical covariate (Zalesky et al., 2010).

Recent work on two-sample testing for samples of networks (e.g., Ginestet et al., 2017; Xia and Li, 2022) has covered either “global” testing, where the null hypothesis is of no difference anywhere in the network, or “local” testing, which considers univariate null hypotheses of no difference for a node pair. Global network testing can often correspond to a scientifically uninteresting null hypothesis. For popular network models like the stochastic block model (SBM, Holland et al., 1983) or the random dot product graph (RDPG, Athreya et al., 2018), which fit relatively low-dimensional models to large networks, the global null hypothesis would nearly always be rejected on real data. On the other hand, local network testing creates a massive multiple testing problem which can be under-powered when we observe few network samples, since there is no information sharing between nodes. Our novel contribution is a flexible framework that spans the spectrum between these two extremes, including them as special cases and allowing for testing at an intermediate or *mesoscale* (Khambhati et al., 2018). Thus, an analyst may specify hypotheses at a scale that is sufficiently local to be scientifically interesting, and yet large enough to have substantial power. In this work, we develop mesoscale network tests for two independent samples of networks on a fixed collection of  $n$  nodes. These tests will identify differences in the means of the edge variables for a fixed *hypothesis set*, a subset of node pairs  $\mathcal{S} \subseteq \{1, \dots, n\}^2$ . If  $\mathcal{S} = \{1, \dots, n\}^2$ , then the mesoscale null coincides with the global null hypothesis (or the difference in means for all node pairs), while if  $\mathcal{S}$  is a singleton set, the mesoscale hypothesis coincides with a local null hypothesis on the difference in the mean for a single node pair.

Mesoscale hypotheses of this form appear naturally in applications. For example, in neuroimaging, it is common to focus on anatomical regions of the brain or on “functional networks” (Fair et al., 2009), consisting of connections within or between known groups of nodes, with the groups determined by a brain atlas. We will refer to these as *rectangles*, as up to a reordering of nodes they correspond to a rectangular block of entries of the adjacency matrices (a square if the comparison is on node pairs within a region, and in general a rectangle if the comparison is on connections between two regions). In an exploratory analysis, Fair et al. (2009) compare samples of child and adult brain images for some of the rectangles induced by functional and lobe-based groupings. Sripada et al. (2020) also work at this scale to identify which functional groupings of brain regions are related to a continuous-valued neurocognitive score. More generally, scientifically interesting rectangular hypothesis sets can arise from any known groupings of nodes. While in some cases given node groupings are used as motivation for inference under a block-constant model like the SBM, homogeneous edge distributions within each rectangle are a restrictive assumption we would like to avoid making. Two-sample comparison at the scale of fixed rows, columns, sub-rows, or sub-columns of the adjacency matrices may also be of interest if we want to isolate the influence of a given node on changes in the two samples (Kuntal et al., 2019).

For the remainder of the paper, we will consider independent samples of networks with independent edges (possibly conditional on latent variables). Much of the literature on two-sample (binary) network testing assumes some form of this model, as it includes the SBM (conditional on latent communities), the RDPG (conditional on latent node positions), and other latent space models (Hoff et al., 2002). The SBM and RDPG are examples of *low-dimensional* latent space network models, which restrict the number of free parameters used to specify the expected adjacency matrix. Under a low-dimensional network model, although the edges in  $\mathcal{S}$  are independent of the edges in its complement (henceforth denoted by  $-\mathcal{S}$ ), these edges still provide information about the mesoscale hypothesis through the

underlying model parameters.

While low-dimensional network models allow us to incorporate information from the entire network in a given mesoscale hypothesis test, model misspecification can invalidate test results. For global network testing, this can occur even under extremely mild model misspecification, for instance incorrect choices of tuning parameters like latent space dimension (Ghoshdastidar and von Luxburg, 2018, Figure 2), or latent position similarity function (cf. Section 4). Both of these tuning parameters are typically unknown and often chosen using heuristic methods.

We propose new methodology for mesoscale two-sample testing which can take advantage of low-dimensional network structure in a much more robust fashion. In contrast to previous network model-based approaches, our methods work with projections of the edges in  $\mathcal{S}$  and thus remain robust to model and tuning parameter misspecification, similar to previous (random) projection-based approaches for high-dimensional two-sample testing and classification (Lopes et al., 2011; Cannings and Samworth, 2017). Assuming independent edges, we have a natural split of the data into the edges in  $\mathcal{S}$ , which will be used for testing the mesoscale hypothesis; and the held out edges in  $-\mathcal{S}$ , which would otherwise be discarded, as they are not directly related to the mesoscale hypothesis. In Section 2.5, we will show that low-dimensional network models imply shared structure inside and outside of  $\mathcal{S}$  that can make such a learned projection informative for mesoscale testing. In summary, our projection-based method makes the most of the available information to test the mesoscale hypothesis: its size properties are robust to any specification of expected adjacency matrices for which the null is satisfied, and when we are in a favorable setting, where the edges in  $-\mathcal{S}$  are informative for the test, that information can still be incorporated.

Next, we review some of the existing literature on global and local network testing, as well as some approaches to testing for equality of individual node positions in latent space models. Both local and mesoscale network testing rely on the *alignment* (also called labeling) of nodes across networks. Without node alignment, one common approach to global network testing is to evaluate a network summary statistic invariant under node permutations, such as modularity or edge density, on the two samples and compare their means either with a  $t$ -test, or a nonparametric permutation test (Wozniak et al., 2013). Several papers in statistical network analysis have taken more complicated model-based approaches. Assuming one sample per group, Agterberg et al. (2020) and Chung et al. (2022) develop tests for differences in two networks generated from the RDPG model (unconditional on positions), by testing for differences in the distributions of latent positions, up to unknown orthogonal transformation. Athreya et al. (2021) instead consider testing for differences in specific functionals of these latent position distributions. Similarly, Sabanayagam et al. (2022) assume each network is sampled from a graphon, and test the equality of those two graphons up to measure preserving transformation. In all of these papers, by positing network models which are well defined for arbitrary node sets, the global test can be performed in terms of some underlying model parameter, without node alignment.

In the aligned node setting, the global network testing problem more closely resembles usual two-sample testing for high-dimensional means. Many statistics in this case are based on some distance between the adjacency matrices of the two samples. Ghoshdastidar et al. (2017) look at a normalized difference between the two samples of adjacency matrices in terms of matrix Frobenius or operator norms. For the Frobenius norm, they propose an asymptotically Gaussian test statistic, as well as a bootstrap algorithm to estimate an empirical null distribution. For the operator norm they apply the same bootstrap algorithm,

and in later work Ghoshdastidar and von Luxburg (2018) also provide an asymptotically Tracy-Widom distributed test statistic. Chen et al. (2020) similarly develop an asymptotically Gaussian test statistic for the global null based on the third power of the normalized adjacency matrix difference.

Other statistics for global network testing are based on graph distances (Donnat and Holmes, 2018). Ginestet et al. (2017) propose an asymptotically  $\chi^2$  statistic based on the geodesic distance between Fréchet means of graph Laplacians in a suitable manifold. Lunagómez et al. (2021) consider more general modeling and Bayesian inference for unimodal distributions of graphs, in which the probability of a particular graph on  $n$  nodes depends on its distance from a fixed graph. Lovato et al. (2020) develop statistics for two-sample testing based on the pairwise distances among the networks, comparing average distances within and between the two samples, and use the bootstrap to estimate an empirical null.

Another branch of the global network testing literature focuses on testing under latent space models, most commonly the RDPG. In this case, the global null hypothesis is equivalent to equality of all the latent positions, up to some unidentifiable transformation. These tests typically assume one network per sample, and that the latent space dimension is known. Tang et al. (2017) evaluate the distance between the two sets of estimated latent positions after a Procrustes alignment, and estimate the null distribution with a parametric bootstrap. Ghoshdastidar and von Luxburg (2018) propose a similar bootstrap-based test which compares estimates of the expected adjacency matrices based on the ASE (Adjacency Spectral Embedding, a standard way of estimating latent positions under RDPG). Li and Li (2018) test for the equality of all node community memberships in the weighted SBM, and develop an asymptotically Gaussian statistic. Levin et al. (2017) and Draves and Sussman (2021) instead analyze an omnibus embedding such that under the global null hypothesis, the estimated embeddings for the two networks are comparable without applying an orthogonal transformation. While Levin et al. (2017) estimate the null distribution with a bootstrap method, Draves and Sussman (2021) compare to a  $\chi^2$  critical value, and calculate power when the expectations of the two adjacency matrices share a common column space. Draves and Sussman (2021) also discuss an adaptation of their global testing methodology to test for differences in individual latent positions, as their statistic decomposes across nodes. However, their theoretical null distribution for a given node’s contribution to the statistic only holds under the global null hypothesis. Other recent work (Du and Tang, 2021) has considered testing for equality of individual node positions under a latent space model. Unlike mesoscale testing for an entire row or column of the adjacency matrix, latent position testing creates challenges due to non-identifiability, which we will discuss in more detail in Appendix A.4. In all of these cases, testing is done assuming a low-dimensional network model, which can greatly increase test power, but these tests can be highly sensitive to unknown tuning parameters like the latent space dimension or the number of communities.

Local network testing can more easily leverage existing methodology, as the local hypothesis for a given node pair is simply a univariate comparison of means. Xia and Li (2022) do treat local network testing in detail, and develop local tests (with control of the false discovery rate) using univariate statistics based on the mean difference between the two samples’ edge variables for each node pair. They provide a power enhancement for their multiple testing procedure which takes advantage of potential sparsity in the network setting. Multiple testing methods can be used to combine local tests and address mesoscale hypotheses, but achieving non-trivial power still relies on large signals at individual node pairs, which may be unrealistic for small samples of sparse networks.

The rest of this paper is organized as follows. In Section 2 we specify a flexible network model with independent, exponential family edges, and develop projection-based mesoscale hypothesis tests, which are motivated by low-dimensional network models and inference for generalized linear models (GLMs). This connection to GLMs provides the starting point for theoretical guarantees in Section 3.1, and ideas from low rank network modeling allow us to prove results about power of the proposed tests in Section 3.2. In Section 4, we provide empirical evaluations of our tests on samples of synthetic networks, as well as an application to single cell interaction data. Section 5 provides conclusions and discussion of future work.

## 2 Mesoscale testing methodology

### 2.1 Notation

We begin by fixing notation. We write  $M_{ij}$  or  $[M]_{ij}$  for the  $(i, j)$  entry of a  $p \times q$  matrix  $M$ . We denote submatrices of  $M$  by  $M_{\mathcal{I}}$  or  $[M]_{\mathcal{I}}$  for a subset  $\mathcal{I} \subseteq \{1, \dots, p\} \times \{1, \dots, q\}$  of the entries. If  $\mathcal{I}$  forms a rectangle, then  $M_{\mathcal{I}}$  will be interpreted as a matrix.

The function  $\text{vec}$  converts a  $p \times q$  matrix to a  $pq$  vector, with inverse  $\text{vec}^{-1}$ . The function  $\text{diag}$ , applied to a  $p$  vector, will construct a  $p \times p$  diagonal matrix with the vector entries on the diagonal. We use  $\otimes$  to denote the Kronecker product, and  $\oplus$  for the matrix direct sum (Bhatia, 1997). The Kronecker product and  $\text{vec}$  satisfy the identity

$$\text{vec}(XMY^T) = (Y \otimes X) \text{vec}(M) \quad (1)$$

for matrices  $X$ ,  $Y$ , and  $M$  of suitable dimensions. We use  $\|\cdot\|_2$  to denote the vector Euclidean norm or matrix operator norm,  $\|\cdot\|_F$  for the matrix Frobenius norm, and  $\|\cdot\|_\infty$  for the maximum absolute entry of a vector. The zero vector in  $\mathbb{R}^p$  is denoted by  $\mathbf{0}_p$ , the vector of all ones by  $\mathbf{1}_p$ , and  $I_p$  is the  $p \times p$  identity matrix. Finally,  $\mathcal{O}_p$  will denote the group of orthonormal  $p \times p$  matrices, and for  $q \leq p$ ,  $\mathcal{O}_{p \times q}$  will denote the set of  $p \times q$  matrices with mutually orthonormal columns.

### 2.2 An exponential family edge model

Throughout the paper, we will assume the data consists of two independent samples of networks on a fixed collection of  $n$  aligned nodes. The edges can be binary or weighted. The layers are represented by  $n \times n$  adjacency matrices

$$\{A_k^{(g)}\}_{k=1}^{m_g}$$

for samples  $g = 1, 2$ , each consisting of  $m_g$  i.i.d. networks. Mesoscale network testing considers mean differences in a fixed collection of node pairs (a *hypothesis set*). For a hypothesis set  $\mathcal{S} \subseteq \{1, \dots, n\}^2$ , the mesoscale null hypothesis is given by

$$\mathcal{H}_{0,\mathcal{S}} : \mathbb{E}[A_1^{(1)}]_{ij} = \mathbb{E}[A_1^{(2)}]_{ij} \quad \forall (i, j) \in \mathcal{S}. \quad (2)$$

We now propose a flexible independent edge model, with the goal of restating (2) in terms of model parameters. For simplicity, assume we have  $m_1 = m_2 = m$  networks in each of the two groups. Assume independent directed edges across groups, and that for  $g = 1, 2$ ,

$k = 1, \dots, m$ , and  $1 \leq i, j \leq n$ , the distribution of  $[A_k^{(g)}]_{ij}$  follows an *exponential family model* with probability function

$$p(z; \Theta_{ij}^{(g)}, \phi_{ij}) = C(z, \phi_{ij}) \cdot \exp \left( \frac{1}{\phi_{ij}^2} \left\{ z[\Theta^{(g)}]_{ij} - H([\Theta^{(g)}]_{ij}) \right\} \right), \quad (3)$$

for a convex log partition function  $H$ . This is a standard exponential family representation, where  $h = H'$  is a function which links  $\Theta^{(g)}$  and the edge expectations via

$$\mathbb{E}[A_k^{(g)}]_{ij} = h([\Theta^{(g)}]_{ij}).$$

Throughout we refer to  $h$  as the *inverse link* function, which is always applied element-wise, though with a slight abuse of notation we will use it with both vector and matrix-valued arguments. We refer to the entries of the matrix  $\Theta^{(g)}$  as the *edge expectation parameters*, and to  $\phi_{ij} > 0$  as the *dispersion parameter* for node pair  $(i, j)$ . This model is similar to exponential family models for independent matrix entries defined in Lin et al. (2021), and for independent multiplex network edges in MacDonald et al. (2022).

This general framework includes several special cases which we will use to prove theoretical guarantees on test size in Section 3 and generate synthetic networks in Section 4. The Gaussian edge model with constant edge variance corresponds to  $H(x) = x^2/2$  for  $x \in \mathbb{R}$  and  $\phi_{ij}^2 = \sigma^2$  for all  $i, j$ . We develop mesoscale hypothesis tests with finite sample guarantees on size for this model, and leave heteroscedastic Gaussian edge models for future work. The logistic binary edge model, with a probability mass function supported on  $\{0, 1\}$ , corresponds to  $H(x) = \log(1 + e^x)$  and  $\phi_{ij} = 1$ . It belongs to the general class of exponential family edge models with a known mean-variance relationship, and thus no unknown dispersion parameters, for which we develop mesoscale hypothesis tests with asymptotic guarantees on size. This methodology can be modified for general exponential family edge models with constant dispersion parameters ( $\phi_{ij} \equiv \phi$ ).

We make some further assumptions to simplify the presentation and notation. We will keep the assumption that the two groups have the same number of networks  $m$  for simplicity, but this is not a requirement and we do not view the samples as paired. We work with directed edges with self-loops allowed, to avoid edge dependence above and below the diagonal, and missing diagonal matrix entries. This can be easily adjusted to the undirected case by using only the upper diagonal of each network, with or without the diagonal (see Appendix A.1).

### 2.3 The general mesoscale null hypotheses and the projection testing approach

With the network model in place, we can state the mesoscale null hypothesis in terms of model parameters. For a hypothesis set  $\mathcal{S}$  of node pairs, the mesoscale null hypothesis can be written as

$$\mathcal{H}_{0,\mathcal{S}} : \Theta_{\mathcal{S}}^{(1)} = \Theta_{\mathcal{S}}^{(2)}, \quad (4)$$

against the two-sided alternative

$$\mathcal{H}_{a,\mathcal{S}} : \Theta_{\mathcal{S}}^{(1)} \neq \Theta_{\mathcal{S}}^{(2)}.$$

Under model (3), the hypothesis (4) is equivalent to (2).

In Section 1, we discussed several examples of rectangular sets  $\mathcal{S}$  which are of interest in applications. To further simplify the presentation in this section, we take  $\mathcal{S}$  to be an  $r \times c$  rectangle, without loss of generality made up of the node pairs corresponding to the first  $r$  rows and the last  $c$  columns in the adjacency matrix. However, (4) is stated for an arbitrary (directed) subset of the node pairs. We discuss adjustments to our method needed for non-rectangular hypothesis sets and networks with undirected edges in Appendix A.1.

Our projection-based approach to mesoscale hypothesis testing, detailed next, is designed to robustly incorporate information from outside a hypothesis set  $\mathcal{S}$ , with the goal of boosting test power under low-dimensional network parameterizations.

The projections in question are onto the column spaces of two orthonormal matrix-valued tuning parameters:  $U \in \mathcal{O}_{r \times d_r}$  and  $V \in \mathcal{O}_{c \times d_c}$  for arbitrary column dimensions  $d_r \leq r$  and  $d_c \leq c$ .  $U$  and  $V$  are chosen adaptively to improve the power of the test for alternatives with differences in a particular subspace of the  $(r \times c)$ -dimensional parameter space. Ideal choices of  $U$  and  $V$  will have low column dimensions, while still keeping the reconstruction error,

$$\min_{\Gamma_g \in \mathbb{R}^{d_r \times d_c}} \left\| \Theta_{\mathcal{S}}^{(g)} - U \Gamma_g V^\top \right\|_F, \quad (5)$$

as small as possible for  $g = 1, 2$ . If (5) was exactly zero, that is, if  $\Theta_{\mathcal{S}}^{(1)}$  and  $\Theta_{\mathcal{S}}^{(2)}$  had low-dimensional representations, a likelihood-based test of  $\Gamma_1 = \Gamma_2$  would retain all of the available signal with many fewer degrees of freedom. In practice, the reconstruction in (5) is only approximate, and our tests will instead leverage quasi-likelihood results for misspecified GLMs (Lv and Liu, 2014).

To summarize, our projection-based approach to mesoscale hypothesis testing proceeds in two stages, described below for a given nominal level  $\alpha \in (0, 1)$  and a generic  $r \times c$  rectangular hypothesis set  $\mathcal{S}$ .

**Stage I** Using node pairs in  $-\mathcal{S}$ , learn orthonormal matrices  $\hat{U} \in \mathbb{R}^{r \times d_r}$  and  $\hat{V} \in \mathbb{R}^{c \times d_c}$ .

**Stage II** Apply a test function

$$\Psi_{\alpha, \hat{U}, \hat{V}} : \mathbb{R}^{(2rc) \times m} \rightarrow \{0, 1\}$$

to the node pairs in  $\mathcal{S}$ , where  $\Psi_{\alpha, \hat{U}, \hat{V}}$  is chosen from a class of test functions indexed by  $U$  and  $V$ .

In order to control type I errors at the nominal level  $\alpha$ , particularly with adaptively chosen projections, we take advantage of a natural independent split of the data induced by  $\mathcal{S}$ , and perform the projection learning step (Stage I) using only the held-out node pairs in  $-\mathcal{S}$ . Under (3), the independence of the data used in each stage of the procedure allows us to specify any learning procedure in Stage I for  $\hat{U}$  and  $\hat{V}$ , as well as their column dimensions  $d_r$  and  $d_c$ .

The flexibility of the learning procedure in Stage I is afforded by the use of a well specified class of tests in Stage II. In particular, if the tests all have (asymptotic) size  $\alpha$ , the test procedure in Stage II has the same (asymptotic) size. For this reason, we begin by detailing Stage II: in Section 2.4 we propose four classes of tests for  $\mathcal{H}_{0, \mathcal{S}}$  for use under different variants of the exponential family edge model (3), and in Section 2.5, we use these test families to suggest appropriate learning procedures for the orthonormal matrices in Stage I.

## 2.4 Classes of projected tests

In this section, we develop four classes of tests which can be used in Stage II of the generic approach. In all cases we specify the family by defining a test procedure for some arbitrary  $U \in \mathbb{R}^{r \times d_r}$  and  $V \in \mathbb{R}^{c \times d_c}$  with orthonormal columns,  $d_r \leq r$ , and  $d_c \leq c$ . Theoretical results establishing test sizes are provided in Section 3.1.

The first class of tests is for the general exponential family edge model (3) with known mean-variance relationship (abbreviated “E”); each test has asymptotic size  $\alpha$ . The second class provides an extension to the case of the general exponential family edge model with unknown dispersion (abbreviated “E-UD”). The third class modifies the first to use the exact null distribution under the Gaussian edge model with unknown dispersion parameter  $\sigma$  (abbreviated “G”). The fourth and final class of tests is a further modification for the Gaussian edge model which operates on only the projected data (abbreviated “G-P”).

### 2.4.1 General exponential family edge model

We begin with the general exponential family edge model (3) with dispersion parameters  $\phi_{ij} \equiv 1$ . Following (5) and applying (1), any  $U$  and  $V$  uniquely define a family of GLMs for the hypothesis set edges. The link function  $h$  is specified in (3), while the design depends on the choices of  $U$  and  $V$ . In particular, the vectorized edge expectation matrices  $\text{vec}(\Theta_S^{(1)})$  and  $\text{vec}(\Theta_S^{(2)})$  are modeled by  $h\{(V \otimes U) \text{vec}(\Gamma_1)\}$  and  $h\{(V \otimes U) \text{vec}(\Gamma_2)\}$ , respectively. Reparameterizing, we write

$$\gamma_1 = \{\text{vec}(\Gamma_1) + \text{vec}(\Gamma_2)\}/2, \quad \gamma_2 = \{\text{vec}(\Gamma_1) - \text{vec}(\Gamma_2)\}/2,$$

where  $\gamma_1$  and  $\gamma_2$  are  $(d_r d_c)$ -dimensional parameter vectors. A classical test for group differences in this parametric setting is a Wald test of  $\gamma_2 = \mathbf{0}_{d_r d_c}$ , based on asymptotic normality of the maximum likelihood estimator (MLE), and an estimator of its asymptotic covariance matrix. However, we only use this GLM parameterization to define a quasi-likelihood function of  $\gamma_1$  and  $\gamma_2$ , we do not actually believe that the model holds. The GLM design will in general be misspecified, but following Lv and Liu (2014), we modify the test so it is robust to this misspecification. In the remainder of this section, we formally define the test statistic and cutoff. Let

$$Y = \begin{pmatrix} \text{vec}([A_1^{(1)}]_S \quad [A_1^{(2)}]_S) & \cdots & \text{vec}([A_m^{(1)}]_S \quad [A_m^{(2)}]_S) \end{pmatrix} \in \mathbb{R}^{(2rc) \times m}, \quad (6)$$

$$\mathbf{X} = \mathbf{1}_m \otimes \begin{pmatrix} V \otimes U & V \otimes U \\ V \otimes U & -(V \otimes U) \end{pmatrix} \in \mathbb{R}^{2rcm \times 2d_r d_c}, \quad (7)$$

and let  $(\hat{\gamma}_1^\top \quad \hat{\gamma}_2^\top)^\top$  be the maximum likelihood estimate from fitting a GLM with inverse link function  $h$ , response vector  $\text{vec}(Y)$ , and design matrix  $\mathbf{X}$ . Define matrices

$$\begin{aligned} \hat{F} &= 2(V \otimes U)^\top \text{diag} \left( h' \left( \tilde{\Theta}_S \right) \right) (V \otimes U), \\ \hat{G} &= 2(V \otimes U)^\top \text{diag} \left( h' \{ (V \otimes U) \hat{\gamma}_1 \} \right) (V \otimes U), \end{aligned} \quad (8)$$



where  $\tilde{\Theta}_S$  is a consistent estimator of  $(\Theta_S^{(1)} + \Theta_S^{(2)})/2$ . Finally, define the test function  $\Psi_{\alpha,U,V}^{(E)}$  by

$$w^{(E)} = m\hat{\gamma}_2^\top \left( \hat{G}\hat{F}^{-1}\hat{G} \right) \hat{\gamma}_2,$$

$$\Psi_{\alpha,U,V}^{(E)}(Y) = \mathbb{I} \left( w^{(E)} > \chi_{d_r d_c, 1-\alpha}^2 \right),$$

where  $\chi_{d_r d_c, 1-\alpha}^2$  denotes the  $(1 - \alpha)$ -th quantile of a  $\chi_{d_r d_c}^2$  distribution.

**Remark 1.** Note that under classical MLE theory, we have

$$\sqrt{m}\hat{G}^{-1/2}\hat{\gamma}_2 \xrightarrow{d} \mathcal{N}(\mathbf{0}, I_{d_r d_c})$$

under the null hypothesis. Comparing to the definition of  $w^{(E)}$ , it is clear that the matrix  $\hat{F}$  provides the additional adjustment for model misspecification. In Section 3.1, we will show that under some regularity conditions on the inverse link function,  $\Psi_{\alpha,U,V}^{(E)}$  controls type I error asymptotically. Moreover, in Section 4, we see that empirically, the asymptotic approximation of test level appears to be quite accurate even for very small values of  $m$  when  $r$  and  $c$  are reasonably large relative to  $d_r$  and  $d_c$ .

**Remark 2.** In (8),  $\hat{F}$  contains an arbitrary consistent estimate of the pooled edge expectation parameters in the hypothesis set. For experiments and real data analysis in Section 4 using the Gaussian edge model, we simply use pooled means for each node pair. For the logistic edge model, we instead use a regularized estimator which provides a more conservative variance estimate, which we describe in detail in Section 4.2.

## 2.4.2 Exponential family edge model with unknown dispersion

We now consider a modified class of tests for general exponential family edges with a single unknown dispersion parameter,  $\phi_{ij} \equiv \phi$ . Building off of classical results for GLMs, we suggest a rescaled statistic for testing  $\mathcal{H}_{0,S}$  based on an estimator of the dispersion parameter. In Section 4, we show that this statistic empirically controls type I error at the nominal level for the logistic link binary edge model with unknown dispersion.

Reusing the notation from Section 2.4.1, and assuming a correctly specified GLM, the asymptotic covariance of  $\hat{\gamma}_2$  is scaled by a factor of  $\phi^2$ . Thus the usual Wald statistic can be corrected by rescaling the statistic by an estimator of  $\phi^2$ . For general exponential family distributions, McCullagh and Nelder (1983) suggest a consistent estimator of  $\phi^2$ . Translating to our setting and notation, they define

$$\hat{\phi}^2 = \frac{1}{2(rcm - d_r d_c)} \{ \text{vec}(Y) - h(\mathbf{1}_m \otimes \hat{\mu}_S) \}^\top \left( \text{diag}\{h'(\mathbf{1}_m \otimes \hat{\mu}_S)\} \right)^{-1} \{ \text{vec}(Y) - h(\mathbf{1}_m \otimes \hat{\mu}_S) \}, \quad (9)$$

where

$$\hat{\mu}_S = \begin{pmatrix} V \otimes U & V \otimes U \\ V \otimes U & -(V \otimes U) \end{pmatrix} \begin{pmatrix} \hat{\gamma}_1 \\ \hat{\gamma}_2 \end{pmatrix}$$

vectorizes the estimates of  $\Theta_S^{(1)}$  and  $\Theta_S^{(2)}$  under the GLM described in Section 2.4.1.

Motivated by these results, we construct the following adjusted test for general exponential family edges with unknown dispersion. Define  $\hat{\phi}^2$  as in (9) and  $w^{(E)}$  as in Section 2.4.1.

Then we can define the test function by

$$w^{(\text{E-UD})} = w^{(\text{E})} / \hat{\phi}^2 ,$$

$$\Psi_{\alpha,U,V}^{(\text{E-UD})}(Y) = \mathbb{I} \left( w^{(\text{E-UD})} > \chi_{d_r d_c, 1-\alpha}^2 \right) ,$$

where  $\chi_{d_r d_c, 1-\alpha}^2$  denotes the  $1 - \alpha$  quantile of a  $\chi_{d_r d_c}^2$  distribution.

**Remark 3.** In Section 4, we use an alternative estimator, also proposed by McCullagh and Nelder (1983),

$$\tilde{\phi}^2 = \frac{1}{2(rc - d_r d_c)} \left\{ \frac{1}{m} Y \mathbf{1}_m - h(\hat{\mu}_S) \right\}^\top \left( \text{diag} \left\{ \frac{1}{m} h'(\hat{\mu}_S) \right\} \right)^{-1} \left\{ \frac{1}{m} Y \mathbf{1}_m - h(\hat{\mu}_S) \right\} , \quad (10)$$

for the dispersion parameter under the logistic link binary edge model, as it is preferred for binary data.

### 2.4.3 Gaussian edge model

If we assume that the edges are Gaussian, we have  $H(x) = x^2/2$ ,  $\phi_{ij} \equiv \sigma$ , and the GLM reduces to a standard linear model with Gaussian errors. In this special case, we can rewrite the statistic  $w^{(\text{E-UD})}$  using orthonormal bases, and define a modified class of tests with rejection thresholds based on the quantiles of the  $F$ -distribution.

Let  $\nu_1 = d_r d_c$  and  $\nu_2 = 2(rcm - d_r d_c)$ , let  $Q$  be an orthonormal basis for the  $(2d_r d_c)$ -dimensional subspace  $\text{col}\{(V \otimes U) \oplus (V \otimes U)\} \subseteq \mathbb{R}^{2rc}$ , and let

$$W = \frac{1}{\sqrt{2}} \begin{pmatrix} V \otimes U \\ -(V \otimes U) \end{pmatrix} \in \mathbb{R}^{2rc \times d_r d_c} .$$

Then we have

$$w^{(\text{G})} = \frac{\nu_2 \|W^\top Y \mathbf{1}_m\|_2^2}{(\nu_1 m) \cdot \|Y - \frac{1}{m} Q Q^\top Y \mathbf{1}_m \mathbf{1}_m^\top\|_F^2} ,$$

$$\Psi_{\alpha,U,V}^{(\text{G})}(Y) = \mathbb{I} \left( w^{(\text{G})} > F_{\nu_1, \nu_2, 1-\alpha} \right) ,$$

where  $F_{\nu_1, \nu_2, 1-\alpha}$  denotes the  $1 - \alpha$  quantile of a  $F_{\nu_1, \nu_2}$  distribution.

In Section 3.1, we show that each  $\Psi_{\alpha,U,V}^{(\text{G})}$  has size  $\alpha$  under the Gaussian edge model.

### 2.4.4 Gaussian edge model with projected data

The tests  $\Psi_{\alpha,U,V}^{(\text{G})}$  are for the Gaussian edge model with constant variance, which assumes the edge covariance matrix is a multiple of the identity. In particular, it requires that the sample variance of  $Q_\perp^\top Y$  is a good estimator of  $\sigma^2$ . While this is true in theory, our applications to real data show that it is a strong assumption in practice, as  $\text{col}(Q)$  may contain a relatively larger proportion of the noise on the hypothesis set edges. Thus, for the Gaussian edge model with  $m > 1$ , we recommend a modified class of tests which takes advantage of replication over  $m$ , and uses only the projected data to get an unbiased estimate of  $\sigma^2$  under a milder assumption on the covariance structure of the edge variables.

Let  $\nu_1 = d_r d_c$  and  $\nu'_2 = 2(m-1)d_r d_c$ , and define  $Q$  and  $W$  as in Section 2.4.3. Then we can define the test function by

$$w^{(G-P)} = \frac{\nu'_2 \|W^\top Y \mathbf{1}_m\|_2^2}{(\nu_1 m) \|Q^\top Y (I_m - \frac{1}{m} \mathbf{1}_m \mathbf{1}_m^\top)\|_F^2},$$

$$\Psi_{\alpha, U, V}^{(G-P)}(Y) = \mathbb{I}\left(w^{(G-P)} > F_{\nu_1, \nu'_2, 1-\alpha}\right),$$

where  $F_{\nu_1, \nu'_2, 1-\alpha}$  denotes the  $1 - \alpha$  quantile of a  $F_{\nu_1, \nu'_2}$  distribution.

**Remark 4.** The test  $\Psi_{\alpha, U, V}^{(G-P)}$  has level  $\alpha$ , and is equivalent to performing an  $F$ -test of equality of group means on projected data

$$(V \otimes U)^\top \text{vec}\left([A_k^{(g)}]_S\right) \in \mathbb{R}^{d_r d_c} \quad (11)$$

for  $k = 1, \dots, m$  and  $g = 1, 2$ . By orthonormality of  $U$  and  $V$ , these low-dimensional vectors are Gaussian, with covariance matrix  $\sigma^2 I_{d_r d_c}$ . Moreover, since the test only depends on these projected data vectors, it only requires that the covariance is correctly specified inside the linear subspace  $\text{col}(V \otimes U)$ .

## 2.4.5 Summary of test classes

In this section, we have defined four classes of projected tests of  $\mathcal{H}_{0, \mathcal{S}}$  indexed by matrices  $U$  and  $V$  with orthonormal columns. In Table 1, we summarize the suggested usage and theoretical guarantees on type I error for testing  $\mathcal{H}_{0, \mathcal{S}}$  for each of these families of tests.

Test	Suggested model	Size guarantees
$\Psi_{\alpha, U, V}^{(E)}$	Exponential family edge model ( $\phi = 1$ )	Asymptotic size $\alpha$ (Corollary 1)
$\Psi_{\alpha, U, V}^{(E-UD)}$	Exponential family edge model (unknown $\phi$ )	n/a
$\Psi_{\alpha, U, V}^{(G)}$	Gaussian edge model ( $m = 1$ )	Size $\alpha$ (Proposition 4)
$\Psi_{\alpha, U, V}^{(G-P)}$	Gaussian edge model ( $m > 1$ )	Size $\alpha$ (Proposition 5)

Table 1: Suggested usage and theoretical guarantees for test families in Sections 2.4.1-2.4.4.

## 2.5 Learning projections from held-out edges

Having described families of tests indexed by pairs  $U, V$  of matrices with orthonormal columns (Stage II), we now propose an approach for learning projections from the independent held out edges in  $-\mathcal{S}$  (Stage I). Under the Gaussian edge model, and with structural assumptions on the edge expectation parameter matrices  $\Theta^{(1)}$  and  $\Theta^{(2)}$ , these projections will approximate the oracle, most powerful projections for a given dimension  $d = d_r = d_c \leq \min\{r, c\}$ , under a fixed alternative.

We will show in Section 3 that under Gaussianity, power depends on a non-centrality parameter

$$\psi(U, V) = \frac{m}{2\sigma^2} \left\| U^\top (\Theta_S^{(1)} - \Theta_S^{(2)}) V \right\|_F^2 \leq \frac{m}{2\sigma^2} \left\| \Theta_S^{(1)} - \Theta_S^{(2)} \right\|_F^2, \quad (12)$$

which implies that the optimal  $d$ -dimensional projections can be recovered directly from the singular value decomposition (SVD) of  $\Theta_S^{(1)} - \Theta_S^{(2)}$ . In particular, they are orthonormal bases for the leading left and right singular subspaces of the difference in hypothesis set edge expectation parameters. While this optimality is only provably true under the Gaussian edge model, in the remainder of the paper we will refer to these singular subspaces as the oracle left and right projections, regardless of the underlying model.

One sensible approach would be to plug in an independent estimate of this difference, then apply the projection test using its leading singular subspaces. Iterative approaches to low rank matrix completion have been developed that are well suited to this problem, either by completing  $m^{-1} \sum_{k=1}^m [A_k^{(g)}]_{-\mathcal{S}}$  for  $g = 1, 2$ , and then taking a difference; or directly completing the difference  $m^{-1} \sum_{k=1}^m \{[A_k^{(1)}]_{-\mathcal{S}} - [A_k^{(2)}]_{-\mathcal{S}}\}$ . Mazumder et al. (2010), for instance, develop a low rank matrix completion approach for the Gaussian setting by using alternating least squares. This approach has been extended to matrices with general exponential family entries in Lin et al. (2021) (eSVD), which can be adapted to the case with missing entries. Mazumder et al. (2010) and Lafond (2015) also consider low rank matrix completion based on solving a convex optimization problem with nuclear norm penalty, in the least squares and general exponential family settings respectively. These existing matrix completion algorithms are generally developed for unstructured or random missingness patterns. They are especially useful for estimating projections with non-rectangular hypothesis node pairs, since they provide estimates of the singular subspaces of the entire expected adjacency matrix, not just for the hypothesis set.

In the remainder of this section, for the case where the hypothesis node pairs form a rectangle, we develop a one-step estimator of the difference in edge expectation parameters. This one-step approach is more amenable to theoretical analysis, and takes advantage of the special block missingness structure. In the following, we partition the indices of the adjacency matrices as four contiguous blocks

$$\begin{pmatrix} \begin{array}{|c|c|} \hline \mathcal{C} & \mathcal{S} \\ \hline \mathcal{D} & \mathcal{R} \\ \hline \end{array} \end{pmatrix},$$

where  $\mathcal{S}$  is the hypothesis set, the columns of  $\mathcal{C}$  have the same dimension as the columns of  $\mathcal{S}$ , and the rows of  $\mathcal{R}$  have the same dimension as the rows of  $\mathcal{S}$ . We also partition the node set into  $[r]$  and its complement  $-[r]$ , where  $[r]$  corresponds to the first  $r$  rows, which are incident to  $\mathcal{S}$ . We analogously partition the nodes into  $[c]$  corresponding to the last  $c$  columns and its complement  $-[c]$ .

Suppose  $\Theta^{(1)} - \Theta^{(2)}$  has rank  $d_*$ , and partition the matrix as

$$\Theta^{(1)} - \Theta^{(2)} = \begin{pmatrix} \Theta_{\mathcal{C}}^{(1)} - \Theta_{\mathcal{C}}^{(2)} & \Theta_{\mathcal{S}}^{(1)} - \Theta_{\mathcal{S}}^{(2)} \\ \Theta_{\mathcal{D}}^{(1)} - \Theta_{\mathcal{D}}^{(2)} & \Theta_{\mathcal{R}}^{(1)} - \Theta_{\mathcal{R}}^{(2)} \end{pmatrix},$$

with SVD

$$USV^\top = \begin{pmatrix} U_{[r]}SV_{-[c]}^\top & U_{[r]}SV_{[c]}^\top \\ U_{-[r]}SV_{-[c]}^\top & U_{-[r]}SV_{[c]}^\top \end{pmatrix}. \quad (13)$$

Note that the blocks of (13) are not the SVD's of the individual blocks, as the first and third factors of each are in general not orthonormal. Moreover, the block corresponding to  $\mathcal{S}$  may have lower rank than the entire matrix. Denote this rank by  $d_{\mathcal{S}} \leq d_*$ . From (12),

we see that the maximum non-centrality parameter can be achieved with  $d = \min\{d_S, r, c\}$ , with additional projection dimensions only increasing the test degrees of freedom.

As discussed above, the oracle projections can be directly recovered from the singular subspaces of  $\Theta^{(1)} - \Theta^{(2)}$ . Define

$$\mathbb{T} = (\Theta_C^{(1)} - \Theta_C^{(2)})(\Theta_D^{(1)} - \Theta_D^{(2)})^\dagger(\Theta_R^{(1)} - \Theta_R^{(2)}) \in \mathbb{R}^{r \times c},$$

where  $\dagger$  denotes the Moore-Penrose pseudoinverse. The following two propositions show conditions on  $\Theta^{(1)} - \Theta^{(2)}$  under which  $\mathbb{T}$  can be used to recover the oracle projections.

**Proposition 1.** Suppose  $U_{-[r]}$  and  $V_{-[c]}$  have linearly independent columns. Then  $\mathbb{T}$  has rank  $d_S$ , and the column and row spaces of  $\mathbb{T}$  coincide with the column and row spaces of  $\Theta_S^{(1)} - \Theta_S^{(2)}$ .

**Proposition 2.** Suppose

$$(U_{-[r]})^\top U_{-[r]} = \rho_U I_{d_*}, \quad (V_{-[c]})^\top V_{-[c]} = \rho_V I_{d_*}$$

for strictly positive  $\rho_U$  and  $\rho_V$ . Then  $\mathbb{T}$  has rank  $d_S$ , and for any  $1 \leq d \leq d_S$  the leading  $d$ -dimensional left and right singular subspaces of  $\mathbb{T}$  coincide with the leading  $d$ -dimensional left and right singular subspaces of  $\Theta_S^{(1)} - \Theta_S^{(2)}$ .

Comparing these two results, Proposition 1 puts a weaker condition on the singular vectors such that  $\mathbb{T}$  has the correct column and row spaces, but without any guarantee that the dimensions will enter the projections in the optimal order. In contrast, Proposition 2 requires that the left and right singular vectors

$$\begin{pmatrix} U_{[r]}^\top & U_{-[r]}^\top \end{pmatrix}^\top, \quad \begin{pmatrix} V_{[c]}^\top & V_{-[c]}^\top \end{pmatrix}^\top$$

are block orthonormal up to rescaling, which correctly orders the singular vectors of  $\mathbb{T}$ . In this sense, when this stronger condition holds, the result in Proposition 2 justifies the optimality of the spectral structure of  $\mathbb{T}$  in the case where  $\Theta_S^{(1)} - \Theta_S^{(2)}$  is not exactly low rank, but still has low effective rank.

Thus, we propose the singular subspaces of an estimate  $\hat{\mathbb{T}}$  as a plug-in for the singular subspaces of  $\Theta_S^{(1)} - \Theta_S^{(2)}$ , where  $\hat{\mathbb{T}}$  itself plugs in estimates for each of the block edge expectation parameters for each group. In the Gaussian case, we naturally use

$$\hat{\Theta}_{\mathcal{I}}^{(g)} = \frac{1}{m} \sum_{k=1}^m [A_k^{(g)}]_{\mathcal{I}}$$

for  $g = 1, 2$  and  $\mathcal{I} \in \{\mathcal{C}, \mathcal{R}, \mathcal{D}\}$ , plus an additional rank truncation step for block  $\mathcal{D}$  to control the error after applying the pseudoinverse. In the case with no self loops, rank truncations may also be used to fill in the missing diagonal entries. With general exponential family edges and a well-behaved link function, we could apply the link function to the group mean adjacency matrices, or otherwise use an eSVD or nuclear norm penalized estimator to perform an initial low rank denoising before calculating  $\hat{\mathbb{T}}$ . We analyze the theoretical performance of this estimator for the Gaussian edge model in Section 3.2.

### 2.5.1 Row and column hypothesis sets

We make some final remarks about learning projections in the special case when  $r = 1$  and  $c = n$ , such that  $\mathcal{S}$  is the first row of the adjacency matrix. This corresponds to testing differences in the edges originating from a particular node. In this case, since  $r = 1$ , the non-centrality parameter can be maximized by a trivial left projection, and a one-dimensional right projection, onto the direction of  $\Theta_{\mathcal{S}}^{(1)} - \Theta_{\mathcal{S}}^{(2)}$ . However, this direction cannot be estimated from the held out edges.

Rewriting the SVD of  $\Theta^{(1)} - \Theta^{(2)}$  with just two blocks,  $\mathcal{S}$  and  $\mathcal{R}$ , as

$$USV^\top = \begin{pmatrix} U_{[r]}SV^\top \\ U_{-[r]}SV^\top \end{pmatrix},$$

note that  $\Theta_{\mathcal{S}}^{(1)} - \Theta_{\mathcal{S}}^{(2)}$  will be in the row space of  $\Theta_{\mathcal{R}}^{(1)} - \Theta_{\mathcal{R}}^{(2)}$ , a subspace which can be recovered from the held out edges. While we cannot get a guarantee as strong as Proposition 2, if  $U_{-[r]}$  has linearly independent columns, then all the signal is captured in an estimable  $d_*$ -dimensional right projection. That is, the projection test with left projection 1 and right projection row  $(\Theta_{\mathcal{R}}^{(1)} - \Theta_{\mathcal{R}}^{(2)})$  will have maximum non-centrality parameter

$$\frac{m}{2\sigma^2} \|\Theta_{\mathcal{S}}^{(1)} - \Theta_{\mathcal{S}}^{(2)}\|_2^2.$$

These remarks apply analogously when  $r = n$ ,  $c = 1$ , and  $\mathcal{S}$  is the last column of the adjacency matrix, and conversely corresponds to testing for differences in the edges which terminate at a particular node.

## 3 Theoretical guarantees

This section presents a number of theoretical properties of our projection testing approach. In Section 3.1 we investigate the asymptotic size properties of the test families defined in Section 2.4, for fixed projections. For the general exponential family edge model with known mean-variance relationship, Proposition 3 gives the asymptotic distribution of  $w^{(E)}$  under a sequence of local alternatives. For the Gaussian edge model, Propositions 4 and 5 establish the exact distributions of  $w^{(G)}$  (see Section 2.4.3) and  $w^{(G-P)}$  (see Section 2.4.4) under any fixed alternative. These results establish the asymptotic size of the test functions  $\Psi_{\alpha,U,V}^{(E)}$ , and the exact size of the test functions  $\Psi_{\alpha,U,V}^{(G)}$  and  $\Psi_{\alpha,U,V}^{(G-P)}$  under respective modeling assumptions. Moreover, they provide intuition about test power and oracle projections.

In Section 3.2, we expand on the properties of the projection test with learned projections based on a plug-in estimate of the matrix  $\mathbb{T}$ , defined in Section 2.5. Under the Gaussian edge model, we prove a non-asymptotic lower bound on power for rectangular hypothesis sets, which depends on the spectral properties of the edge expectation parameter matrices.

Throughout this section, for simplicity we assume a rectangular hypothesis set of size  $r \times c$ , although the results in Section 3.1 hold similarly in the non-rectangular case (see Appendix A.1).

### 3.1 Results for fixed projections

In this section we assume the matrices  $U$  and  $V$  are fixed and have orthonormal columns, with column dimensions  $1 \leq d_r \leq r$  and  $1 \leq d_c \leq c$ , respectively.

#### 3.1.1 The general exponential family edge model

Under the general exponential family edge model with a known mean-variance relationship, we will establish the asymptotic distribution for our test statistic as  $m \rightarrow \infty$  for fixed  $r$  and  $c$ . The edge expectation parameters  $\Theta_{\mathcal{S},m}^{(1)}$  and  $\Theta_{\mathcal{S},m}^{(2)}$ , under a local alternative reparameterization, can be written as

$$\Theta_{\mathcal{S},m}^{(1)} = \text{vec}^{-1}(\tau) + \frac{\text{vec}^{-1}(\Delta)}{\sqrt{m}}, \quad \Theta_{\mathcal{S},m}^{(2)} = \text{vec}^{-1}(\tau) - \frac{\text{vec}^{-1}(\Delta)}{\sqrt{m}}$$

for constant  $(rc)$ -dimensional vectors  $\tau$  and  $\Delta$ .

In the fixed projection setting, the edge expectation parameters for node pairs in  $-\mathcal{S}$  are completely unused, and thus these results also apply in the asymptotic regime when  $n \rightarrow \infty$  while the size of the hypothesis set remains fixed.

We now state two additional regularity assumptions on the exponential family edge model required for Proposition 3, before stating the main result.

#### Assumption 1.

(A)  $h$  is strictly increasing and continuously differentiable.

(B) For all  $g = 1, 2$ ,  $(i, j) \in \mathcal{S}$ , and  $m \geq 1$ ,  $\mathbb{E} \left| [A_1^{(g)}]_{ij} - [\Theta_{\mathcal{S},m}^{(g)}]_{ij} \right|^3$  is uniformly bounded.

#### Assumption 2. Define

$$\mu_{\mathcal{S},m} = \text{vec} \begin{pmatrix} \Theta_{\mathcal{S},m}^{(1)} \\ \Theta_{\mathcal{S},m}^{(2)} \end{pmatrix} \in \mathbb{R}^{2rc}, \quad \bar{X} = \begin{pmatrix} V \otimes U & V \otimes U \\ V \otimes U & -(V \otimes U) \end{pmatrix} \in \mathbb{R}^{2rc \times 2d_r d_c},$$

and let  $\gamma_m = (\gamma_{1,m} \quad \gamma_{2,m})$  be the vector that solves the system of equations

$$\mathbf{0}_{2d_r d_c} = \bar{X}^\top \{h(\mu_{\mathcal{S},m}) - h(\bar{X}\gamma_m)\}, \quad (14)$$

which has a unique solution under Assumption 1. We assume that

$$\sup_{m \geq 1} \{ \|(\gamma_{1,m}, \sqrt{m}\gamma_{2,m})\|_2 \} = K_\gamma < \infty.$$

Assumption 1 provides standard regularity for the misspecified GLM setting (Lv and Liu, 2014). Assumption 2 controls the size of the “population” GLM coefficients which minimize the Kullback-Leibler divergence to the true model (Lv and Liu, 2014). Essentially, we require that the coefficient vector  $\gamma_{1,m}$ , which captures the common part, must scale like a constant in  $m$ ; the coefficient vector  $\gamma_{2,m}$  which captures the difference must scale like  $m^{-1/2}$ , the same order as the difference in edge expectations  $\Theta_{\mathcal{S},m}^{(1)} - \Theta_{\mathcal{S},m}^{(2)}$ .

**Proposition 3.** Assume the exponential family edge model (3) satisfies Assumptions 1 and 2. Let  $(\hat{\gamma}_1^\top \ \hat{\gamma}_2^\top)^\top$  be the maximum likelihood estimate from fitting a GLM with responses  $\text{vec}(Y)$ , and design matrix  $\mathbf{X}$  as in Section 2.4.1. Define  $\gamma_m$  as in Assumption 2, and define matrices  $\hat{F}$  and  $\hat{G}$  as in (8).

Define the function

$$Q(x, y) = 2 \left( \begin{array}{c} (V \otimes U)^\top \{h(\tau) - h((V \otimes U)x)\} \\ (V \otimes U)^\top \{\text{diag}\{h'(\tau)\}\Delta - \text{diag}\{h'((V \otimes U)x)\}(V \otimes U)y\} \end{array} \right).$$

It has a (unique) root defined by  $\mathbf{0}_{2d_r d_c} = Q(\tilde{\tau}, \tilde{\Delta})$ . Finally, define

$$\tilde{F} = 2(V \otimes U)^\top \text{diag}\{h'(\tau)\}(V \otimes U), \quad \tilde{G} = 2(V \otimes U)^\top \text{diag}\{h'\{(V \otimes U)\tilde{\tau}\}\}(V \otimes U).$$

Then  $w^{(E)}$  has an asymptotic  $\chi_{d_r d_c}^2(\tilde{\psi})$  distribution as  $m \rightarrow \infty$ , with non-centrality parameter

$$\tilde{\psi} = \tilde{\Delta}^\top \tilde{G} \tilde{F}^{-1} \tilde{G} \tilde{\Delta}.$$

The proof of Proposition 3 can be found in Section B.2 in the Appendix.

Under the null hypothesis ( $\Delta = \mathbf{0}_{r \times c}$ ), it can be shown that  $\tilde{\Delta} = \mathbf{0}_{d_r d_c}$  regardless of the choices of  $U$  and  $V$ , so that  $\tilde{\psi} = 0$ , which establishes the asymptotic sizes of the tests given in Section 2.4.1. It can also be shown that Assumption 2 holds trivially for  $K_\gamma = \|\tau\|_F$ . We summarize these remarks in the following Corollary.

**Corollary 1.** Assume an exponential family edge model as in (3) which satisfies Assumption 1. Define  $w^{(E)}$  as in Proposition 3. Then, under  $\mathcal{H}_{0,S}$ ,  $w^{(E)}$  has an asymptotic  $\chi_{d_r d_c}^2$  distribution as  $m \rightarrow \infty$ .

As discussed in Section 2.4,  $U$  and  $V$  are arbitrary and may not have any relationship with the true  $\Theta^{(1)}$  and  $\Theta^{(2)}$ . Thus the coefficient estimate  $\hat{\gamma}_2$  is based on a misspecified GLM likelihood. Lv and Liu (2014) establish a central limit theorem for coefficient estimates under misspecified GLMs, and their main results are key to establishing the asymptotic distribution in Proposition 3. Note that  $\hat{G}$  is the usual asymptotic covariance under the GLM, while  $\hat{F}$  is the asymptotic covariance under the saturated model, which is estimable in this setting since we have  $2m$  edge observations for each node pair.

We also provide some interpretation of the non-centrality parameter. Given  $\tilde{\tau}$ ,  $\tilde{\Delta}$  solves a generalized least squares problem and satisfies

$$\tilde{\Delta} = \{(V \otimes U)^\top \text{diag}\{h'((V \otimes U)\tilde{\tau})\}(V \otimes U)\}^{-1} (V \otimes U)^\top \text{diag}\{h'(\tau)\}\Delta.$$

Moreover,  $\Delta$  can be reparameterized as

$$\Delta = \frac{\sqrt{m}}{2} \text{vec} \left( \Theta_{S,m}^{(1)} - \Theta_{S,m}^{(2)} \right).$$

Hence, modulo possible heteroscedasticity introduced by the link function, the non-centrality parameter under a sequence of local alternatives depends on how much of the vectorized difference in edge expectations is in the linear subspace  $\text{col}(V \otimes U)$ , equivalent to applying left and right-hand side projections onto  $\text{col}(U)$  and  $\text{col}(V)$ , respectively.



### 3.1.2 Gaussian edge model

Under the Gaussian edge model, we have the following two results, which hold under arbitrary fixed alternatives.

**Proposition 4.** Under the Gaussian edge model with edge variance  $\sigma^2$ ,  $w^{(G)}$  (see Section 2.4.3) has a doubly non-central  $F_{\nu_1, \nu_2}(\psi, \zeta)$  distribution (Bulgren, 1971), where

$$\psi = \frac{m}{2\sigma^2} \left\| U^\top (\Theta_S^{(1)} - \Theta_S^{(2)}) V \right\|_F^2, \quad \zeta = \frac{m}{\sigma^2} \left\| (I_{2rc} - QQ^\top) \text{vec} \begin{pmatrix} \Theta_S^{(1)} & \Theta_S^{(2)} \end{pmatrix} \right\|_2^2,$$

and  $Q$  is an orthonormal basis for  $\text{col}\{(V \otimes U) \oplus (V \otimes U)\}$ .

Note that the first non-centrality parameter ( $\psi$ ) corresponds to the non-centrality in the numerator, and the second ( $\zeta$ ) to the non-centrality in the denominator. Moreover, under the mesoscale null hypothesis, we have  $\psi = 0$  regardless of the choices of  $U$  and  $V$ , so that  $1/w^{(G)}$  follows a non-central  $F$ -distribution with non-centrality parameter  $\zeta > 0$ . As the non-central  $F$ -distribution is stochastically monotone in its non-centrality parameter, this establishes the sizes of the tests given in Section 2.4.3.

**Proposition 5.** Suppose  $m > 1$ . Under the Gaussian edge model with edge variance  $\sigma^2$ ,  $w^{(G-P)}$  (see Section 2.4.4) has a non-central  $F_{\nu_1, \nu_2'}(\psi)$  distribution, where  $\psi$  is defined in Proposition 4.

Under the mesoscale null hypothesis,  $\psi = 0$  regardless of the choices of  $U$  and  $V$ , which establishes the sizes of the tests given in Section 2.4.4. Propositions 4 and 5 show that test power depends on the model parameters through the non-centrality parameter  $\psi$ , and hence motivates choices of  $U$  and  $V$  which maximize  $\psi$ . The non-centrality parameter  $\psi$  is a special case of the non-centrality parameter  $\tilde{\psi}$  defined in Proposition 3.

As noted in Section 2.5, for any choice of  $d = d_r = d_c$ , the optimal asymptotic power is the result of choosing the projection space to be correspond to the top  $d$  left and right singular vectors of  $\Theta_S^{(1)} - \Theta_S^{(2)}$ . While this oracle power is well-defined for fixed  $d$ , even with known edge expectation parameters, the optimal choice of  $d$  does not simply maximize  $\psi$ , but depends on the trade-off between adding to the non-centrality parameter, and adding more (numerator) degrees of freedom to the test statistic (Das Gupta and Perlman, 1974).

To help interpret the oracle projections, we consider a particular class of low rank alternatives for ranks  $d_0, d_1$  and  $d_2$  satisfying  $d_0 + d_1 + d_2 \leq \min\{r, c\}$ . Suppose the edge expectation parameter matrices in  $\mathcal{S}$  have SVDs given by

$$U^{(0)} \text{diag}(\Gamma^{(g)})(V^{(0)})^\top + U^{(g)} \text{diag}(\Lambda^{(g)}) \left\{ V^{(g)} \right\}^\top.$$

for  $g = 1, 2$ , up to reordering of columns. That is, the entries  $\Gamma^{(g)} \in \mathbb{R}^{d_0}$  and  $\Lambda^{(g)} \in \mathbb{R}^{d_g}$  need not be in decreasing order, internally or relative to each other. Under this parameterization,  $U^{(0)}$  and  $V^{(0)}$  describe the column and row space structure shared between both samples, while  $U^{(g)}$  and  $V^{(g)}$  for  $g = 1, 2$  describe structure which is individual to one sample, similar to models for multilayer networks in MacDonald et al. (2022), Zhang et al. (2020), Loyal and Chen (2021), and others. Also suppose that the columns of  $U^{(1)}$  and  $U^{(2)}$  are mutually orthogonal, and the same for the right singular vectors. In this way, the parameterization decomposes both  $\mathbb{R}^r$  and  $\mathbb{R}^c$  into four mutually orthogonal subspaces: a common part, an

individual part for each sample, and a residual part which appears in neither sample's edge expectation parameter matrix.

Under this alternative, we can write the SVD of the difference of edge expectations  $\Theta_S^{(1)} - \Theta_S^{(2)}$  (up to sign flips and reordering of columns) as

$$(U^{(0)} \quad U^{(1)} \quad U^{(2)}) \left\{ \text{diag} \left( \Gamma^{(1)} - \Gamma^{(2)} \quad \Lambda^{(1)} \quad \Lambda^{(2)} \right) \right\} (V^{(0)} \quad V^{(1)} \quad -V^{(2)})^\top.$$

Thus for any choice of  $d \leq d_0 + d_1 + d_2$ , the optimal asymptotic power is the result of choosing the projection spaces correspond to the top singular subspaces, ordered according to the the entries of

$$(|\Gamma^{(1)} - \Gamma^{(2)}| \quad \Lambda^{(1)} \quad \Lambda^{(2)}).$$

For directions in the space common to both samples, the priority is to include dimensions with different singular values, while for directions in the individual spaces are ordered according to the magnitude of their singular values. In particular, directions in  $\text{col}(U^{(0)})$  and  $\text{col}(V^{(0)})$  corresponding to large singular values in the means of each sample may cancel in the difference, and thus no longer be useful for discriminating those two samples. Moreover, even if the expected adjacency matrices are not low rank, if  $d_0$  is large and many entries of  $\Gamma^{(1)} - \Gamma^{(2)}$  are close to zero, we may still be able to identify low-dimensional projections which capture much of the discriminative signal in the difference.

## 3.2 Results for learned projections

### 3.2.1 Gaussian edge model

In this section, in a non-asymptotic setting with a fixed alternative under the Gaussian edge model, we will establish a bound on the difference in power between an oracle projection test  $\mathcal{H}_{0,S}$ , and one using learned projections based on an estimator  $\hat{\mathbb{T}}$ , as described in Section 2.5.

We present this result in two parts. First, we state a generic bound on the difference in power between the oracle and learned projection tests given a high probability bound on the subspace errors. Then we will give a high probability bound on the subspace errors of our learned projections.

**Proposition 6.** For a fixed alternative, let  $U$  and  $V$  denote the oracle  $d_r$  and  $d_c$  dimensional projections for testing  $\mathcal{H}_{0,S}$ . Let

$$\psi_{\text{orc}} = \frac{m}{2\sigma^2} \|U^\top (\Theta_S^{(1)} - \Theta_S^{(2)}) V\|_F^2$$

denote the oracle non-centrality parameter for  $w^{(\text{G-P})}$ , and

$$\psi_{\text{max}} = \frac{m}{2\sigma^2} \|\Theta_S^{(1)} - \Theta_S^{(2)}\|_F^2,$$

the maximum non-centrality parameter for any choice of dimension. For some  $\alpha \in (0, 1)$ , denote the type II error rate of the level  $\alpha$  oracle projection test by  $\beta_{\text{orc}}$  and the type II error rate of the level  $\alpha$  learned projection test by  $\beta_{\text{learn}}$ .

Suppose the learned projection test is performed with orthonormal bases  $\hat{U} \in \mathbb{R}^{r \times d_r}$  and  $\hat{V} \in \mathbb{R}^{c \times d_c}$  which are independent of the test statistics, and satisfy

$$\min_{O \in \mathcal{O}_{d_r}} \|\hat{U} - UO\|_2 + \min_{O \in \mathcal{O}_{d_c}} \|\hat{V} - VO\|_2 \leq \epsilon < \min \left\{ \sqrt{\frac{\psi_{\text{orc}}}{\psi_{\text{max}}}}, \frac{1}{\sqrt{\psi_{\text{orc}} \psi_{\text{max}}}} \right\} \quad (15)$$

with probability at least  $1 - \xi$ .

Then

$$\beta_{\text{orc}} \leq \beta_{\text{learn}} \leq \left( \frac{1}{1 - \epsilon \sqrt{\psi_{\text{orc}} \psi_{\text{max}}}} \right) \beta_{\text{orc}} + \xi.$$

As one would expect, if the subspace errors are small with high probability, the power of the tests using oracle and learned projections will be similar.

To complete the main result of this section, we will now prove a high probability bound on the subspace errors of our learned projections. We first recall some of the notation introduced in Section 2.5. We split  $\Theta^{(1)} - \Theta^{(2)}$  into four blocks

$$\Theta^{(1)} - \Theta^{(2)} = \begin{pmatrix} \Theta_{\mathcal{C}}^{(1)} - \Theta_{\mathcal{C}}^{(2)} & \Theta_{\mathcal{S}}^{(1)} - \Theta_{\mathcal{S}}^{(2)} \\ \Theta_{\mathcal{D}}^{(1)} - \Theta_{\mathcal{D}}^{(2)} & \Theta_{\mathcal{R}}^{(1)} - \Theta_{\mathcal{R}}^{(2)} \end{pmatrix},$$

with SVD

$$USV^\top = \begin{pmatrix} U_{[r]}SV_{-[c]}^\top & U_{[r]}SV_{[c]}^\top \\ U_{-[r]}SV_{-[c]}^\top & U_{-[r]}SV_{[c]}^\top \end{pmatrix},$$

and assume that this matrix has rank  $d_* < \min\{r, c\}$ . Denote the maximum and minimum entries of  $S$  by  $s_{\text{max}}$  and  $s_{\text{min}}$  respectively.

We also make an assumption on the left and right singular vectors which is intermediate to the conditions assumed in Propositions 1 and 2.

**Assumption 3.**

$$\begin{aligned} \rho_U I_{d_*} &\preceq (U_{[r]})^\top U_{[r]} \preceq \kappa_U I_{d_*}, \\ \rho_V I_{d_*} &\preceq (V_{[c]})^\top V_{[c]} \preceq \kappa_V I_{d_*}. \end{aligned}$$

for  $0 < \rho_U \leq \kappa_U < 1$  and  $0 < \rho_V \leq \kappa_V < 1$ .

Finally, we formally define our plug-in estimator of  $\mathbb{T}$ ,

$$\hat{\mathbb{T}} = (\hat{\Theta}_{\mathcal{C}}^{(1)} - \hat{\Theta}_{\mathcal{C}}^{(2)}) \left( \left[ \hat{\Theta}_{\mathcal{D}}^{(1)} - \hat{\Theta}_{\mathcal{D}}^{(2)} \right]_{(d_*)} \right)^\dagger (\hat{\Theta}_{\mathcal{R}}^{(1)} - \hat{\Theta}_{\mathcal{R}}^{(2)}), \quad (16)$$

where  $[\cdot]_{(d_*)}$  denotes the best rank  $d_*$  approximation of its matrix argument, and

$$\hat{\Theta}_{\mathcal{I}}^{(g)} = \frac{1}{m} \sum_{k=1}^m [A_k^{(g)}]_{\mathcal{I}} \quad (17)$$

for  $g = 1, 2$  and  $\mathcal{I} \in \{\mathcal{C}, \mathcal{D}, \mathcal{R}\}$ . The learned projections will have orthonormal bases  $\hat{U}$  and  $\hat{V}$  given by the leading  $d_*$  left and right singular vectors of  $\hat{\mathbb{T}}$ . Note that by Assumption 3 and Proposition 1, the leading  $d_*$  left and right singular vectors of  $\mathbb{T}$  are orthonormal bases for the oracle projections.

We will state our subspace perturbation bound in two parts. First, we state a simultaneous high probability bound on the error of each factor of  $\hat{\mathbb{T}}$ , before stating a high probability bound on the resulting subspace error.

**Lemma 1.** Assume the Gaussian edge model holds. For integers  $p, q \geq 1$ , define

$$\delta(p, q) = \frac{15}{2 \log(3/2)} \cdot \frac{\sqrt{\log(\min\{p, q\})}}{\sqrt{p} + \sqrt{q}}.$$

Note that  $\delta(p, q) < 5$  for all  $p, q \geq 1$ , and  $\delta(p, q) \rightarrow 0$  as  $\max\{p, q\} \rightarrow \infty$ .

Define

$$\xi = 2 \left( \exp \left\{ -\frac{\sigma^2}{8m} (\sqrt{r} + \sqrt{n-c})^2 \right\} + \exp \left\{ -\frac{\sigma^2}{8m} (\sqrt{n-r} + \sqrt{c})^2 \right\} + \exp \left\{ -\frac{\sigma^2}{8m} (\sqrt{n-r} + \sqrt{n-c})^2 \right\} \right).$$

Then, with probability at least  $1 - \xi$ , we have that

$$\begin{aligned} \|(\hat{\Theta}_{\mathcal{C}}^{(1)} - \hat{\Theta}_{\mathcal{C}}^{(2)}) - (\Theta_{\mathcal{C}}^{(1)} - \Theta_{\mathcal{C}}^{(2)})\|_2 &\leq 2\{2 + \delta(r, n-c)\} \sigma \frac{\sqrt{r} + \sqrt{n-c}}{\sqrt{m}} =: \epsilon_{\mathcal{C}}, \\ \|(\hat{\Theta}_{\mathcal{R}}^{(1)} - \hat{\Theta}_{\mathcal{R}}^{(2)}) - (\Theta_{\mathcal{R}}^{(1)} - \Theta_{\mathcal{R}}^{(2)})\|_2 &\leq 2\{2 + \delta(n-c, r)\} \sigma \frac{\sqrt{n-c} + \sqrt{r}}{\sqrt{m}} =: \epsilon_{\mathcal{R}}, \\ \left\| \left[ \hat{\Theta}_{\mathcal{D}}^{(1)} - \hat{\Theta}_{\mathcal{D}}^{(2)} \right]_{(d_*)} - (\Theta_{\mathcal{D}}^{(1)} - \Theta_{\mathcal{D}}^{(2)}) \right\|_2 &\leq 4\{2 + \delta(n-r, n-c)\} \sigma \frac{\sqrt{n-r} + \sqrt{n-c}}{\sqrt{m}} =: \epsilon_{\mathcal{D}}. \end{aligned}$$

simultaneously over blocks  $\mathcal{C}$ ,  $\mathcal{R}$ , and  $\mathcal{D}$ .

**Proposition 7.** Under the Gaussian edge model, suppose the difference in expected adjacency matrices has rank  $d_*$  and Assumption 3 holds. Define  $U$  and  $V$  as in Proposition 6; and  $\xi$ ,  $\epsilon_{\mathcal{C}}$ ,  $\epsilon_{\mathcal{R}}$ , and  $\epsilon_{\mathcal{D}}$  as in Lemma 1. Suppose that

$$2\epsilon_{\mathcal{D}} \leq s_{\min} \sqrt{(1 - \rho_U)(1 - \rho_V)}. \quad (18)$$

Define

$$\begin{aligned} \epsilon_{\mathbb{T}} &= \sum_{j=1}^7 \epsilon_{\mathbb{T}}^{(j)}, \\ \epsilon_{\mathbb{T}}^{(1)} &= \frac{\epsilon_{\mathcal{C}} \epsilon_{\mathcal{R}}}{s_{\min} \sqrt{(1 - \rho_U)(1 - \rho_V)}}, & \epsilon_{\mathbb{T}}^{(2)} &= \frac{(1 + \sqrt{5}) \epsilon_{\mathcal{C}} \epsilon_{\mathcal{R}} \epsilon_{\mathcal{D}}}{s_{\min}^2 (1 - \rho_U)(1 - \rho_V)}, \\ \epsilon_{\mathbb{T}}^{(3)} &= \frac{\epsilon_{\mathcal{C}} s_{\max} \sqrt{(1 - \kappa_U) \rho_V}}{s_{\min} \sqrt{(1 - \rho_U)(1 - \rho_V)}}, & \epsilon_{\mathbb{T}}^{(4)} &= \frac{\epsilon_{\mathcal{R}} s_{\max} \sqrt{\rho_U (1 - \kappa_V)}}{s_{\min} \sqrt{(1 - \rho_U)(1 - \rho_V)}}, \\ \epsilon_{\mathbb{T}}^{(5)} &= \frac{(1 + \sqrt{5}) \epsilon_{\mathcal{C}} \epsilon_{\mathcal{D}} s_{\max} \sqrt{\rho_U (1 - \kappa_V)}}{s_{\min}^2 (1 - \rho_U)(1 - \rho_V)}, & \epsilon_{\mathbb{T}}^{(6)} &= \frac{(1 + \sqrt{5}) \epsilon_{\mathcal{R}} \epsilon_{\mathcal{D}} s_{\max} \sqrt{(1 - \kappa_U) \rho_V}}{s_{\min}^2 (1 - \rho_U)(1 - \rho_V)}, \\ \epsilon_{\mathbb{T}}^{(7)} &= \frac{(1 + \sqrt{5}) \epsilon_{\mathcal{D}} s_{\max}^2 \sqrt{\rho_U (1 - \kappa_U) \rho_V (1 - \kappa_V)}}{s_{\min}^2 (1 - \rho_U)(1 - \rho_V)}. \end{aligned}$$

Then with probability at least  $\xi$ ,

$$\min_{O \in \mathcal{O}_{d_*}} \|\hat{U} - UO\|_2 + \min_{O \in \mathcal{O}_{d_*}} \|\hat{V} - VO\|_2 \leq \frac{4\sqrt{2} s_{\max} \epsilon_{\mathbb{T}}}{(1 - \rho_U)(1 - \rho_V) s_{\min}^2}.$$

As  $\hat{\mathbb{T}}$  is independent of the test statistics, the main result of this section is complete, by plugging Proposition 7 into Proposition 6.

Although this result is fully non-asymptotic, to understand the bounds, we can consider an asymptotic regime where the overall network size  $n$  grows, while  $m$ ,  $r$ ,  $c$ , and  $\sigma$  remain fixed.

In this case, if the singular vectors are *coherent* (Cape et al., 2019), we would expect  $\rho_U$ ,  $\kappa_U$ ,  $\rho_V$  and  $\kappa_V$  to all have asymptotic order  $1/n$ , with  $\psi_{\text{orc}} = \psi_{\text{max}}$ , and  $\psi_{\text{orc}}$  asymptotically bounded. Note that for fixed  $m$  and  $\sigma$ ,  $\xi$  will go to zero exponentially in  $n$ , so all that remains for convergence in type II error is that (18) holds for sufficiently large  $n$ , and

$$\frac{s_{\text{max}}\epsilon_{\mathbb{T}}}{s_{\text{min}}^2} \rightarrow 0 \quad (19)$$

as  $n \rightarrow \infty$ . In this regime, the asymptotic leading term of  $\epsilon_{\mathbb{T}}$  will be either  $\epsilon_{\mathbb{T}}^{(1)}$  or  $\epsilon_{\mathbb{T}}^{(2)}$ . Both (18) and (19) are satisfied if the difference in adjacency matrices is well conditioned (i.e.,  $s_{\text{max}}/s_{\text{min}}$  is asymptotically bounded), and its singular values dominate  $\sqrt{n}$  asymptotically, similar to a spiked singular value condition seen in random matrix theory (Gavish and Donoho, 2017).

## 4 Experiments on simulated and real data

In this section, we apply our projection tests to mesoscale network testing with synthetic networks from the Gaussian edge model with unknown edge variance  $\sigma^2$ , and the logistic link binary edge model with both known and unknown dispersion parameters. We verify the size of our testing procedures under any choice of projection dimension  $d$ , as well as their empirical power properties compared to classical tests which ignore the network structure, and bootstrap tests based on a latent space model, which are expensive to calibrate, and are not robust to model misspecification. We then apply our tests to cell-cell interaction (CCI) networks between patients exhibiting moderate or severe coronavirus disease 2019 (COVID-19) symptoms. As an additional analysis, in Appendix C we use our tests to compare functional magnetic resonance imaging (fMRI) brain images between patients with Parkinson’s disease and healthy controls.

### 4.1 Synthetic Gaussian edge networks

In this section, we generate synthetic networks from a Gaussian edge model on  $n = 100$  nodes, with variance  $\sigma^2 = 50$ . We test the equality of a  $20 \times 30$  off-diagonal rectangle with nominal level  $\alpha = 0.05$ , and vary  $m$ , the number of networks per sample from 1 to 10. For each of 500 independent replications, the expected adjacency matrices are generated according to the following setup.

1. The network is generated from a 3-dimensional inner product latent space model, with  $\Theta^{(g)} = X^{(g)}[Y^{(g)}]^\top$ . The entries of  $X^{(g)}$  and  $Y^{(g)}$  are Gaussian random variables.
2. In the null setting,

$$\begin{aligned} X_i^{(1)} &\sim \mathcal{N}(0, I_3), & X_i^{(2)} &= X_i^{(1)} & (i = 1, \dots, 20), \\ X_i^{(1)} &\sim \mathcal{N}(0, I_3), & X_i^{(2)} &\sim \mathcal{N}(0, I_3) & (i = 21, \dots, 100), \\ Y_i^{(1)} &\sim \mathcal{N}(0, I_3), & Y_i^{(2)} &\sim \mathcal{N}(0, I_3) & (i = 1, \dots, 70), \\ Y_i^{(1)} &\sim \mathcal{N}(0, I_3), & Y_i^{(2)} &= Y_i^{(1)} & (i = 71, \dots, 100). \end{aligned}$$

3. In the alternative setting,

$$\begin{aligned}
X_i^{(1)} &\sim \mathcal{N}(0, I_3), & X_i^{(2)} &= X_i^{(1)} + \mathcal{N}(0, \frac{1}{3\sqrt{2}}I_3) & (i = 1, \dots, 20), \\
X_i^{(1)} &\sim \mathcal{N}(0, I_3), & X_i^{(2)} &\sim \mathcal{N}(0, I_3) & (i = 21, \dots, 100), \\
Y_i^{(1)} &\sim \mathcal{N}(0, I_3), & Y_i^{(2)} &\sim \mathcal{N}(0, I_3) & (i = 1, \dots, 70), \\
Y_i^{(1)} &\sim \mathcal{N}(0, I_3), & Y_i^{(2)} &= Y_i^{(1)} + \mathcal{N}(0, \frac{1}{3\sqrt{2}}I_3) & (i = 71, \dots, 100).
\end{aligned}$$

This setup produces networks with exactly low rank edge expectation matrices in both the null and alternative cases. Moreover, since the positions are generated with spherical covariance, the conditions of Proposition 2 should hold in expectation, and thus  $\hat{\mathbb{T}}$  should provide a good estimate of the oracle projections for any choice of dimension.

The first competing method (“Basic”) is a baseline approach which ignores the network structure, discards the edges in  $-\mathcal{S}$ , and applies the classical  $F$ -test of equality of means to the two vectorized samples,

$$\{\text{vec}([A_k^{(1)}]_{\mathcal{S}})\}_{k=1}^m, \quad \{\text{vec}([A_k^{(2)}]_{\mathcal{S}})\}_{k=1}^m.$$

Note that this test is only possible for  $m > 1$ . In these settings with relatively small  $m$ , this amounts to 600 univariate comparisons, each based on at most 20 Gaussian samples. While this test does pool the univariate comparisons, it does no dimension reduction.

The second competing method (“Posn- $p$ ”) is a bootstrap test based on an inner product latent space model for the networks in each sample. For  $p = 2, 3, 4$ , we estimate expected adjacency matrices for each group under both the null and alternative mesoscale hypotheses and assuming a  $p$ -dimensional latent space model. Under the alternative,  $\hat{\Theta}^{(1)}$  and  $\hat{\Theta}^{(2)}$  amount to rank  $p$  truncation of the mean adjacency matrix for each sample. Under the null we fit low rank estimates  $\tilde{\Theta}^{(1)}$  and  $\tilde{\Theta}^{(2)}$  constrained to have  $\tilde{\Theta}_{\mathcal{S}}^{(1)} = \tilde{\Theta}_{\mathcal{S}}^{(2)}$ . Our implementation of this constrained estimation is described in Appendix D.

Then, similar to the “Boot-EPA” test described in Ghoshdastidar and von Luxburg (2018), we calculate a Frobenius norm statistic  $\|\hat{\Theta}_{\mathcal{S}}^{(1)} - \hat{\Theta}_{\mathcal{S}}^{(2)}\|_F$ , and calibrate a cutoff based on 500 replications under a parametric bootstrap, fit using the estimated expected adjacency matrices and edge variance under the null. In this setting, the models with  $p \geq 3$  are correctly specified, although the model with  $p = 4$  is overparameterized.

Finally, for  $m > 1$  we apply our projection tests with statistic  $w^{(\text{G-P})}$  (“OrcProj”, “Proj- $d$ ”) using both oracle and learned left and right projections. For  $m = 1$  we instead use the projection test with statistic  $w^{(\text{G})}$ . Under the oracle, the left and right projections are the 6-dimensional singular subspaces of the true difference  $\Theta_{\mathcal{S}}^{(1)} - \Theta_{\mathcal{S}}^{(2)}$ , while our learned projections will be based on the leading  $d$ -dimensional singular subspaces of  $\hat{\mathbb{T}}$ , for  $d = 4, 6, 8$ . We implement these projection tests with twice the dimensions since this is the analogous dimension to the one used in the position model bootstrap test. The results for all of these methods are shown in Figure 1.

In the left panel of Figure 1, we compare the methods under the null. As expected, the basic and all the projection tests control the type I error at the nominal level. On the other hand, the position model bootstrap tests have at best asymptotic control—the rejection rate for

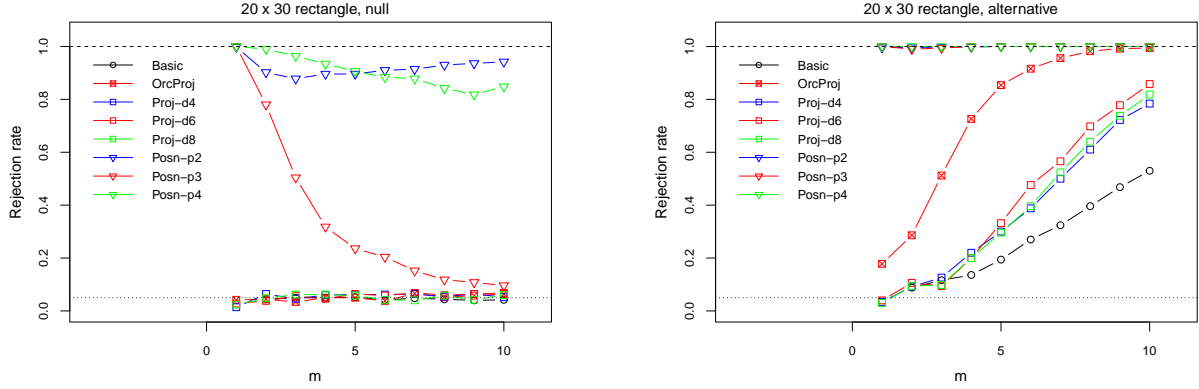


Figure 1: Rejection rate for Gaussian edge networks with inner product latent space model. The dotted line denotes the nominal level  $\alpha = 0.05$ , while the dashed line denotes 1. Points are colored by fitted dimension.

$p = 3$  appears to be decreasing towards the nominal level, but this is not the case for the misspecified model with  $p = 2$  or the overparameterized model with  $p = 4$ .

In the right panel of Figure 1, we compare the methods under the alternative. The position model bootstrap tests have the highest empirical power, but this is not comparable given their issues maintaining control of the type I error rate. The projection tests show increased power compared to the basic test, especially as  $m$  grows and the learned projections approach the oracle. The rejection rates of the tests based on learned projections are also fairly insensitive to the choice of dimension.

As a second comparison, we demonstrate the efficacy of our method when the expected adjacency matrices are not exactly low rank, but instead have low effective rank. Similar to the first setting, we test the equality of a  $20 \times 30$  off-diagonal rectangle with nominal level  $\alpha = 0.05$ , in Gaussian edge networks on  $n = 100$  nodes, and again varying  $m$  from 1 to 10. We generate the expected adjacency matrices according to the following setup.

1. The network is generated from a 3-dimensional Euclidean distance latent space model with  $\Theta_{ij}^{(g)} = \|X_i^{(g)} - Y_j^{(g)}\|_2$ . The entries of  $X^{(g)}$  and  $Y^{(g)}$  are Gaussian random variables.
2. In the null setting,

$$\begin{aligned}
 X_i^{(1)} &\sim \mathcal{N}(0, I_3), & X_i^{(2)} &= X_i^{(1)} & (i = 1, \dots, 20), \\
 X_i^{(1)} &\sim \mathcal{N}(0, I_3), & X_i^{(2)} &\sim \mathcal{N}(0, I_3) & (i = 21, \dots, 100), \\
 Y_i^{(1)} &\sim \mathcal{N}(0, I_3), & Y_i^{(2)} &\sim \mathcal{N}(0, I_3) & (i = 1, \dots, 70), \\
 Y_i^{(1)} &\sim \mathcal{N}(0, I_3), & Y_i^{(2)} &= Y_i^{(1)} & (i = 71, \dots, 100).
 \end{aligned}$$

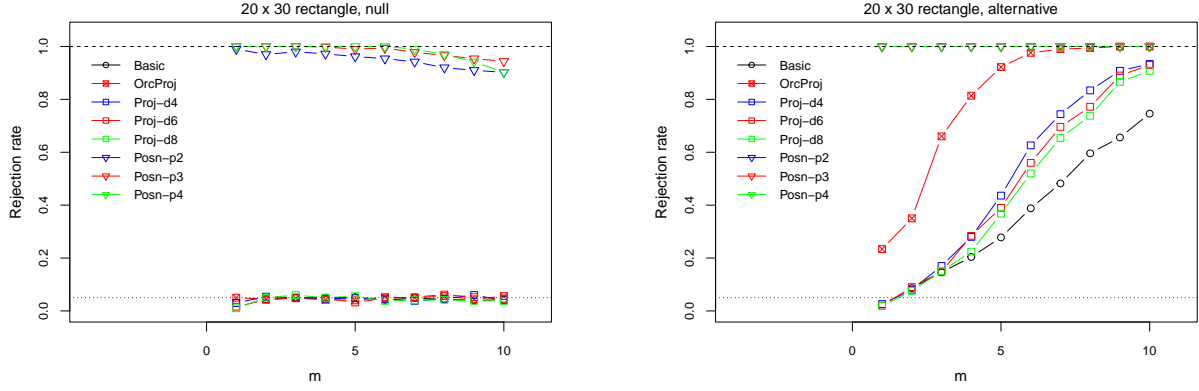


Figure 2: Rejection rate for Gaussian edge networks with Euclidean distance latent space model. The dotted line denotes the nominal level  $\alpha = 0.05$ , while the dashed line denotes 1. Points are colored by fitted dimension.

3. In the alternative setting,

$$\begin{aligned}
 X_i^{(1)} &\sim \mathcal{N}(0, I_3), & X_i^{(2)} &= X_i^{(1)} + \mathcal{N}(0, \frac{\sqrt{2}}{3} I_3) & (i = 1, \dots, 20), \\
 X_i^{(1)} &\sim \mathcal{N}(0, I_3), & X_i^{(2)} &\sim \mathcal{N}(0, I_3) & (i = 21, \dots, 100), \\
 Y_i^{(1)} &\sim \mathcal{N}(0, I_3), & Y_i^{(2)} &\sim \mathcal{N}(0, I_3) & (i = 1, \dots, 70), \\
 Y_i^{(1)} &\sim \mathcal{N}(0, I_3), & Y_i^{(2)} &= Y_i^{(1)} + \mathcal{N}(0, \frac{\sqrt{2}}{3} I_3) & (i = 71, \dots, 100).
 \end{aligned}$$

In this setting, the expected adjacency matrices have low dimensional, nonlinear structure. However, they still exhibit a low effective rank, with visual inspection of a scree plot showing 5 spiked singular values. We apply the same methods, but for the projection tests the learned projections are the left and right singular subspaces of a rank  $d$  imputation of the mean difference in adjacency matrices, after removing the edges in  $\mathcal{S}$  (Mazumder et al., 2010). The results are shown in Figure 2.

In the left panel of Figure 2, we compare the methods under the null. As before, the basic and all the projection tests exactly control type I error at the nominal level, but now all of the position model bootstrap tests are misspecified, and nearly always reject under the null.

In the right panel of Figure 2, we compare the methods under the alternative. Even though the expected adjacency matrices are not exactly low rank, the projection tests show increased power compared to the basic test. Although the scree plot for  $\Theta^{(g)}$  would suggest a 5-dimensional low rank model for each sample, the highest rejection rate for the projection test is with  $d = 4$ , decreasing as  $d$  grows. This implies that the dimensions corresponding to the smaller spiked singular values either cannot be reliably recovered due to the noise, or are no longer spiked after taking the difference between the adjacency matrices.



## 4.2 Synthetic binary edge networks

To evaluate mesoscale two-sample comparisons of networks with binary edges, we test two different mesoscale hypotheses with nominal level  $\alpha = 0.05$  using our test based on  $w^{(E)}$  and its competitors. Our first setting considers a  $20 \times 30$  off-diagonal rectangle in two samples of networks on  $n = 100$  nodes. In both cases we generate synthetic logistic link binary edge networks, under the general exponential family edge model with support  $\{0, 1\}$ , dispersion  $\phi = 1$ , and inverse link function  $h(x) = e^x / (1 + e^x)$ . Once again we vary  $m$  from 1 to 10. For each of 500 independent replications, we generate edge expectation parameters according to the following setup.

1. The network is generated from a 2-dimensional inner product latent space model with  $h^{-1}(\mathbb{E}A_1^{(g)}) = \Theta^{(g)} = X^{(g)}[Y^{(g)}]^\top$ . The entries of  $X^{(g)}$  and  $Y^{(g)}$  are Gaussian random variables.
2. In the null setting,

$$\begin{aligned} X_i^{(1)} &\sim \mathcal{N}(0, I_2), & X_i^{(2)} &= X_i^{(1)} & (i = 1, \dots, 20), \\ X_i^{(1)} &\sim \mathcal{N}(0, I_2), & X_i^{(2)} &\sim \mathcal{N}(0, I_2) & (i = 21, \dots, 100), \\ Y_i^{(1)} &\sim \mathcal{N}(0, I_2), & Y_i^{(2)} &\sim \mathcal{N}(0, I_2) & (i = 1, \dots, 70), \\ Y_i^{(1)} &\sim \mathcal{N}(0, I_2), & Y_i^{(2)} &= Y_i^{(1)} & (i = 71, \dots, 100). \end{aligned}$$

3. In the alternative setting,

$$\begin{aligned} X_i^{(1)} &\sim \mathcal{N}(0, I_2), & X_i^{(2)} &= X_i^{(1)} + \mathcal{N}(0, \frac{1}{4\sqrt{2}}I_2) & (i = 1, \dots, 20), \\ X_i^{(1)} &\sim \mathcal{N}(0, I_2), & X_i^{(2)} &\sim \mathcal{N}(0, I_2) & (i = 21, \dots, 100), \\ Y_i^{(1)} &\sim \mathcal{N}(0, I_2), & Y_i^{(2)} &\sim \mathcal{N}(0, I_2) & (i = 1, \dots, 70), \\ Y_i^{(1)} &\sim \mathcal{N}(0, I_2), & Y_i^{(2)} &= Y_i^{(1)} + \mathcal{N}(0, \frac{1}{4\sqrt{2}}I_2) & (i = 71, \dots, 100). \end{aligned}$$

After applying the inverse link function, this model produces expected edge parameter matrices with are exactly low rank. The expected adjacency matrices  $h(\Theta^{(g)})$  for  $g = 1, 2$  still have low effective rank, with visual inspection of a scree plot showing 3 spiked singular values

The “Basic” approach now performs 600 univariate (two-sided) binomial proportion tests, without a continuity correction. Each of the resulting statistics has an independent asymptotic  $\chi_1^2$  distribution, so the results are pooled by summation and compared to a  $\chi_{600}^2$  null distribution. When  $m = 1$ , this test is trivial and will never reject the null hypothesis.

The position model bootstrap tests for  $p = 2, 3, 4$  are performed exactly as for the Gaussian edge model, but with the parametric bootstrap generating binary edge networks. While this no longer agrees with the model likelihood, it is common in the RDGP literature to apply such spectral approaches directly to the adjacency matrix, under a semiparametric signal-plus-noise assumption.

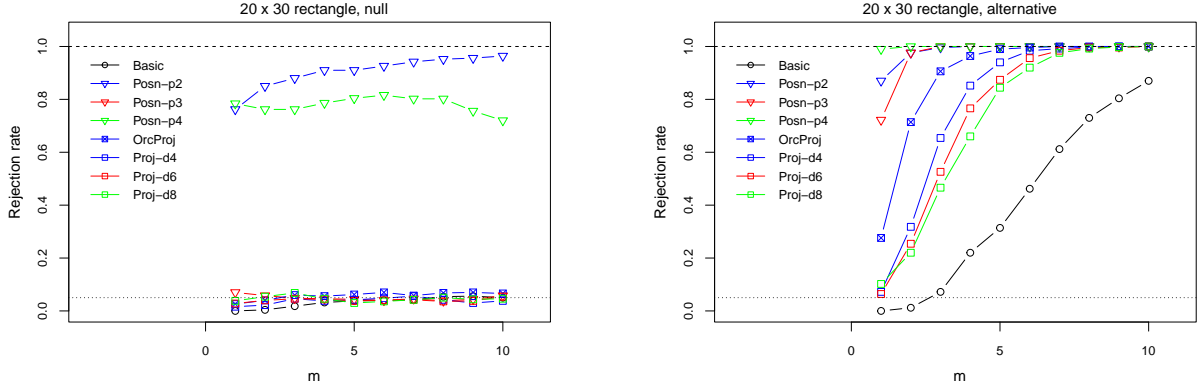


Figure 3: Rejection rates for binary edge logistic link networks with inner product latent space model. The dotted line denotes the nominal level  $\alpha = 0.05$ , while the dashed line denotes 1. Points are colored by fitted dimension.

Finally, our projection test based on  $w^{(E)}$  is applied with both oracle and learned projections. In the computation of the test statistic, we use a regularized estimator  $\hat{\Theta}_S$  to compute  $\hat{F}$  (see (8)). In this special case, the binomial variance is maximized for proportion  $1/2$ , so for each node pair we shrink the pooled means towards  $1/2$  by a constant shift of  $1/(4m)$ . For small values of  $m$ , this helps control the type I error rate by increasing the correction for misspecification made by  $\hat{F}^{-1}$ . The learned projections are based on an estimate  $\hat{T}$ , after plugging in estimates of the matrix blocks learned from a rank  $d$  truncation of  $h^{-1}(m^{-1} \sum_k A_k^{(g)})$ , with elements trimmed above and below at  $h^{-1}(1 - 1/3m)$  and  $h^{-1}(1/3m)$  respectively.

In the left panels of Figure 3, we compare test performance under the null. We see that our projection tests empirically control the type I error at the nominal level for any choice of projection dimension. The good performance of the asymptotic approximation in Proposition 3, even for very small  $m$ , suggests that these approximations may also hold for growing  $r$  and  $c$ , when the projection dimension of the test remains small. The position model bootstrap test empirically controls the type I error for  $p = 3$  but does not do as well for either  $p = 2$  or  $p = 4$ .

In the right panel of Figure 3, we compare the methods under the alternative. The rejection rates of the projection tests are larger than the basic test, and once again fairly insensitive to the choice of projection dimension. As before the smallest projection dimension,  $d = 4$ , gives the best empirical power.

As a final comparison, and to demonstrate more robustness properties of our projection tests, we apply our method and its competitors to overdispersed binary edges. In the context of logistic regression with grouped data (McCullagh and Nelder, 1983), overdispersion can occur when there is positive correlation among the trials in each group, such that the sum of those trials has variance greater than what would be expected from a binomial distribution with the same mean. In our specific setting, the “grouping” comes from the  $m$  binary edges for each fixed  $(g, i, j)$  triple for  $g = 1, 2$  and  $1 \leq i, j \leq n$ .

We generate expected adjacency matrices as in the previous binary edge logistic link model comparison, but introduce overdispersion with a beta-binomial model. For  $m > 1$  and a constant (over node pairs) overdispersion parameter  $\eta \in [1, m)$ , we generate overdispersed

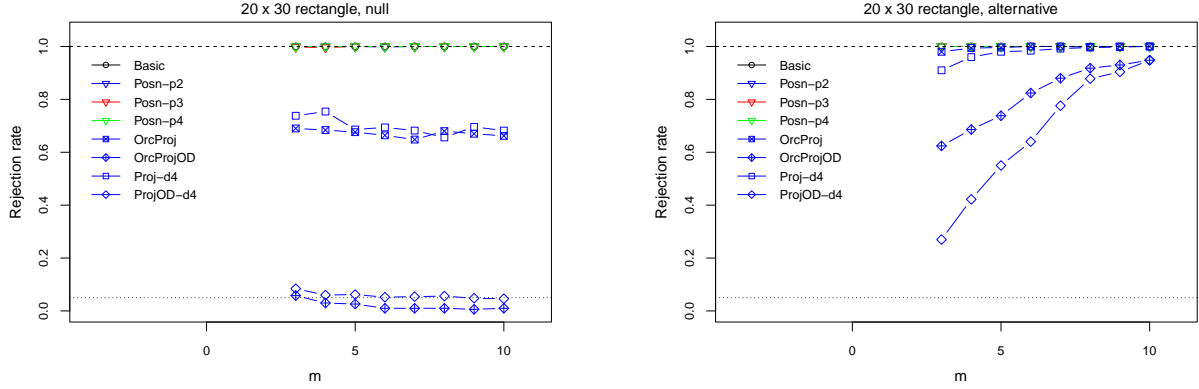


Figure 4: Rejection rates for binary edge logistic link networks with inner product latent space model and overdispersion parameter  $\eta = 2$ . The dotted line denotes the nominal level  $\alpha = 0.05$ , while the dashed line denotes 1. Points are colored by fitted dimension.

edge variables by sampling

$$B_{ij,g} \sim \text{Beta} \left( \frac{h(\Theta_{ij}^{(g)})(m - \eta)}{\eta - 1}, \frac{\{1 - h(\Theta_{ij}^{(g)})\}(m - \eta)}{\eta - 1} \right),$$

$$\sum_{k=1}^m [A_k^{(g)}]_{ij} \sim \text{Binomial}(m, B_{ij,g}).$$

then choosing a configuration of 1's and 0's for the  $m$  layers uniformly at random. Ahn and Chen (1995) show that this hierarchical sampling strategy produces edges which are independent over  $(g, i, j)$  triples, and satisfy

$$\mathbb{E}([A_k^{(g)}]_{ij}) = h(\Theta_{ij}^{(g)}), \quad \text{Var} \left( \sum_{k=1}^m [A_k^{(g)}]_{ij} \right) = \eta m h(\Theta_{ij}^{(g)}) \{1 - h(\Theta_{ij}^{(g)})\}$$

for  $g = 1, 2$ ,  $k = 1, \dots, m$  and node pairs  $(i, j)$ . In this simulation we set  $\eta = 2$ , and vary  $m$  from 3 to 10.

We apply the projection test described in Section 2.4.2, using the modified statistic  $w^{(\text{E-UD})}$  (“OrcProjOD”, “ProjOD- $d$ ”). For comparison we also apply the usual projection test based on  $w^{(\text{E})}$ , and the same competing basic and position model bootstrap tests. For both the usual and modified projection tests, we use a learned 4-dimensional projection. The results are shown in Figure 4.

In the left panel of Figure 4, we see that other than the projection tests, all the methods nearly always reject the mesoscale null hypothesis. The usual projection tests do not control type I error at the nominal level, while the modified projection tests do appear to have asymptotic control. In the right panel of Figure 4, under the alternative, the modified projection tests have good power, with the power of the learned projection test approaching that of the oracle projection test as  $m$  grows. With overdispersion parameter  $\eta = 2$ , the effective sample size in terms of  $m$  is essentially halved compared to independent Bernoulli trials, and after making this adjustment, the rejection rates under this model are very close to the corresponding rates in Figure 3.

### 4.3 An application to cell-cell interaction networks

In this section, we apply our projection test to mesoscale network testing for cell-cell interaction (CCI) data. The samples are comprised of 38 COVID-19 patients who exhibited either moderate ( $m_1 = 23$ ) or severe ( $m_2 = 19$ ) symptoms. Single cell sequencing data for each patient is summarized to construct an undirected binary network of aggregated CCIs among different types of immune cells. The single cell gene sequencing data was originally collected by Wilk et al. (2020), and the data processing was done by the Sydney Precision Data Science Center using a workflow described in Lin et al. (2022). Briefly, each patient’s data begins as a large matrix of gene expressions for a sample of immune cells, which are then annotated with one of  $n = 32$  cell types. The recently developed method “CellChat” (Jin et al., 2021) then uses these gene expressions to identify significantly communicating ligand-receptor pairs, by aggregating over all the cells in a given pair of cell types. Finally, communications are further aggregated over ligand-receptor pairs related to inflammation, to produce a final interaction score between any two cell types. These scores are non-negative, but often zero, so they are binarized and symmetrized for our network analysis, and analyzed under the logistic link binary edge model.

We construct mesoscale hypotheses based on two classes of immune cells: T cells, and natural killer (NK) cells. T cells comprise 8 of the 32 cell types, while NK cells comprise 4 of the 32. T cells are known to play an important role in COVID-19 infection, and Chen and Wherry (2020); Kuri-Cervantes et al. (2020), among others, have previously identified differential T cell behavior depending on COVID-19 case severity. Chen and Wherry (2020) also suggest that T cell activation may have an effect on their expression of NK cell-related markers. Thus, we test for differences in the edge expectation parameters among the T cells (“T/T”), and between the T and NK cells (“T/NK”). We do not test the edge expectation parameters among the NK cells, as this rectangle is too small and the edges too sparse to have sufficient signal, even with dimension reduction. We denote the blocks of each adjacency matrix as

$$\left( \begin{array}{cc|c} \text{T/T} & \text{T/NK} & \mathcal{R} \\ \hline \text{T/NK}^\top & \text{NK/NK} & \mathcal{R} \\ \hline \mathcal{R}^\top & \mathcal{D} & \end{array} \right). \quad (20)$$

We compare our projection test, with and without modification for unknown dispersion (“ProjOD”, “Proj”), to the basic proportion test described in Section 4.2 (“Basic”). For the projection tests of the T/T mesoscale null, we adjust for symmetry of the hypothesis set by using only the edges on or above the main diagonal. We perform density corrected versions of the projection tests (see Appendix A.2), allowing for group-specific intercept terms under the null.

To learn projections, we use a low rank imputation (Mazumder et al., 2010) of  $\hat{\Theta}^{(1)} - \hat{\Theta}^{(2)}$ , after centering, where the gray blocks of (20) are treated as missing, and the white blocks as observed. Each  $\hat{\Theta}^{(g)}$  for  $g = 1, 2$  is estimated by applying  $h^{-1}$  elementwise to the mean adjacency matrix for each group, and trimming the entries above and below at  $h^{-1}(1 - 1/m_g)$  and  $h^{-1}(1/m_g)$ . Visual inspection of the scree plot of

$$\begin{pmatrix} \hat{\Theta}_{\mathcal{R}}^{(1)} - \hat{\Theta}_{\mathcal{R}}^{(2)} \\ \hat{\Theta}_{\mathcal{D}}^{(1)} - \hat{\Theta}_{\mathcal{D}}^{(2)} \end{pmatrix},$$

Test	$p$ -value		Rej. rate ( $\alpha = 0.05$ )	
	T/T	T/NK	T/T	T/NK
Basic	0.880	0.995	0	0
Proj ( $d = 1$ )	<b><math>1.0 \times 10^{-4}</math></b>	<b>0.033</b>	1	1
ProjOD ( $d = 1$ )	<b>0.016</b>	0.078	1	0
RandProj ( $d = 1$ )	0.382	0.627	0.13	0.03
BlockProj	<b>0.018</b>	0.621	1	0
BlockProjOD	0.228	0.701	0	0

Table 2:  $p$ -values for CCI data mesoscale testing. For uniform random projections, the median and rejection rate over 100 replications is reported.  $p$ -values below  $\alpha = 0.05$  are bolded.

after centering, shows only one large singular value, so we perform the projection tests with dimension  $d_r = d_c = 1$ . Note that we do not claim that one dimension is sufficient to model the mean structure of the network difference, just that it is a good choice to balance signal to noise for mesoscale testing. As additional comparisons, we also apply the projection test (without modification for overdispersion) using projections generated uniformly at random (“RandProj”) and a block-constant projection (with and without modification for overdispersion) which only looks at local changes in edge density across the two groups (“BlockProj”, “BlockProjOD”). Results are shown in Table 2.

For the T/T hypothesis set, the projection test rejects the mesoscale null hypothesis at the  $\alpha = 0.05$  level, even after accounting for possible overdispersion. This is in contrast to the basic proportion test, which cannot find sufficient signal due to the sparsity of the networks. For the T/NK hypothesis set, the usual projection test rejects the null hypothesis, but this is no longer the case after accounting for overdispersion. It is clear that the projections learned by matrix imputation provide useful dimension reduction, as they lead to smaller  $p$ -values than the corresponding tests using uniform random projections, or the naive block-constant projections.

We can interpret the decision of the projection test to reject these mesoscale null hypotheses by inspecting the learned projection direction, and the sign of the logistic regression coefficient internal to the test. For the T/T hypothesis set, the evidence against the null is driven by increased connection probability in the moderate patients relative to the severe patients among a clique of three cell types: CD4 naive, CD4 central memory, and CD8 naive. For the T/NK hypothesis set, the evidence against the null is driven by these same 3 subtypes of T cells showing increased connection probability with two types of NK cell (NK-56hi and NK-16hi) in the moderate patients relative to the severe patients.

We also demonstrate the sensitivity of these testing approaches to changes in the number of networks in each sample. For  $\underline{m} = 4, 8, 12, 16, 19$ , we form subsamples from each population without replacement and test the mesoscale hypothesis for the T/T hypothesis set, which was rejected by the usual projection test on the full data. Both the learned and uniform random projection tests use dimension 1. This process is repeated 200 times, and the results are summarized in Figure 5.

For all values of  $\underline{m}$ , the learned projection test leads to a smaller  $p$ -value on average than the competing methods, with the differences increasing as  $\underline{m}$  grows, suggesting that in addition to the signal provided by the additional networks, the projection test learns more informative

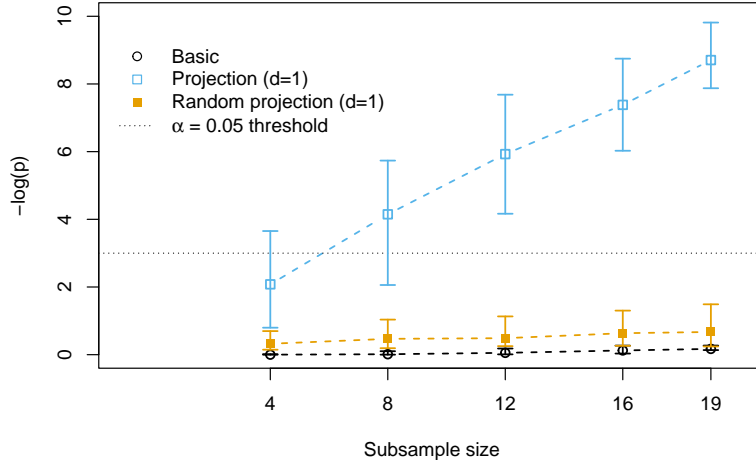


Figure 5: Median  $-\log(p)$  for testing the T/T hypothesis in CCI data, varying subsample sizes  $\underline{m}$ . Vertical bars span from the 25th to 75th empirical quantiles over 200 replications.

projections to isolate this signal.

## 5 Discussion and future work

In this paper, we have developed mesoscale two-sample testing methodology for networks. These mesoscale tests allow for comparisons at local (individual node pair), intermediate (a subnetwork) and global (full network) scales, for samples of aligned networks. Mesoscale questions of interest arise naturally in many applications, and allow the analyst to effectively balance power and localization of two-sample network comparisons. We show how, in the presence of low rank or low effective rank structure, information can be shared across the entire network to produce powerful tests that are robust to structural misspecification. We prove finite sample type I error control and exact power calculations for Gaussian edge networks, and propose methodology for networks with general exponential family edges, with provable asymptotic type I error control.

Future directions in theory for this problem could focus on obtaining stronger asymptotic results for general exponential family edges. We conjecture that the asymptotic distribution result in Proposition 3 should still hold when  $r, c$  and  $n$  grow, even for fixed  $m$ , provided we are in a suitable asymptotic regime. Such a result would give a better understanding of test control and power in this more general setting.

In Appendix A.3, we discuss further simple modifications to methodology and theory to understand simultaneous mesoscale testing for several hypothesis sets. Additional methodological extensions of interest include adjustments for edge dependence or heteroscedasticity, perhaps motivated by nested model comparison procedures for generalized linear mixed models with more flexible covariance structures. There is also potential to work with more general non-linear projected null hypotheses, essentially extending the use of linear subspaces to submanifolds of  $\mathbb{R}^r$  and  $\mathbb{R}^c$ . Finally, it would be valuable to tailor our mesoscale

hypothesis testing methodology to robustly test for equality of positions in latent position models, perhaps by developing a procedure to adaptively learn a suitable set of “null” nodes to align the network embeddings.

The setting of multiple matrix-valued observations split into two samples is not unique to networks, and arises in other applications. For example, one could observe a matrix of counts (e.g., of microbiotic taxa), or subject-specific covariance or precision matrix estimates (Xia et al., 2018, 2020). Many models in those settings also reduce the intrinsic dimension of data using low rank or other latent variable models, and thus our methodology would be applicable to two-sample testing for fixed rows, columns, or blocks of general matrix data, as long as suitable assumptions can be worked out.

## References

- Agterberg, J., Tang, M., and Priebe, C. E. (2020). Nonparametric two-sample hypothesis testing for random graphs with negative and repeated eigenvalues. *arXiv:2012.09828 [math, stat]*.
- Ahn, H. and Chen, J. J. (1995). Generation of over-dispersed and under-dispersed binomial variates. *Journal of Computational and Graphical Statistics*, 4(1):55–64.
- Athreya, A., Fishkind, D. E., Tang, M., Priebe, C. E., Park, Y., Vogelstein, J. T., Levin, K., Lyzinski, V., Qin, Y., and Sussman, D. L. (2018). Statistical inference on random dot product graphs: A survey. *The Journal of Machine Learning Research*, 18:92.
- Athreya, A., Tang, M., Park, Y., and Priebe, C. E. (2021). On estimation and inference in latent structure random graphs. *Statistical Science*, 36(1).
- Badea, L., Onu, M., Wu, T., Roceanu, A., and Bajenaru, O. (2017). Exploring the reproducibility of functional connectivity alterations in Parkinson’s disease. *PLOS ONE*, 12(11):e0188196.
- Bandeira, A. S. and van Handel, R. (2016). Sharp nonasymptotic bounds on the norm of random matrices with independent entries. *The Annals of Probability*, 44(4).
- Bhatia, R. (1997). *Matrix Analysis*. Springer.
- Breusch, T. S. (1986). Hypothesis testing in unidentified models. *The Review of Economic Studies*, 53(4):635–651.
- Bulgren, W. G. (1971). On representations of the doubly non-central  $F$  distribution. *Journal of the American Statistical Association*, 66(333):184–186.
- Cannings, T. I. and Samworth, R. J. (2017). Random-projection ensemble classification. *Journal of the Royal Statistical Society, Series B*, 79(4):959–1035.
- Cape, J., Tang, M., and Priebe, C. E. (2019). The two-to-infinity norm and singular subspace geometry with applications to high-dimensional statistics. *Annals of Statistics*, 47(5):2405–2439.
- Chen, L., Josephs, N., Lin, L., Zhou, J., and Kolaczyk, E. D. (2020). A spectral-based framework for hypothesis testing in populations of networks. *arXiv:2011.12416 [math, stat]*.

- Chen, Z. and Wherry, E. J. (2020). T cell responses in patients with COVID-19. *Nature Reviews Immunology*, 20(9):529–536.
- Chung, J., Varjavand, B., Arroyo-Reli3n, J., Alyakin, A., Agterberg, J., Tang, M., Priebe, C. E., and Vogelstein, J. T. (2022). Valid two-sample graph testing via optimal transport Procrustes and multiscale graph correlation with applications in connectomics. *Stat*, 11(1):e429.
- Das Gupta, S. and Perlman, M. D. (1974). Power of the noncentral  $F$ -test: Effect of additional variates on Hotelling’s T2-test. *Journal of the American Statistical Association*, 69(345):174–180.
- Donnat, C. and Holmes, S. (2018). Tracking network dynamics: A survey of distances and similarity metrics. *arXiv:1801.07351 [physics, stat]*.
- Draves, B. and Sussman, D. L. (2021). Bias-variance tradeoffs in joint spectral embeddings. *arXiv:2005.02511 [math, stat]*.
- Du, X. and Tang, M. (2021). Hypothesis testing for equality of latent positions in random graphs. *arXiv:2105.10838 [stat]*.
- Fair, D. A., Cohen, A. L., Power, J. D., Dosenbach, N. U. F., Church, J. A., Miezin, F. M., Schlaggar, B. L., and Petersen, S. E. (2009). Functional brain networks develop from a “local to distributed” organization. *PLoS Computational Biology*, 5(5):e1000381.
- Gavish, M. and Donoho, D. L. (2017). Optimal shrinkage of singular values. *IEEE Transactions on Information Theory*, 63(4):2137–2152.
- Ghoshdastidar, D., Gutzeit, M., Carpentier, A., and von Luxburg, U. (2017). Two-sample tests for large random graphs using network statistics. In *Proceedings of the 2017 Conference on Learning Theory*, pages 954–977.
- Ghoshdastidar, D. and von Luxburg, U. (2018). Practical methods for graph two-sample testing. In *Advances in Neural Information Processing Systems*.
- Ginestet, C. E., Li, J., Balachandran, P., Rosenberg, S., and Kolaczyk, E. D. (2017). Hypothesis testing for network data in functional neuroimaging. *The Annals of Applied Statistics*, 11(2):725–750.
- Hoff, P. D., Raftery, A. E., and Handcock, M. S. (2002). Latent space approaches to social network analysis. *Journal of the American Statistical Association*, 97(460):1090–1098.
- Holland, P. W., Laskey, K. B., and Leinhardt, S. (1983). Stochastic blockmodels: First steps. *Social Networks*, 5(2):109–137.
- Huang, D. T., Gururajapathy, S. S., Ke, Y., Qiao, M., Wang, A., Kumar, H., and Yang, Y. (2022). Data-driven network neuroscience: On data collection and benchmark. *arXiv:2211.12421 [cs, eess, q-bio]*.
- Jin, S., Guerrero-Juarez, C. F., Zhang, L., Chang, I., Ramos, R., Kuan, C.-H., Myung, P., Plikus, M. V., and Nie, Q. (2021). Inference and analysis of cell-cell communication using CellChat. *Nature Communications*, 12(1):1088.
- Keener, R. W. (2010). *Theoretical statistics: topics for a core course*. Springer.



- Khambhati, A. N., Sizemore, A. E., Betzel, R. F., and Bassett, D. S. (2018). Modeling and interpreting mesoscale network dynamics. *NeuroImage*, 180:337–349.
- Kuntal, B. K., Chandrakar, P., Sadhu, S., and Mande, S. S. (2019). “NetShift”: A methodology for understanding “driver microbes” from healthy and disease microbiome datasets. *The ISME Journal*, 13(2):442–454.
- Kuri-Cervantes, L., Pampera, M. B., Meng, W., Rosenfeld, A. M., Ittner, C. A., Weisman, A. R., Agyekum, R. S., Mathew, D., Baxter, A. E., Vella, L. A., et al. (2020). Comprehensive mapping of immune perturbations associated with severe COVID-19. *Science Immunology*, 5(49):eabd7114.
- Lafond, J. (2015). Low rank matrix completion with exponential family noise. In *Conference on Learning Theory*, pages 1224–1243.
- Levin, K., Athreya, A., Tang, M., Lyzinski, V., and Priebe, C. E. (2017). A central limit theorem for an omnibus embedding of multiple random dot product graphs. In *2017 IEEE International Conference on Data Mining Workshops*, pages 964–967.
- Li, Y. and Li, H. (2018). Two-sample test of community memberships of weighted stochastic block models. *arXiv:1811.12593 [math, stat]*.
- Lin, K. Z., Lei, J., and Roeder, K. (2021). Exponential-family embedding with application to cell developmental trajectories for single-cell RNA-Seq data. *Journal of the American Statistical Association*, 116(534):457–470.
- Lin, Y., Loo, L., Tran, A., Lin, D. M., Moreno, C., Hesselton, D., Neely, G. G., and Yang, J. Y. H. (2022). Scalable workflow for characterization of cell-cell communication in COVID-19 patients. *PLOS Computational Biology*, 18(10):e1010495.
- Lopes, M., Jacob, L., and Wainwright, M. J. (2011). A more powerful two-sample test in high dimensions using random projection. In *Advances in Neural Information Processing Systems*.
- Lovato, I., Pini, A., Stamm, A., and Vantini, S. (2020). Model-free two-sample test for network-valued data. *Computational Statistics & Data Analysis*, 144:106896.
- Loyal, J. D. and Chen, Y. (2021). An eigenmodel for dynamic multilayer networks. *arXiv:2103.12831 [stat]*.
- Lunagómez, S., Olhede, S. C., and Wolfe, P. J. (2021). Modeling network populations via graph distances. *Journal of the American Statistical Association*, 116(536):2023–2040.
- Lv, J. and Liu, J. S. (2014). Model selection principles in misspecified models. *Journal of the Royal Statistical Society, Series B*, 76(1):141–167.
- Ma, Z., Ma, Z., and Yuan, H. (2020). Universal latent space model fitting for large networks with edge covariates. *The Journal of Machine Learning Research*, 21:67.
- MacDonald, P. W., Levina, E., and Zhu, J. (2022). Latent space models for multiplex networks with shared structure. *Biometrika*, 109(3):683–706.
- Mazumder, R., Hastie, T., and Tibshirani, R. (2010). Spectral regularization algorithms for learning large incomplete matrices. *The Journal of Machine Learning Research*, 11:2287–2322.

- McCullagh, P. and Nelder, J. A. (1983). *Generalized Linear Models*. Chapman and Hall.
- Qi, X., Wang, J., and Shao, J. (2022). Minimax perturbation bounds of the low-rank matrix under Ky Fan norm. *AIMS Mathematics*, 7(5):7595–7605.
- Sabanayagam, M., Vankadara, L. C., and Ghoshdastidar, D. (2022). Graphon based clustering and testing of networks: Algorithms and theory. In *International Conference on Learning Representations*.
- Sripada, C., Rutherford, S., Angstadt, M., Thompson, W. K., Luciana, M., Weigard, A., Hyde, L. H., and Heitzeg, M. (2020). Prediction of neurocognition in youth from resting state fMRI. *Molecular Psychiatry*, 25(12):3413–3421.
- Storey, J. D., Taylor, J. E., and Siegmund, D. (2004). Strong control, conservative point estimation and simultaneous conservative consistency of false discovery rates: A unified approach. *Journal of the Royal Statistical Society, Series B*, 66(1):187–205.
- Tang, M., Athreya, A., Sussman, D. L., Lyzinski, V., Park, Y., and Priebe, C. E. (2017). A semiparametric two-sample hypothesis testing problem for random graphs. *Journal of Computational and Graphical Statistics*, 26(2):344–354.
- Taylor, A. E., Saint-Cyr, J. A., and Lang, A. E. (1986). Frontal lobe dysfunction in Parkinson’s disease: The cortical focus of neostriatal outflow. *Brain*, 109(5):845–883.
- Tiku, M. L. (1967). Tables of the power of the  $F$ -test. *Journal of the American Statistical Association*, 62(318):525–539.
- Tzourio-Mazoyer, N., Landeau, B., Papathanassiou, D., Crivello, F., Etard, O., Delcroix, N., Mazoyer, B., and Joliot, M. (2002). Automated anatomical labeling of activations in SPM using a macroscopic anatomical parcellation of the MNI MRI single-subject brain. *Neuroimage*, 15(1):273–289.
- Wedin, P.-Å. (1973). Perturbation theory for pseudo-inverses. *BIT*, 13(2):217–232.
- Wilk, A. J., Rustagi, A., Zhao, N. Q., Roque, J., Martínez-Colón, G. J., McKechnie, J. L., Ivison, G. T., Ranganath, T., Vergara, R., Hollis, T., Simpson, L. J., Grant, P., Subramanian, A., Rogers, A. J., and Blish, C. A. (2020). A single-cell atlas of the peripheral immune response in patients with severe COVID-19. *Nature Medicine*, 26(7):1070–1076.
- Wozniak, J. R., Mueller, B. A., Bell, C. J., Muetzel, R. L., Hoecker, H. L., Boys, C. J., and Lim, K. O. (2013). Global functional connectivity abnormalities in children with fetal alcohol spectrum disorders. *Alcohol: Clinical and Experimental Research*, 37(5):748–756.
- Wu, T. and Hallett, M. (2013). The cerebellum in Parkinson’s disease. *Brain*, 136(3):696–709.
- Xia, Y., Cai, T., and Cai, T. T. (2018). Multiple testing of submatrices of a precision matrix with applications to identification of between pathway interactions. *Journal of the American Statistical Association*, 113(521):328–339.
- Xia, Y. and Li, L. (2022). Hypothesis testing for network data with power enhancement. *Statistica Sinica*, 32:293–321.
- Xia, Y., Li, L., Lockhart, S. N., and Jagust, W. J. (2020). Simultaneous covariance inference for multimodal integrative analysis. *Journal of the American Statistical Association*, 115(531):1279–1291.

- Zalesky, A., Fornito, A., and Bullmore, E. T. (2010). Network-based statistic: Identifying differences in brain networks. *NeuroImage*, 53(4):1197–1207.
- Zhang, X., Xue, S., and Zhu, J. (2020). A flexible latent space model for multilayer networks. In *Proceedings of the 37th International Conference on Machine Learning*, pages 11288–11297.

## A Methodological extensions

### A.1 Non-rectangular or undirected hypothesis sets

One interpretation of the tests in Section 2 is as the comparison of nested GLMs. When the hypothesis node pairs form a rectangle, the left and right projections are easy to write compactly with matrices, but the underlying idea is still compatible with non-rectangular hypotheses. For projections with dimensions  $d_r$  and  $d_c$ , the edge expectations under the corresponding projection null will have at most  $d_r d_c$  free parameters, and thus whether or not it is rectangular, whenever  $|\mathcal{S}| \geq d_r d_c$ , projection will reduce the test dimension.

In the general non-rectangular case, we require left and right subspaces of  $\mathbb{R}^n$ , with orthonormal bases  $\bar{U} \in \mathbb{R}^{n \times d_r}$  and  $\bar{V} \in \mathbb{R}^{n \times d_c}$ . These subspaces, along with  $\mathcal{S}$ , will define a subspace of  $\mathbb{R}^{|\mathcal{S}|}$ . We will restrict our estimates of the (vectorized) group means to this low dimensional subspace.

Let  $\mathcal{P}_{\mathcal{M}}$  denote the  $p \times p$  matrix of the projection operator onto a subspace  $\mathcal{M} \subseteq \mathbb{R}^p$ , and for a non-empty subset  $\mathcal{N} \subseteq \{1, \dots, p\}$ , let  $\pi_{\mathcal{N}}$  denote the  $|\mathcal{N}| \times p$  matrix made up of the rows of  $I_p$  which correspond to the elements in  $\mathcal{N}$ .

Given left and right-hand side projections, we can write a projected null in the following general form

$$\text{vec}(\Theta_S^{(g)}) \in \pi_{\mathcal{S}}(\bar{V} \otimes \bar{U}) \quad (21)$$

for  $g = 1, 2$ .

Assuming  $\pi_{\mathcal{S}}(\bar{V} \otimes \bar{U})$  has full rank, the corresponding projection-based tests are exactly the ones in the previous sections; motivated by the comparison of groupwise (generalized) linear models with coefficients  $\gamma_1, \gamma_2 \in \mathbb{R}^{d_r d_c}$ , the means are given by

$$\{\pi_{\mathcal{S}}(\bar{V} \otimes \bar{U})\} (\gamma_1 + \gamma_2)$$

for group 1,

$$\{\pi_{\mathcal{S}}(\bar{V} \otimes \bar{U})\} (\gamma_1 - \gamma_2)$$

for group 2, and  $\gamma_2 = \mathbf{0}_{d_r d_c}$  under the projected null hypothesis.

This extension to general hypothesis sets also suggests a modification of the above tests for undirected networks, and networks with no self loops. For networks with no self loops, we can simply remove diagonal entries from  $\mathcal{S}$ . For instance, if  $\mathcal{S} = \mathcal{T} \times \mathcal{T}$  for  $\mathcal{T} \subseteq \{1, \dots, n\}$  which forms a square, we modify  $\mathcal{S}$  to include only (without loss of generality) the upper triangle of  $\mathcal{S}$ , with or without the diagonal.

For undirected networks, we must discard dependent edge variables below the diagonal from  $\mathcal{S}$ , but the methodological modification takes slightly more care, since symmetry can also induce rank deficiency in the projected data (for the Gaussian edge model) or GLM design matrix (for general exponential family edges). As a simple example, again suppose the hypothesis set is  $\mathcal{S} = \mathcal{T} \times \mathcal{T}$  in an undirected network, and denote both the left and right-hand side projections by  $V$ , then the projected data

$$V^{\top} [A_k^{(g)}]_{\mathcal{S}} V \in \mathbb{R}^{d \times d}$$

for  $g = 1, 2$  and  $k = 1, \dots, m$  will also be symmetric, and thus restricted to a subspace of  $\mathbb{R}^{d \times d}$ , where  $d$  is the column dimension of  $V$ .

In the undirected case, we assume that the hypothesis set contains the symmetric counterpart of all of its node pairs, and that the learned left and right-hand side projections are equal ( $\bar{V} = \bar{U}$ ). Given left and right-hand side projections, the mesoscale test operates under a working GLM, with mean structure

$$\mathbb{E} \left\{ \pi_{\mathcal{S}} \text{vec} \left( A_k^{(g)} \right) \right\} = h \{ \pi_{\mathcal{S}} (\bar{U} \otimes \bar{U}) \beta^{(g)} \}. \quad (22)$$

Let  $\pi_{\mathcal{S}}^{\Delta}$  denote the operator which restricts to only node pairs on or above the diagonal, and suppose  $G_{\mathcal{S}}$  is the linear mapping which satisfies

$$\pi_{\mathcal{S}} \text{vec}(M) = G_{\mathcal{S}} \pi_{\mathcal{S}}^{\Delta} \text{vec}(M)$$

for any  $n \times n$  matrix  $M$ . By construction,  $G_{\mathcal{S}}$  has a (left) pseudo-inverse  $G_{\mathcal{S}}^{\dagger}$ , and (22) can be rewritten as

$$\mathbb{E} \left\{ \pi_{\mathcal{S}}^{\Delta} \text{vec} \left( A_k^{(g)} \right) \right\} = G_{\mathcal{S}}^{\dagger} h \{ \pi_{\mathcal{S}} (\bar{U} \otimes \bar{U}) \beta^{(g)} \}. \quad (23)$$

In words, application of the linear map  $G_{\mathcal{S}}^{\dagger}$  on the right-hand side of (23) replaces the edge expectation of a given node pair by the average of its expectation and that of its symmetric counterpart. Then by injectivity of  $h$  we can move  $G_{\mathcal{S}}^{\dagger}$  inside the link function and reparametrize

$$\mathbb{E} \left\{ \pi_{\mathcal{S}}^{\Delta} \text{vec} \left( A_k^{(g)} \right) \right\} = h(\tilde{W} \tilde{\beta}^{(g)}),$$

where  $\tilde{W}$  is an orthonormal basis for  $\text{col} \left\{ G_{\mathcal{S}}^{\dagger} \pi_{\mathcal{S}} (\bar{U} \otimes \bar{U}) \right\}$ . In general,

$$\text{col} \left\{ G_{\mathcal{S}}^{\dagger} \pi_{\mathcal{S}} (\bar{U} \otimes \bar{U}) \right\}$$

will not coincide with

$$\text{col} \left\{ \pi_{\mathcal{S}}^{\Delta} (\bar{U} \otimes \bar{U}) \right\},$$

the “naive” choice of subspace under undirectedness, and they may even have different dimensions.

In summary, for undirected networks, we augment the general working assumption in (21) as

$$\pi_{\mathcal{S}}^{\Delta} \text{vec}(\Theta^{(g)}) \in \text{col} \left\{ G_{\mathcal{S}}^{\dagger} \pi_{\mathcal{S}} (\bar{U} \otimes \bar{U}) \right\}$$

for  $g = 1, 2$ .

## A.2 Density and degree correction with restricted projections

In the previous section, we noted that the projected null hypothesis is conservative, and restricts the class of alternatives for which the projection test has non-trivial power. This same property of projection testing can be used to design modified testing procedures which ignore some linear classes of differences between the edge expectation parameter matrices. In this section, we will describe two such modifications which are of particular interest in applications. We will refer to these as density corrected and degree corrected two-sample mesoscale tests, as that is their interpretation for binary edge networks. As above, we restrict to the case of rectangular hypothesis sets for simplicity, but these modifications apply in the non-rectangular case as well (see Section A.1).

In the density corrected case, note that under the model (3), two-sample differences in edge density will correspond to differences in  $\text{vec}(\Theta_S^{(1)})$  and  $\text{vec}(\Theta_S^{(2)})$  in a one-dimensional subspace

$$\text{span}(\mathbf{1}_c \otimes \mathbf{1}_r).$$

Thus the density corrected projection test will center the left and right projections  $U$  and  $V$ , restricting them to satisfy

$$(V \otimes U)^\top (\mathbf{1}_c \otimes \mathbf{1}_r) = \mathbf{0}_{d_r d_R}$$

such that changes in the sum of the entries of  $\Theta_S^{(1)}$  and  $\Theta_S^{(2)}$  will be ignored by the corresponding projection test. Practically, while this centering step can be applied to  $U$  and  $V$  estimated as in Section 2.5, it is helpful to modify the projection learning method, applying imputation or one-step estimation to a centered estimate of the difference in edge expectation parameters. The result is an improved ordering of the projection directions tailored to density corrected testing, as the learned orthonormal matrix is already approximately centered. We apply a density corrected projection test to real data in Section 4.3.

Under model (3), degree corrections are typically modeled with additive row and column fixed effects  $\delta_i^{(g)}$  for  $g = 1, 2$  and  $i = 1, \dots, n$ , such that

$$\mathbb{E}[A_k^{(g)}]_{ij} = h \left( \delta_i^{(g)} + \delta_j^{(g)} + \Theta_{ij}^{(g)} \right)$$

for  $g = 1, 2$ ,  $k = 1, \dots, m$ , and  $1 \leq i, j \leq n$ , with additional centering assumptions on  $\Theta^{(g)}$  (e.g., Ma et al., 2020). Thus, restricted to the hypothesis set, two sample differences in these fixed effect parameters will correspond to a linear subspace,

$$\text{col} \left( \mathbf{1}_c \otimes I_r \quad \mathbf{1}_r \otimes I_c \right),$$

which has  $(r + c - 1)$  linearly independent directions. Just as for density correction, the degree corrected projection test will restrict the left and right projections so that  $\text{col}(V \otimes U)$  is orthogonal to changes in the degree effects, analogous to allowing sample-specific row and column fixed effect terms under the null.

### A.3 Multiple testing and false discovery rates

In many applications, we may be interested in simultaneous multiple testing for several non-overlapping hypothesis sets, denoted by  $\mathcal{S}_1, \dots, \mathcal{S}_K$  for  $K > 1$ . For instance, we may want to test for two-sample differences in several rectangles induced by known node communities, or several rows corresponding to different nodes of interest. While the flexibility of the mesoscale framework means that we can easily test the intersection hypothesis by setting the hypothesis set to be  $\mathcal{S} = \mathcal{S}_1 \cup \dots \cup \mathcal{S}_K$ , selecting smaller non-null hypothesis sets to control a multiple testing error metric like the false discovery rate (FDR) is a distinct problem. Under the same independent edge assumption made in model (3), testing with fixed projections will render the  $p$ -values independent, and thus standard thresholding approaches control the FDR at the nominal level (Storey et al., 2004).

However, our methodology for mesoscale testing with learned projections will lead to dependent test statistics, as the edges in  $\mathcal{S}_1$  will be used directly for testing  $\mathcal{H}_{0, \mathcal{S}_1}$ , and indirectly for learning projections to test  $\mathcal{H}_{0, \mathcal{S}_j}$  for  $j = 2, \dots, K$ .

Some simple alterations to the data splitting strategy can be used to produce independent  $p$ -values. First, if  $\mathcal{S}_1 \cup \dots \cup \mathcal{S}_K \neq \{1, \dots, n\}^2$ , we may use the remaining edges to learn projections for all the tests. A conditioning argument, integrating over these remaining edge variables, shows that standard thresholding approaches for independent  $p$ -values will still control the FDR. If this first strategy is not feasible, but  $m > 1$ , we may instead do an initial layer of data splitting, using a subset of the networks to learn projections, and the held out set to test the mesoscale hypotheses. The same conditioning argument justifies control of the FDR at the nominal level.

In future work, we will consider both empirical and theoretical analysis of the effect of dependence among multiple mesoscale hypothesis test statistics, both when edges are re-used, directly and indirectly, for different hypotheses; and when the hypothesis sets are overlapping. While this will render the test statistics dependent, it is unclear if and when this dependence will affect FDR control.

#### A.4 Relationship to latent position testing

In this section, we will expand on the relationship between mesoscale network testing and testing for equality of individual node positions under a latent space model. As is typical of two-sample testing under latent space models, in this section we will assume that the expected adjacency matrices are symmetric.

Fixing notation, a general latent space model assumes that the expected adjacency matrices for each sample are parameterized by  $d$ -dimensional latent positions  $Z_i^{(g)}$  for  $i = 1, \dots, n$  and  $g = 1, 2$ , and specifies

$$[\Theta^{(g)}]_{ij} = D\left(Z_i^{(g)}, Z_j^{(g)}\right) \quad (24)$$

for a similarity function  $D : \mathbb{R}^d \times \mathbb{R}^d \rightarrow \mathbb{R}$ . For instance,  $D$  may be the (generalized) inner product or a linear function of the Euclidean distance. It is typical that this model is identifiable only up to some group of invariant transformations; for instance, when  $D$  is the inner product, the model is invariant under orthogonal transformations of latent positions.

Under this general latent space model, we may formally state a *positional* null hypothesis

$$\mathcal{H}_{0,i}^{(\text{posn})} : Z_i^{(1)} = Z_i^{(2)},$$

to test the equality of node  $i$ 's latent position in two samples. The positional null has both pros and cons. It can be of scientific value to isolate changes in the behavior of a given node  $i$ . On the other hand, it can be difficult to interpret since it depends on latent variables which are not fully identified.

Using terminology introduced by Breusch (1986), model unidentifiability renders  $\mathcal{H}_{0,i}^{(\text{posn})}$  *untestable* for any  $i = 1, \dots, n$ . In particular, it is not *confirmable*: for any parameter set where the positional null is true, there is an equivalent parameter set where it is false. While in some cases  $\mathcal{H}_{0,i}^{(\text{posn})}$  may be *refutable* (with an inner product similarity we can distinguish between latent positions with different Euclidean norms), in others it is completely vacuous (with a Euclidean distance similarity, the latent space model is invariant to translation of the latent positions).

In recent work, Du and Tang (2021) test this positional null hypothesis under the generalized RDPG by making an additional identifying assumption. They assume a known “seed” set

of nodes  $\mathcal{J} \subseteq \{1, \dots, n\}$  such that the positional null hypothesis holds for all  $j \in \mathcal{J}$ , and the map

$$z \mapsto \left\{ D(z, Z_j^{(1)}) \right\}_{j \in \mathcal{J}} \quad (25)$$

is injective. In their specific setting with generalized inner product similarity, this injectivity condition requires that the  $|\mathcal{J}| \times d$  matrix of seed node positions has linearly independent columns.

The condition in (25) renders the positional null hypothesis testable, and in fact makes it equivalent to a mesoscale null hypothesis. In particular, under the general latent space model (24), and if (25) holds for a seed set  $\mathcal{J}$ ,  $\mathcal{H}_{0,i}^{(\text{posn})}$  is equivalent to the mesoscale null hypothesis  $\mathcal{H}_{0, \mathcal{S}_i^{(\mathcal{J})}}$ , where

$$\mathcal{S}_i^{(\mathcal{J})} = \{(i, j) : j \in \mathcal{J}\}.$$

While (25) makes  $\mathcal{H}_{0,i}^{(\text{posn})}$  theoretically testable, any practical test, including the one used in Du and Tang (2021), will depend on the correct specification of  $\mathcal{J}$ , and validity of the test cannot be guaranteed otherwise. On the other hand, the corresponding mesoscale hypothesis based on the node pairs in  $\mathcal{S}_i^{(\mathcal{J})}$  is defined in terms of identified parameters, and although it may no longer coincide with the positional null, it will remain a well-defined mesoscale null hypothesis, even when  $\mathcal{J}$  is misspecified. In summary, while our mesoscale testing methodology does not specifically address the positional null, it can be used to more robustly test closely related hypotheses, written in terms of fully identified model parameters.

## B Technical proofs

### B.1 Proofs of Propositions 1 and 2

*Proof of Proposition 1.* Recall the definition of  $\mathbb{T}$ ,

$$\mathbb{T} = (\Theta_{\mathcal{C}}^{(1)} - \Theta_{\mathcal{C}}^{(2)})(\Theta_{\mathcal{D}}^{(1)} - \Theta_{\mathcal{D}}^{(2)})^\dagger (\Theta_{\mathcal{R}}^{(1)} - \Theta_{\mathcal{R}}^{(2)}) \in \mathbb{R}^{r \times c}.$$

From (13), we expand

$$\mathbb{T} = \left( U_{[r]} S V_{-[c]}^\top \right) \left( U_{-[r]} S V_{-[c]}^\top \right)^\dagger \left( U_{-[r]} S V_{[c]}^\top \right).$$

Then by the definition of the Moore-Penrose pseudo-inverse,

$$\mathbb{T} = U_{[r]} S \left( V_{-[c]}^\top V_{-[c]} \right) S^{-1} \left( U_{-[r]}^\top U_{-[r]} \right) S V_{[c]}^\top, \quad (26)$$

where  $S^{-1}$  exists since  $\Theta^{(1)} - \Theta^{(2)}$  has rank  $d_*$ .

By assumption,  $V_{-[c]}^\top V_{-[c]}$  and  $U_{-[r]}^\top U_{-[r]}$  are full rank, so we can write

$$\begin{aligned} \Theta_{\mathcal{S}}^{(1)} - \Theta_{\mathcal{S}}^{(2)} &= U_{[r]} S V_{[c]}^\top \\ \mathbb{T} &= U_{[r]} \left\{ S \left( V_{-[c]}^\top V_{-[c]} \right) S^{-1} \left( U_{-[r]}^\top U_{-[r]} \right) S \right\} V_{[c]}^\top, \end{aligned}$$

and both  $S$  and  $\{S(V_{-[c]}^\top V_{-[c]})S^{-1}(U_{-[r]}^\top U_{-[r]})S\}$  are full rank. It follows that the  $d_{\mathcal{S}}$ -dimensional column and row spaces of  $\Theta_{\mathcal{S}}^{(1)} - \Theta_{\mathcal{S}}^{(2)}$  and  $\mathbb{T}$  coincide, which completes the proof.  $\square$



*Proof of Proposition 2.* Beginning from (26), we have by assumption that

$$\begin{aligned}\mathbb{T} &= U_{[r]} S \left( V_{-[c]}^\top V_{-[c]} \right) S^{-1} \left( U_{-[r]}^\top U_{-[r]} \right) S V_{[c]}^\top \\ &= (\rho_U \rho_V) U_{[r]} S V_{[c]}^\top \\ &= (\rho_U \rho_V) \left( \Theta_S^{(1)} - \Theta_S^{(2)} \right).\end{aligned}$$

Since  $\mathbb{T}$  is a scalar multiple of  $\Theta_S^{(1)} - \Theta_S^{(2)}$ , it follows that they have the same leading left and right singular subspaces for any  $d \in \{1, \dots, d_S\}$ .  $\square$

## B.2 Proof of Proposition 3 and Corollary 1

*Proof of Proposition 3 and Corollary 1.* To begin, we define  $(2d_r d_c) \times (2d_r d_c)$  covariance matrices  $F_m$  and  $G_m(\tilde{\gamma})$  as a function of an arbitrary  $\tilde{\gamma} \in \mathbb{R}^{d_r d_c}$ :

$$F_m = \bar{X}^\top \text{diag}(h'(\mu_{S,m})) \bar{X}, \quad G_m(\tilde{\gamma}) = \bar{X}^\top \text{diag}(h'(\bar{X}\tilde{\gamma})) \bar{X}.$$

The proof will proceed in three steps. First, we verify Conditions 1 to 4 required for Lv and Liu (2014), Theorem 7, which shows the asymptotic normality of the GLM coefficients. Then we verify that under this particular local alternative setup, the MLEs  $\hat{\gamma}_1$  and  $\hat{\gamma}_2$  are asymptotically independent, and the rescaled limit  $\sqrt{m}\gamma_{m,2}$  converges. Finally, we will prove that  $\hat{G}\hat{F}^{-1}\hat{G}$  is a consistent estimator of  $\tilde{G}\tilde{F}^{-1}\tilde{G}$ , and the result will follow by Slutsky's theorem.

Recall the definition of the population target  $\gamma_m = (\gamma_{1,m} \quad \gamma_{2,m})$  which solves the population score equations.

For a given  $m$  and arbitrary  $\tilde{\gamma}$ , the covariance under the misspecified GLM is

$$\mathbf{X}^\top \text{diag} \{h'(\mathbf{X}\tilde{\gamma})\} \mathbf{X} = mG_m(\tilde{\gamma}),$$

while the covariance under the saturated model is

$$\mathbf{X}^\top \text{diag} \{h'(\mathbf{1}_m \otimes \mu_{S,m})\} \mathbf{X} = mF_m$$

Condition 1 of Lv and Liu (2014) follows immediately from Assumption 1, part (A), and orthonormality of  $U$  and  $V$ .

To verify Condition 2 of Lv and Liu (2014), define

$$V(\tilde{\gamma}) = F_m^{-1/2} G_m(\tilde{\gamma}) F_m^{-1/2}, \quad N_m(\kappa) = \left\{ \tilde{\gamma} : \|\sqrt{m} F_m^{1/2}(\tilde{\gamma} - \gamma_m)\|_2 \leq \kappa \right\} \subseteq \mathbb{R}^{2d_r d_c},$$

and let  $\lambda_{\min}(M)$  denote the smallest eigenvalue of a symmetric matrix  $M$ . Note that by Assumption 1, part (A),  $V$  is a continuous function of  $\tilde{\gamma}$ .

Define

$$\delta = \inf_{m \geq 1} \min_{g \in \{1,2\}} \min_{(i,j) \in \mathcal{S}} \left\{ h'([\Theta_{S,m}^{(g)}]_{ij}) \right\}.$$

Note that  $\delta > 0$  by assumption, since  $h'$  is strictly positive, continuous, and the entries of  $\Theta_{S,m}^{(1)}$  and  $\Theta_{S,m}^{(2)}$  are uniformly bounded. The first part of the condition holds since for any  $m$ ,

$$\lambda_{\min}(F_m) \geq 2\delta > 0,$$

where the inequality holds by definition of  $\delta$  and since  $2^{-1/2}\bar{X}$  is orthonormal.

This minimum eigenvalue condition also implies that for any  $m$  and  $\kappa > 0$ ,  $N_m(\kappa)$  is contained in a ball centered at  $\gamma$  with radius proportional to  $m^{-1/2}$ . Thus, by continuity of  $V$ , for any  $\kappa > 0$ ,

$$\min_{\tilde{\gamma} \in N_m(\kappa)} \lambda_{\min} \{V(\tilde{\gamma})\} \geq \min_{\|\tilde{\gamma} - \gamma\|_2 \leq 1} (\lambda_{\min} \{V(\tilde{\gamma})\}) > 0$$

for sufficiently large  $m$ .

To verify Condition 3 of Lv and Liu (2014), define

$$\tilde{V}(\tilde{\gamma}_1, \dots, \tilde{\gamma}_{2d_r d_c}) = F_m^{-1/2} \tilde{G}_m(\tilde{\gamma}_1, \dots, \tilde{\gamma}_{2d_r d_c}) F_m^{-1/2},$$

where

$$\tilde{G}(\tilde{\gamma}_1, \dots, \tilde{\gamma}_{2d_r d_c}) = \bar{X}^\top \left\{ \begin{pmatrix} \vdots & & \vdots \\ h'(\bar{X}\tilde{\gamma}_1) & \cdots & h'(\bar{X}\tilde{\gamma}_{2d_r d_c}) \\ \vdots & & \vdots \end{pmatrix} \circ \bar{X} \right\},$$

and  $\circ$  denotes the Hadamard (element-wise) product of two matrices. By Assumption 1, part (A),  $\tilde{V}$  is a continuous function of its arguments. Thus, similar to the verification of Condition 2, for any  $\kappa > 0$

$$\max_{\tilde{\gamma}_1, \dots, \tilde{\gamma}_{2d_r d_c} \in N_m(\kappa)} \|\tilde{V}(\tilde{\gamma}_1, \dots, \tilde{\gamma}_{2d_r d_c}) - V(\gamma_m)\|_2 \rightarrow 0$$

as  $m \rightarrow \infty$ , by construction of  $N_m(\kappa)$  and continuity of  $\tilde{V}$ .

The first part of Condition 4 of Lv and Liu (2014) follows from Assumption 1, part (B). For the second part, let  $\bar{x}_i$  denote the  $i$ th row of  $\bar{X}$  for  $i = 1, \dots, 2rc$ . Then

$$\begin{aligned} \sum_{k=1}^m \sum_{i=1}^{2rc} \left( \bar{x}_i^\top \{mF_m\}^{-1} \bar{x}_i \right)^{3/2} &= m^{-3/2} \sum_{k=1}^m \sum_{i=1}^{2rc} \left( \bar{x}_i^\top F_m^{-1} \bar{x}_i \right)^{3/2} \\ &\leq m^{-3/2} \sum_{k=1}^m \sum_{i=1}^{2rc} (2\delta \bar{x}_i^\top \bar{x}_i)^{3/2} \\ &= m^{-1/2} \sum_{i=1}^{2rc} (2\delta \bar{x}_i^\top \bar{x}_i)^{3/2} \\ &\rightarrow 0 \end{aligned}$$

as  $m \rightarrow \infty$ . This completes the verification of the four conditions.

Thus, by Lv and Liu (2014), Theorem 7,

$$\sqrt{m} F_m^{-1/2} G_m(\gamma_m) (\hat{\gamma}_m - \gamma_m) \xrightarrow{d} \mathcal{N}(\mathbf{0}_{2d_r d_c}, I_{2d_r d_c}). \quad (27)$$

Next, we characterize the limiting behavior of  $\gamma_m$ . Note that the system of equations which  $\gamma_m$  solves can be rewritten as

$$\begin{aligned} \mathbf{0}_{d_l d_c} &= (V \otimes U)^\top \left\{ h \left( \tau + \frac{\Delta}{\sqrt{m}} \right) + h \left( \tau - \frac{\Delta}{\sqrt{m}} \right) - h \{ (V \otimes U)(\gamma_{m,1} + \gamma_{m,2}) \} - h \{ (V \otimes U)(\gamma_{m,1} - \gamma_{m,2}) \} \right\} \\ \mathbf{0}_{d_l d_c} &= (V \otimes U)^\top \left\{ h \left( \tau + \frac{\Delta}{\sqrt{m}} \right) - h \left( \tau - \frac{\Delta}{\sqrt{m}} \right) - h \{ (V \otimes U)(\gamma_{m,1} + \gamma_{m,2}) \} + h \{ (V \otimes U)(\gamma_{m,1} - \gamma_{m,2}) \} \right\}. \end{aligned}$$

Equivalently, we define

$$Q_m(x, y) = \begin{pmatrix} (V \otimes U)^\top \left\{ h\left(\tau + \frac{\Delta}{\sqrt{m}}\right) + h\left(\tau - \frac{\Delta}{\sqrt{m}}\right) - h\left\{(V \otimes U)\left(x + \frac{y}{\sqrt{m}}\right)\right\} - h\left\{(V \otimes U)\left(x - \frac{y}{\sqrt{m}}\right)\right\} \right\} \\ \sqrt{m}(V \otimes U)^\top \left\{ h\left(\tau + \frac{\Delta}{\sqrt{m}}\right) - h\left(\tau - \frac{\Delta}{\sqrt{m}}\right) - h\left\{(V \otimes U)\left(x + \frac{y}{\sqrt{m}}\right)\right\} + h\left\{(V \otimes U)\left(x - \frac{y}{\sqrt{m}}\right)\right\} \right\} \end{pmatrix}$$

so that  $\mathbf{0}_{2d_r d_c} = Q_m(\gamma_{m,1}, \sqrt{m}\gamma_{m,2})$ . Similarly recall the definition

$$Q(x, y) = 2 \begin{pmatrix} (V \otimes U)^\top \{h(\tau) - h((V \otimes U)x)\} \\ (V \otimes U)^\top \{\text{diag}\{h'(\tau)\}\Delta - \text{diag}\{h'((V \otimes U)x)\}(V \otimes U)y\} \end{pmatrix}$$

which also has a unique solution  $\mathbf{0}_{2d_r d_c} = Q(\tilde{\tau}, \tilde{\Delta})$ . Consider the compact set  $\mathbf{K} = \{(x, y) : \|(x, y)\|_2 \leq K_\gamma\}$ . We will first show that  $Q_m$  converges uniformly to  $Q$  on  $\mathbf{K}$ .

First, it is easy to see that

$$(V \otimes U)^\top \{h(\tau + \Delta/\sqrt{m}) + h(\tau - \Delta/\sqrt{m})\} \rightarrow 2(V \otimes U)^\top h(\tau),$$

free of  $(x, y)$ .

Next consider

$$(V \otimes U)^\top \{h((V \otimes U)(x + y/\sqrt{m})) + h((V \otimes U)(x - y/\sqrt{m}))\}.$$

By compactness of  $\mathbf{K}$ ,  $x \pm y/\sqrt{m}$  converges uniformly to  $x$ . Then note that the composition of a continuous function on compact domains preserves uniform continuity, so this term converges uniformly to

$$2(V \otimes U)^\top h((V \otimes U)x).$$

Thus convergence holds for the first  $d_r d_c$  coordinates.

For the remaining coordinates, consider a single element

$$\sqrt{m} \{h([(V \otimes U)(x - y/\sqrt{m})]_{ij}) - h([(V \otimes U)(x + y/\sqrt{m})]_{ij})\}.$$

By a linear expansion of both terms around  $h([(V \otimes U)x]_{ij})$ , we have that it equals

$$(h'(\xi_{ij}^{(m+)}) + h'(\xi_{ij}^{(m-)}))[(V \otimes U)y]_{ij}$$

for intermediate values  $\xi_{ij}^{(m\pm)}$ . By compactness of  $\mathbf{K}$ , these intermediate values both converge uniformly to  $[(V \otimes U)x]_{ij}$ . Combining over all the elements, we conclude that

$$\sqrt{m}(V \otimes U)^\top \{h((V \otimes U)(x - y/\sqrt{m})) - h((V \otimes U)(x + y/\sqrt{m}))\} \rightarrow 2\{\text{diag } h'((V \otimes U)x)\}(V \otimes U)y$$

uniformly over  $\mathbf{K}$ . Similarly,

$$\sqrt{m}(V \otimes U)^\top \{h(\tau - \Delta/\sqrt{m}) - h(\tau + \Delta/\sqrt{m})\} \rightarrow 2\{\text{diag } h'(\tau)\}\Delta,$$

free of  $(x, y)$ .

Then by uniform convergence, and the definition of  $\mathbf{K}$ , we conclude that the roots of  $Q_m$  also converge to the roots of  $Q$  (Keener, 2010, Theorem 9.4-3), that is

$$\gamma_{m,1} \rightarrow \tilde{\tau}, \quad \sqrt{m}\gamma_{m,2} \rightarrow \tilde{\Delta}$$

as  $m \rightarrow \infty$ . Note that  $\gamma_{m,2} \rightarrow \mathbf{0}$ .

Let  $S_{g,m}^F = \text{diag}(h'(\tau + (-1)^{g-1}\Delta/\sqrt{m}))$  and rewrite

$$F_m = \begin{pmatrix} (V \otimes U)^\top (S_{1,m}^F + S_{2,m}^F)(V \otimes U) & (V \otimes U)^\top (S_{1,m}^F - S_{2,m}^F)(V \otimes U) \\ (V \otimes U)^\top (S_{1,m}^F - S_{2,m}^F)(V \otimes U) & (V \otimes U)^\top (S_{1,m}^F + S_{2,m}^F)(V \otimes U) \end{pmatrix}.$$

Thus,

$$F_m \rightarrow \begin{pmatrix} \tilde{F} & 0 \\ 0 & \tilde{F} \end{pmatrix},$$

where  $\tilde{F} = 2(V \otimes U)^\top \text{diag}(h'(\tau))(V \otimes U)$ .

Similarly let  $S_{g,m}^G = \text{diag}(h'((V \otimes U)(\gamma_{m,1} + (-1)^{g-1}\gamma_{m,2})))$  and rewrite

$$G_m(\gamma_m) = \begin{pmatrix} (V \otimes U)^\top (S_{1,m}^G + S_{2,m}^G)(V \otimes U) & (V \otimes U)^\top (S_{1,m}^G - S_{2,m}^G)(V \otimes U) \\ (V \otimes U)^\top (S_{1,m}^G - S_{2,m}^G)(V \otimes U) & (V \otimes U)^\top (S_{1,m}^G + S_{2,m}^G)(V \otimes U) \end{pmatrix}.$$

Thus,

$$G_m(\gamma_m) \rightarrow \begin{pmatrix} \tilde{G} & 0 \\ 0 & \tilde{G} \end{pmatrix}$$

where  $\tilde{G} = 2(V \otimes U)^\top \text{diag}(h'((V \otimes U)\tilde{\tau}))(V \otimes U)$ .

By (27) and Slutsky's theorem, the last  $d_r d_c$  coordinates of  $\hat{\gamma}_m$  satisfy

$$\sqrt{m}\tilde{F}^{-1/2}\tilde{G}\hat{\gamma}_{m,2} \xrightarrow{d} \mathcal{N}(\tilde{F}^{-1/2}\tilde{G}\tilde{\Delta}, I_{d_r d_c}),$$

and by continuous mapping theorem,

$$m\hat{\gamma}_{m,2}^\top \tilde{G}\tilde{F}^{-1}\tilde{G}\hat{\gamma}_{m,2} \xrightarrow{d} \chi_{d_r d_c}^2(\tilde{\Delta}^\top \tilde{G}\tilde{F}^{-1}\tilde{G}\tilde{\Delta}).$$

To complete the proof, we will show that  $\hat{G}\hat{F}^{-1}\hat{G}$  is a consistent estimator of  $\tilde{G}\tilde{F}^{-1}\tilde{G}$ , in the sense that

$$\|\hat{G}\hat{F}^{-1}\hat{G} - \tilde{G}\tilde{F}^{-1}\tilde{G}\|_2 = o_{\mathbb{P}}(1).$$

First, by (27),  $\|\hat{\gamma}_1 - \tilde{\tau}\|_2 = o_{\mathbb{P}}(1)$ , thus by continuity,

$$\|\hat{G} - \tilde{G}\|_2 = o_{\mathbb{P}}(1). \quad (28)$$

Which implies that

$$\|\hat{G}\|_2 \leq \|\tilde{G}\|_2 + \|\hat{G} - \tilde{G}\|_2 = O_{\mathbb{P}}(1). \quad (29)$$

Define

$$\delta' = \min_{(i,j) \in \mathcal{S}} \{h'(\tau_{ij})\}.$$

Then

$$\frac{1}{2}\lambda_{\min}(\hat{F}) \geq \min_{(i,j) \in \mathcal{S}} \{h'([\tilde{\Theta}_{\mathcal{S}}]_{ij})\} \geq \delta' + o_{\mathbb{P}}(1)$$

since  $\tilde{\Theta}_{\mathcal{S}}$  is a consistent estimator of  $\tau$ . This implies that

$$\|\hat{F}^{-1}\|_2 \leq \frac{1}{\lambda_{\min}(\hat{F})} = O_{\mathbb{P}}(1), \quad (30)$$

and finally

$$\begin{aligned}\|\widehat{F}^{-1} - \tilde{F}^{-1}\|_2 &\leq \frac{\|\widehat{F} - \tilde{F}\|_2}{\lambda_{\min}(\widehat{F})\lambda_{\min}(\tilde{F})} \\ &\leq \frac{1}{2\delta'\lambda_{\min}(\widehat{F})} \left\| h' \left\{ \text{vec}(\tilde{\Theta}_S) \right\} - h' \left\{ \text{vec}(\tau) \right\} \right\|_\infty = o_{\mathbb{P}}(1)\end{aligned}\quad (31)$$

by the law of large numbers and Assumption 1, part (A). Combining (28)-(31), we conclude that

$$\|\widehat{G}\widehat{F}^{-1}\widehat{G} - \tilde{G}\tilde{F}^{-1}\tilde{G}\|_2 = o_{\mathbb{P}}(1),$$

which completes the proof of Proposition 3

To prove Corollary 1, it is sufficient to show that  $\Delta = \mathbf{0}_{rc}$  implies  $\tilde{\Delta} = \mathbf{0}_{d_r d_c}$ .

Under the mesoscale null  $\Delta = \mathbf{0}_{rc}$ , the second  $d_r d_c$  coordinates of  $Q_m$  reduce to

$$\mathbf{0}_{d_r d_c} = (V \otimes U)^\top \{h\{(V \otimes U)(\gamma_{m,1} - \gamma_{m,2})\} - h\{(V \otimes U)(\gamma_{m,1} + \gamma_{m,2})\}\}. \quad (32)$$

Equivalently, for fixed  $\gamma_{m,1}, \gamma_{m,2}$  minimizes the objective

$$H\{(V \otimes U)(\gamma_{m,1} - \gamma_{m,2})\} + H\{(V \otimes U)(\gamma_{m,1} + \gamma_{m,2})\}. \quad (33)$$

For arbitrary  $\gamma_{m,1}, \gamma_{m,2} = \mathbf{0}_{d_r d_c}$  solves (32), and (33) is strictly convex in  $\gamma_{m,2}$ . Thus,  $\gamma_{m,2} = \mathbf{0}_{d_r d_c}$ , and thus from the previous development  $\tilde{\Delta} = \lim_{m \rightarrow \infty} \sqrt{m}\gamma_{m,2} = \mathbf{0}$ , which completes the proof. Note that this also shows that under the mesoscale null, we have  $\gamma_m$  is constant in  $m$ , with  $\gamma_{1,m} \equiv \gamma_1$  and  $\gamma_{2,m} = \mathbf{0}$ . Thus Assumption 2 is trivially satisfied for constant  $K_\gamma = \|\gamma\|_2$ .

□

### B.3 Proofs of Propositions 4 and 5

*Proof of Proposition 4.* This proof follows from three claims and the definition of the doubly non-central  $F$  distribution. The first claim,

$$\frac{1}{m\sigma^2} \|W^\top Y \mathbf{1}_m\|_2^2 \sim \chi_{v_1}^2(\psi), \quad (34)$$

is established in the proof of Proposition 5. The second claim is that

$$\frac{1}{\sigma^2} \left\| Y - \frac{1}{m} Q Q^\top Y \mathbf{1}_m \mathbf{1}_m^\top \right\|_F^2 \sim \chi_{v_2'}^2(\zeta), \quad (35)$$

and the final claim is that (34) and (35) are independent. To establish the second claim, we rewrite

$$\begin{aligned}\frac{1}{\sigma} \text{vec} \left( Y - \frac{1}{m} Q Q^\top Y \mathbf{1}_m \mathbf{1}_m^\top \right) &= \frac{1}{\sigma} \text{vec}(Y) - \frac{1}{m\sigma} (\mathbf{1}_m \mathbf{1}_m^\top \otimes Q Q^\top) \text{vec}(Y) \\ &= \left( I_{2mrc} - \left\{ \left( \frac{1}{m} \mathbf{1}_m \mathbf{1}_m^\top \right) \otimes (Q Q^\top) \right\} \right) \left\{ \frac{1}{\sigma} \text{vec}(Y) \right\}\end{aligned}$$

Note that  $(I_{2mrc} - \{(m^{-1} \mathbf{1}_m \mathbf{1}_m^\top) \otimes (Q Q^\top)\})$  is an idempotent matrix with rank  $2(mrc - d_r d_c) = v_2'$ . Moreover,  $\text{vec}(Y)/\sigma$  is a Gaussian vector with mean

$$\frac{1}{\sigma} (\mathbf{1}_m \otimes \mu_S),$$

and covariance matrix  $I_{2mrc}$ . Thus

$$\frac{1}{\sigma^2} \left\| Y - \frac{1}{m} QQ^\top Y \mathbf{1}_m \mathbf{1}_m^\top \right\|_F^2 \sim \chi_{\nu'_2}^2 \left( \frac{1}{\sigma^2} \left\| \left( I_{2mrc} - \left\{ \left( \frac{1}{m} \mathbf{1}_m \mathbf{1}_m^\top \right) \otimes (QQ^\top) \right\} \right) (\mathbf{1}_m \otimes \mu_S) \right\|_2^2 \right).$$

We further simplify

$$\begin{aligned} & \frac{1}{\sigma^2} \left\| \left( I_{2mrc} - \left\{ \left( \frac{1}{m} \mathbf{1}_m \mathbf{1}_m^\top \right) \otimes (QQ^\top) \right\} \right) (\mathbf{1}_m \otimes \mu_S) \right\|_2^2 \\ &= \frac{1}{\sigma^2} \|(\mathbf{1}_m \otimes \mu_S) - (\mathbf{1}_m \otimes QQ^\top \mu_S)\|_2^2 \\ &= \frac{1}{\sigma^2} \|\{\mathbf{1}_m \otimes (I_{2rc} - QQ^\top) \mu_S\}\|_2^2 \\ &= \frac{1}{\sigma^2} \{\mathbf{1}_m \otimes (I_{2rc} - QQ^\top) \mu_S\}^\top \{\mathbf{1}_m \otimes (I_{2rc} - QQ^\top) \mu_S\} \\ &= \frac{m}{\sigma^2} \mu_S^\top (I_{2rc} - QQ^\top) \mu_S \\ &= \zeta, \end{aligned}$$

which completes the proof of the second claim. The final claim holds since  $W^\top Y \mathbf{1}_m$  and  $\text{vec}(Y - m^{-1} QQ^\top Y \mathbf{1}_m \mathbf{1}_m^\top)$  are Gaussian vectors, and satisfy

$$\begin{aligned} & \text{Cov} \left\{ W^\top Y \mathbf{1}_m, \text{vec} \left( Y - \frac{1}{m} QQ^\top Y \mathbf{1}_m \mathbf{1}_m^\top \right) \right\} \\ &= \text{Cov} \left\{ (\mathbf{1}_m \otimes W)^\top \text{vec}(Y), \left( I_{2mrc} - \left\{ \left( \frac{1}{m} \mathbf{1}_m \mathbf{1}_m^\top \right) \otimes (QQ^\top) \right\} \right) \text{vec}(Y) \right\} \\ &= (\mathbf{1}_m \otimes W)^\top (\sigma^2 I_{2mrc}) \left( I_{2mrc} - \left\{ \left( \frac{1}{m} \mathbf{1}_m \mathbf{1}_m^\top \right) \otimes (QQ^\top) \right\} \right) \\ &= \sigma^2 \left\{ (\mathbf{1}_m \otimes W)^\top - \frac{1}{m} (\mathbf{1}_m^\top \otimes W^\top) (\mathbf{1}_m \mathbf{1}_m^\top \otimes QQ^\top) \right\} \\ &= \sigma^2 \left\{ (\mathbf{1}_m \otimes W)^\top - \frac{1}{m} (\mathbf{1}_m \otimes QQ^\top W)^\top \right\} \\ &= \sigma^2 \{\mathbf{1}_m \otimes (I_{2rc} - QQ^\top) W\}^\top \\ &= \mathbf{0}_{\nu_1 \times 2mrc} \end{aligned}$$

since  $\text{col}(W) \subseteq \text{col}(Q)$ . □

*Proof of Proposition 5.* To prove this result, we will show three claims. First,

$$\frac{1}{m\sigma^2} \|W^\top Y \mathbf{1}_m\|_2^2 \sim \chi_{\nu_1}^2(\psi). \quad (36)$$

Second,

$$\frac{1}{\sigma^2} \|Q^\top Y (I_m - \frac{1}{m} \mathbf{1}_m \mathbf{1}_m^\top)\|_F^2 \sim \chi_{\nu_2}^2 \quad (37)$$

and finally, that (36) and (37) are independent. Then the result will follow by the definition of the non-central  $F$  distribution.

Denote

$$\mu_S = \text{vec} \begin{pmatrix} \Theta_S^{(1)} & \Theta_S^{(2)} \end{pmatrix}, \quad (38)$$

and note that by the Gaussian edge model assumption

$$\text{vec}(Y) \sim \mathcal{N}(\mathbf{1}_m \otimes \mu_{\mathcal{S}}, \sigma^2 I_{2rcm}).$$

To show the first claim, we consider the distribution of the Gaussian vector

$$\frac{1}{\sigma\sqrt{m}} W^\top Y \mathbf{1}_m = \frac{1}{\sigma\sqrt{m}} (\mathbf{1}_m \otimes W)^\top \text{vec}(Y),$$

which has mean

$$\begin{aligned} \frac{1}{\sigma\sqrt{m}} (\mathbf{1}_m \otimes W)^\top (\mathbf{1}_m \otimes \mu_{\mathcal{S}}) &= \frac{1}{\sigma\sqrt{m}} \{(\mathbf{1}_m^\top \mathbf{1}_m) \otimes (W^\top \mu_{\mathcal{S}})\} \\ &= \frac{\sqrt{m}}{\sigma} W^\top \mu_{\mathcal{S}}, \end{aligned}$$

and covariance matrix

$$\begin{aligned} \frac{1}{\sigma^2 m} (\mathbf{1}_m \otimes W)^\top (\sigma^2 I_{2mrc}) (\mathbf{1}_m \otimes W) &= \frac{1}{m} \{(\mathbf{1}_m^\top \mathbf{1}_m) \otimes (W^\top W)\} \\ &= I_{\nu_1}, \end{aligned}$$

where the final equality holds since  $W$  is orthonormal. Thus

$$\frac{1}{m\sigma^2} \|W^\top Y \mathbf{1}_m\|_2^2 \sim \chi_{\nu_1}^2 \left( \left\| \frac{\sqrt{m}}{\sigma} W^\top \mu_{\mathcal{S}} \right\|_2^2 \right).$$

We further simplify

$$\begin{aligned} \left\| \frac{\sqrt{m}}{\sigma} W^\top \mu_{\mathcal{S}} \right\|_2^2 &= \frac{m}{\sigma^2} \|W^\top \mu_{\mathcal{S}}\|_2^2 \\ &= \frac{m}{2\sigma^2} \left\| \begin{pmatrix} V \otimes U \\ -(V \otimes U) \end{pmatrix} \text{vec} \begin{pmatrix} \Theta_S^{(1)} & \Theta_S^{(2)} \end{pmatrix} \right\|_2^2 \\ &= \frac{m}{2\sigma^2} \|(V \otimes U) \text{vec}(\Theta_S^{(1)} - \Theta_S^{(2)})\|_2^2 \\ &= \frac{m}{2\sigma^2} \|U^\top (\Theta_S^{(1)} - \Theta_S^{(2)}) V\|_F^2 = \psi, \end{aligned}$$

which completes the first claim.

For the second claim, let

$$C_m = I_m - \frac{1}{m} \mathbf{1}_m \mathbf{1}_m^\top,$$

an  $m \times m$  idempotent matrix with rank  $m - 1$ . Rewrite

$$\begin{aligned} \frac{1}{\sigma} \text{vec}(Q^\top Y C_m) &= \frac{1}{\sigma} (C_m \otimes Q)^\top \text{vec}(Y) \\ &= (C_m \otimes I_{2d_r d_c}) \left\{ \frac{1}{\sigma} (I_m \otimes Q)^\top \text{vec}(Y) \right\}, \end{aligned}$$

Note that  $(C_m \otimes I_{2d_r d_c})$  is an idempotent matrix with rank  $2(m - 1)d_r d_c = \nu_2$ , and

$$\frac{1}{\sigma} (I_m \otimes Q)^\top \text{vec}(Y)$$

is a Gaussian vector with mean

$$\frac{1}{\sigma}(I_m \otimes Q)^\top (\mathbf{1}_m \otimes \mu_S) = \frac{1}{\sigma} (\mathbf{1}_m \otimes Q^\top \mu_S)$$

and covariance matrix

$$\begin{aligned} \frac{1}{\sigma^2 m} (I_m \otimes Q)^\top (\sigma^2 I_{2mrc}) (I_m \otimes Q) &= \{(C_m^\top C_m) \otimes (Q^\top Q)\} \\ &= I_m \otimes I_{2d_r d_c} \\ &= I_{2md_r d_c}. \end{aligned}$$

Moreover, the mean vector satisfies

$$\frac{1}{\sigma^2} (\mathbf{1}_m \otimes Q^\top \mu_S)^\top (C_m \otimes I_{2d_r d_c}) (\mathbf{1}_m \otimes Q^\top \mu_S) = 0$$

since  $\mathbf{1}_m^\top C_m \mathbf{1}_m = 0$ . Thus,

$$\begin{aligned} \frac{1}{\sigma^2} \|Q^\top Y C_m\|_F^2 &= \frac{1}{\sigma^2} \|\text{vec}(Q^\top Y C_m)\|_2^2 \\ &= \frac{1}{\sigma^2} \{(I_m \otimes Q)^\top \text{vec}(Y)\}^\top (C_m \otimes I_{2d_r d_c}) \{(I_m \otimes Q)^\top \text{vec}(Y)\} \sim \chi_{v_2}^2, \end{aligned}$$

completing the second claim. The final claim holds since  $W^\top Y \mathbf{1}_m$  and  $\text{vec}(Q^\top Y C_m)$  are Gaussian vectors, and satisfy

$$\begin{aligned} \text{Cov}\{W^\top Y \mathbf{1}_m, \text{vec}(Q^\top Y C_m)\} &= \text{Cov}\{(\mathbf{1}_m \otimes W)^\top \text{vec}(Y), (C_m \otimes Q)^\top \text{vec}(Y)\} \\ &= (\mathbf{1}_m \otimes W)^\top (\sigma^2 I_{2mrc}) (C_m \otimes Q) \\ &= \sigma^2 \{(\mathbf{1}_m^\top C_m) \otimes (W^\top Q)\} \\ &= \sigma^2 \{(\mathbf{0}_m^\top) \otimes (W^\top Q)\} \\ &= \mathbf{0}_{\nu_1 \times 2md_r d_c}. \end{aligned}$$

□

## B.4 Proof of Proposition 6

Before proving Proposition 6, we state and prove two lemmas. The first is a property of Kronecker products of orthonormal matrices, and the second is a property of the CDF of the non-central  $F$ -distribution.

**Lemma 2.** Suppose  $d_1 d_2 \leq n$ , and  $\hat{U}_1, U_1 \in \mathbb{R}^{n \times d_1}$  and  $\hat{U}_2, U_2 \in \mathbb{R}^{n \times d_2}$  are orthonormal matrices which satisfy

$$\|\hat{U}_1 - U_1 O_1\|_2 \leq \epsilon_1, \quad \|\hat{U}_2 - U_2 O_2\|_2 \leq \epsilon_2$$

for some orthonormal matrices  $O_1 \in \mathbb{R}^{d_1 \times d_1}$  and  $O_2 \in \mathbb{R}^{d_2 \times d_2}$ . Then  $\hat{U}_1 \otimes \hat{U}_2, U_1 \otimes U_2$ , and  $O_1 \otimes O_2$  are orthonormal matrices, and

$$\|(\hat{U}_1 \otimes \hat{U}_2) - (U_1 \otimes U_2)(O_1 \otimes O_2)\|_2 \leq \epsilon_1 + \epsilon_2.$$



*Proof of Lemma 2.* For orthonormal  $U \in \mathbb{R}^{n \times r}$  and  $V \in \mathbb{R}^{n \times s}$ , we have

$$(U \otimes V)^\top (U \otimes V) = (U^\top U) \otimes (V^\top V) = I_{rs},$$

Which shows that  $\hat{U}_1 \otimes \hat{U}_2$ ,  $U_1 \otimes U_2$ , and  $O_1 \otimes O_2$  are orthonormal matrices. Then,

$$\begin{aligned} & \|(\hat{U}_1 \otimes \hat{U}_2) - (U_1 \otimes U_2)(O_1 \otimes O_2)\|_2 \\ &= \|(\hat{U}_1 \otimes \hat{U}_2) - (U_1 O_1 \otimes U_2 O_2)\|_2 \\ &= \|(\hat{U}_1 \otimes \hat{U}_2) - (\hat{U}_1 \otimes U_2 O_2) + (\hat{U}_1 \otimes U_2 O_2) - (U_1 O_1 \otimes U_2 O_2)\|_2 \\ &\leq \|\hat{U}_1 \otimes (\hat{U}_2 - U_2 O_2)\|_2 + \|(\hat{U}_1 - U_1 O_1) \otimes U_2 O_2\|_2 \\ &= \|\hat{U}_1\|_2 \|\hat{U}_2 - U_2 O_2\|_2 + \|\hat{U}_1 - U_1 O_1\|_2 \|U_2 O_2\|_2 \\ &\leq \epsilon_1 + \epsilon_2. \end{aligned}$$

□

**Lemma 3.** For a fixed cutoff  $t > 0$ , and degrees of freedom parameters  $\nu_1$  and  $\nu_2$ , define the function

$$\Phi(z; t, \nu_1, \nu_2) = \mathbb{P}(F_{\nu_1, \nu_2}(z) \leq t),$$

the CDF of a non-central  $F$  distribution with non-centrality parameter  $z$ . Then for constants  $0 < c_1 < c_2 < \infty$ ,  $\Phi(z; t, \nu_1, \nu_2)$  is differentiable with respect to  $z$  for  $z \in [c_1, c_2]$ , and

$$|\Phi'(z; t, \nu_1, \nu_2)| \leq \frac{1}{2} \Phi(z; t, \nu_1, \nu_2).$$

*Proof of Lemma 3.* The function  $\Phi$  is defined in terms of an infinite series,

$$\Phi(z; t, \nu_1, \nu_2) = \sum_{j=0}^{\infty} \exp(-z/2) \frac{(z/2)^j}{j!} \mathcal{I}\left(\frac{\nu_1 t}{\nu_2 + \nu_1 t}; \frac{\nu_1}{2} + j, \frac{\nu_2}{2}\right),$$

where  $\mathcal{I}(x; a, b)$  is the regularized incomplete beta function Tiku (1967). Note that  $\exp(z/2)\Phi(z)$  is a power series, which converges for any  $z$ . Thus it is uniformly convergent for  $z \in [c_1, c_2]$ , and we can interchange differentiation and summation:

$$\Phi'(z; t, \nu_1, \nu_2) = \sum_{j=0}^{\infty} \frac{\partial}{\partial z} \left\{ \exp(-z/2) \frac{(z/2)^j}{j!} \mathcal{I}\left(\frac{\nu_1 t}{\nu_2 + \nu_1 t}; \frac{\nu_1}{2} + j, \frac{\nu_2}{2}\right) \right\}.$$

Each term on the inside is a product and so the derivative splits into two terms. The first terms form the convergent series

$$\sum_{j=0}^{\infty} (-1/2) \left\{ \exp(-z/2) \frac{(z/2)^j}{j!} \mathcal{I}\left(\frac{\nu_1 t}{\nu_2 + \nu_1 t}; \frac{\nu_1}{2} + j, \frac{\nu_2}{2}\right) \right\} = -\frac{1}{2} \Phi(z; t, \nu_1, \nu_2).$$

Then the second terms form another convergent series

$$\sum_{j=1}^{\infty} (1/2) \left\{ \exp(-z/2) \frac{(z/2)^{j-1}}{(j-1)!} \mathcal{I}\left(\frac{\nu_1 t}{\nu_2 + \nu_1 t}; \frac{\nu_1}{2} + j, \frac{\nu_2}{2}\right) \right\}.$$

Define  $\omega_1 = \nu_1 + 2$  and  $s = \nu_1 t / (\nu_1 + 2)$ , and  $i = j - 1$ . This series can be rewritten as

$$\frac{1}{2} \sum_{i=0}^{\infty} \left\{ \exp(-z/2) \frac{(z/2)^i}{i!} \mathcal{I}\left(\frac{\omega_1 s}{\nu_2 + \omega_1 s}; \frac{\omega_1}{2} + i, \frac{\nu_2}{2}\right) \right\},$$

which is a non-central  $F$  CDF evaluated at a smaller cutoff  $s$ , and with larger numerator degrees of freedom parameter  $\omega_1$ . Note that these changes in cutoff and degrees of freedom imply  $\Phi(z; s, \omega_1, \nu_2) < \Phi(z; t, \nu_1, \nu_2)$ . This is consistent with the stochastic monotonicity of the non-central  $F$  distribution in its non-centrality parameter.

Adding these two convergent series, we have

$$\Phi'(z; t, \nu_1, \nu_2) = \frac{1}{2} \{ \Phi(z; s, \omega_1, \nu_2) - \Phi(z; t, \nu_1, \nu_2) \} < 0.$$

Then since  $\Phi(z; s, \omega_1, \nu_2) < \Phi(z; t, \nu_1, \nu_2)$ , we conclude that

$$|\Phi'(z; t, \nu_1, \nu_2)| \leq \frac{1}{2} \Phi(z; t, \nu_1, \nu_2),$$

as desired.  $\square$

*Proof of Proposition 6.* To begin, we bound the learned projection test's type II error rates compared to the oracle test, for fixed left and right projections  $\hat{U}$  and  $\hat{V}$  which satisfy (15).

Denote the type II error rate for this test by  $\beta_{\text{learn}}^{\hat{U}, \hat{V}}$ . By the independence of the test statistics and the learned projections, it only depends on  $\hat{U}$  and  $\hat{V}$  through the non-centrality parameter of the test statistic. Using notation from Lemma 3,

$$\beta_{\text{learn}}^{\hat{U}, \hat{V}} = \Phi(\psi_{\text{learn}}^{\hat{U}, \hat{V}}; t^*, \nu_1, \nu_2),$$

where  $\nu_1$  and  $\nu_2$  are defined as in Proposition 5,  $t^*$  is the level  $\alpha$  threshold, and

$$\psi_{\text{learn}}^{\hat{U}, \hat{V}} = \frac{m}{2\sigma^2} \|\hat{U}^\top (\Theta_S^{(1)} - \Theta_S^{(2)}) \hat{V}\|_F^2.$$

Similarly,

$$\beta_{\text{orc}} = \Phi(\psi_{\text{orc}}; t^*, \nu_1, \nu_2),$$

where by construction,  $\psi_{\text{orc}} \geq \psi_{\text{learn}}^{\hat{U}, \hat{V}}$ , and therefore  $\beta_{\text{orc}} \leq \beta_{\text{learn}}^{\hat{U}, \hat{V}}$ .

To prove an upper bound, we first bound the difference in non-centrality parameters. Let  $O^*$  denote the orthogonal transformation matrix which aligns  $(\hat{V} \otimes \hat{U})$  and  $(V \otimes U)$ . Then

$$\begin{aligned} \psi_{\text{learn}}^{\hat{U}, \hat{V}} &= \frac{m}{2\sigma^2} \|(\hat{V} \otimes \hat{U})^\top \text{vec}(\Theta_S^{(1)} - \Theta_S^{(2)})\|_2^2 \\ &= \frac{m}{2\sigma^2} \left\| \left\{ (\hat{V} \otimes \hat{U}) - (V \otimes U)O^* + (V \otimes U)O^* \right\}^\top \text{vec}(\Theta_S^{(1)} - \Theta_S^{(2)}) \right\|_2^2 \\ &\geq \frac{m}{2\sigma^2} \left\{ \|(V \otimes U)^\top \text{vec}(\Theta_S^{(1)} - \Theta_S^{(2)})\|_2 - \|(\hat{V} \otimes \hat{U}) - (V \otimes U)O^*\|_2 \|\text{vec}(\Theta_S^{(1)} - \Theta_S^{(2)})\|_2 \right\}^2 \\ &\geq \frac{m}{2\sigma^2} \left\{ \left( \frac{2\sigma^2 \psi_{\text{orc}}}{m} \right)^{1/2} - \epsilon \left( \frac{2\sigma^2 \psi_{\text{max}}}{m} \right)^{1/2} \right\}^2 \\ &= \psi_{\text{orc}} \left( 1 - \epsilon \sqrt{\frac{\psi_{\text{orc}}}{\psi_{\text{max}}}} \right)^2, \end{aligned}$$

where the second inequality uses Lemma 2, and the fact that  $\epsilon < \sqrt{\psi_{\text{orc}}/\psi_{\text{max}}}$ . It then

follows that

$$\begin{aligned}
\psi_{\text{orc}} - \psi_{\text{learn}}^{\hat{U}, \hat{V}} &\leq \psi_{\text{orc}} \left\{ 1 - \left( 1 - \epsilon \sqrt{\frac{\psi_{\text{orc}}}{\psi_{\text{max}}}} \right)^2 \right\} \\
&\leq 2\psi_{\text{orc}} \left( \epsilon \sqrt{\frac{\psi_{\text{orc}}}{\psi_{\text{max}}}} \right) \\
&= 2\epsilon \sqrt{\psi_{\text{orc}} \psi_{\text{max}}}.
\end{aligned} \tag{39}$$

We now proceed to upper bound the type II error rate. By the mean value theorem, there exists  $\tilde{\psi} \in (\psi_{\text{learn}}^{\hat{U}, \hat{V}}, \psi_{\text{orc}})$  such that

$$\beta_{\text{orc}} - \beta_{\text{learn}}^{\hat{U}, \hat{V}} = \Phi'(\tilde{\psi}; t^*, \nu_1, \nu_2) (\psi_{\text{orc}} - \psi_{\text{learn}}^{\hat{U}, \hat{V}}).$$

Thus,

$$\begin{aligned}
\beta_{\text{learn}}^{\hat{U}, \hat{V}} &\leq \beta_{\text{orc}} + \left| \Phi'(\tilde{\psi}; t^*, \nu_1, \nu_2) \right| (\psi_{\text{orc}} - \psi_{\text{learn}}^{\hat{U}, \hat{V}}) \\
&\leq \beta_{\text{orc}} + \frac{1}{2} \Phi(\tilde{\psi}; t^*, \nu_1, \nu_2) (\psi_{\text{orc}} - \psi_{\text{learn}}^{\hat{U}, \hat{V}}) \\
&\leq \beta_{\text{orc}} + \frac{1}{2} \beta_{\text{learn}}^{\hat{U}, \hat{V}} (\psi_{\text{orc}} - \psi_{\text{learn}}^{\hat{U}, \hat{V}}),
\end{aligned} \tag{40}$$

where the second inequality uses Lemma 3, and the third uses stochastic monotonicity.

Combining (39) and (40), we have

$$\beta_{\text{learn}}^{\hat{U}, \hat{V}} \leq \beta_{\text{orc}} + \beta_{\text{learn}}^{\hat{U}, \hat{V}} \epsilon \sqrt{\psi_{\text{orc}} \psi_{\text{max}}},$$

which implies

$$\beta_{\text{learn}}^{\hat{U}, \hat{V}} \leq \left( \frac{1}{1 - \epsilon \sqrt{\psi_{\text{orc}} \psi_{\text{max}}}} \right) \beta_{\text{orc}} \tag{41}$$

since  $\epsilon < 1/\sqrt{\psi_{\text{orc}} \psi_{\text{max}}}$ .

To complete the proof, we integrate over learned projections, noting that

$$\beta_{\text{learn}} = \int \beta_{\text{learn}}^{\tilde{U}, \tilde{V}} d\mathbb{P}(\tilde{U}, \tilde{V}).$$

Let  $\mathcal{G}$  denote the event (15). By assumption  $\mathbb{P}(\mathcal{G}) \geq 1 - \xi$ , independently of the test statistics. The lower bound holds directly from the pointwise lower bounds:

$$\beta_{\text{orc}} = \int \beta_{\text{orc}} d\mathbb{P}(\tilde{U}, \tilde{V}) \leq \int \beta_{\text{learn}}^{\tilde{U}, \tilde{V}} d\mathbb{P}(\tilde{U}, \tilde{V}) = \beta_{\text{learn}}.$$

For the upper bound, we have

$$\beta_{\text{learn}} = \int_{\mathcal{G}} \beta_{\text{learn}}^{\tilde{U}, \tilde{V}} d\mathbb{P}(\tilde{U}, \tilde{V}) + \int_{\mathcal{G}^c} \beta_{\text{learn}}^{\tilde{U}, \tilde{V}} d\mathbb{P}(\tilde{U}, \tilde{V}).$$

By (41), the first term is bounded above by

$$\left( \frac{1}{1 - \epsilon \sqrt{\psi_{\text{orc}} \psi_{\text{max}}}} \right) \beta_{\text{orc}};$$

by construction of  $\mathcal{G}$ , and since  $\beta_{\text{learn}}^{\tilde{U}, \tilde{V}} \leq 1$  uniformly, the second term is bounded above by  $\xi$ , which completes the proof.  $\square$

## B.5 Proof of Proposition 7

We will begin by proving Lemma 1, followed by the proof of Proposition 7. For the proof of Lemma 1, we state a special form of Bandeira and van Handel (2016), Corollary 3.11 which will be applied to bound the operator norm error of each block  $\mathcal{C}$ ,  $\mathcal{R}$ ,  $\mathcal{D}$ , for  $g = 1, 2$ .

**Lemma 4** (Bandeira and van Handel (2016), Corollary 3.11). Suppose  $Z$  is a  $p \times q$  matrix with iid  $\mathcal{N}(0, \sigma^2)$  entries. Then, with probability at least

$$1 - \exp \left\{ -\frac{\sigma^2}{8} (\sqrt{p} + \sqrt{q})^2 \right\}$$

we have

$$\|Z\|_2 \leq \{2 + \delta(p, q)\} \sigma (\sqrt{p} + \sqrt{q}),$$

where  $\delta(p, q)$  is defined as in Lemma 1.

*Proof of Lemma 1.* To begin, we will apply Lemma 4 to bound the operator norm error of each block  $\mathcal{C}$ ,  $\mathcal{R}$ ,  $\mathcal{D}$ , for  $g = 1, 2$ .

By (17), for block  $\mathcal{C}$ , and  $g \in \{1, 2\}$ , we have that

$$\widehat{\Theta}_{\mathcal{C}}^{(g)} - \Theta_{\mathcal{C}}^{(g)}$$

is an  $r \times (n - c)$  matrix, and has iid Gaussian entries with variance  $\sigma^2/m$ . Thus, by Lemma 4, union bound, and triangle inequality,

$$\|(\widehat{\Theta}_{\mathcal{C}}^{(1)} - \widehat{\Theta}_{\mathcal{C}}^{(2)}) - (\Theta_{\mathcal{C}}^{(1)} - \Theta_{\mathcal{C}}^{(2)})\|_2 \leq \epsilon_{\mathcal{C}} \quad (42)$$

with probability at least

$$1 - 2 \exp \left\{ -\frac{\sigma^2}{8m} (\sqrt{r} + \sqrt{n - c})^2 \right\}.$$

Similarly, for block  $\mathcal{R}$ ,

$$\|(\widehat{\Theta}_{\mathcal{R}}^{(1)} - \widehat{\Theta}_{\mathcal{R}}^{(2)}) - (\Theta_{\mathcal{R}}^{(1)} - \Theta_{\mathcal{R}}^{(2)})\|_2 \leq \epsilon_{\mathcal{R}} \quad (43)$$

with probability at least

$$1 - 2 \exp \left\{ -\frac{\sigma^2}{8m} (\sqrt{n - r} + \sqrt{c})^2 \right\}.$$

For block  $\mathcal{D}$ , first suppose  $\widehat{M}$  and  $M$  are matrices, and  $M$  has rank  $R$ . Then

$$\|[\widehat{M}]_{(R)} - M\|_2 \leq \|[\widehat{M}]_{(R)} - \widehat{M}\|_2 + \|\widehat{M} - M\|_2 \leq 2\|\widehat{M} - M\|_2,$$

where the second inequality follows from Eckhart-Young theorem. Thus, by a similar argument using Lemma 4, union bound, and triangle inequality,

$$\left\| \left[ \widehat{\Theta}_{\mathcal{D}}^{(1)} - \widehat{\Theta}_{\mathcal{D}}^{(2)} \right]_{(d_*)} - (\Theta_{\mathcal{D}}^{(1)} - \Theta_{\mathcal{D}}^{(2)}) \right\|_2 \leq \epsilon_{\mathcal{D}} \quad (44)$$

with probability at least

$$1 - 2 \exp \left\{ -\frac{\sigma^2}{8m} (\sqrt{n - r} + \sqrt{n - c})^2 \right\}.$$

A final union bound over the three blocks  $\mathcal{C}$ ,  $\mathcal{R}$ , and  $\mathcal{D}$  completes the proof.  $\square$

*Proof of Proposition 7.* Suppose the event in Lemma 1 holds. We will begin by proving a perturbation upper bound

$$\|\hat{\mathbb{T}} - \mathbb{T}\|_2 \leq \epsilon_{\mathbb{T}}. \quad (45)$$

Note that both  $\mathbb{T}$  and  $\hat{\mathbb{T}}$  are given by the product of three matrices.

In general, suppose we have matrices  $A, B$  and  $C$  such that the product  $ABC$  is well-defined, and perturbed versions of those matrices  $\hat{A}, \hat{B}$  and  $\hat{C}$  such that

$$\|\hat{A} - A\|_2 \leq \epsilon_A, \quad \|\hat{B} - B\|_2 \leq \epsilon_B, \quad \|\hat{C} - C\|_2 \leq \epsilon_C.$$

Also suppose that

$$\|A\|_2 \leq \lambda_A, \quad \|B\|_2 \leq \lambda_B, \quad \|C\|_2 \leq \lambda_C,$$

Then

$$\begin{aligned} \|\hat{A}\hat{B}\hat{C} - ABC\|_2 &\leq \epsilon_A \lambda_B \epsilon_C + \epsilon_A \epsilon_B \epsilon_C + \epsilon_A \lambda_B \lambda_C + \lambda_A \lambda_B \epsilon_C \\ &\quad + \epsilon_A \epsilon_B \lambda_C + \lambda_A \epsilon_B \epsilon_C + \lambda_A \epsilon_B \lambda_C \end{aligned} \quad (46)$$

Thus we can establish a the upper bound with bounds on the largest singular value of each factor of  $\mathbb{T}$ , as well as operator norm perturbations for each factor.

For the first factor of  $\mathbb{T}$ ,  $\Theta_{\mathcal{C}}^{(1)} - \Theta_{\mathcal{C}}^{(2)}$ , the operator norm perturbation is bounded above by  $\epsilon_{\mathcal{C}}$  by Lemma 1, and

$$\|\Theta_{\mathcal{C}}^{(1)} - \Theta_{\mathcal{C}}^{(2)}\|_2 \leq \|U_{[r]} S V_{[-c]}^T\|_2 \leq s_{\max} \sqrt{\rho_U (1 - \kappa_V)}$$

by assumption. Similarly, for the third factor we have operator norm perturbation bounded above by  $\epsilon_{\mathcal{R}}$ , and

$$\|\Theta_{\mathcal{R}}^{(1)} - \Theta_{\mathcal{R}}^{(2)}\|_2 \leq s_{\max} \sqrt{(1 - \kappa_U) \rho_V}.$$

For the second factor, we need to take additional steps due to the pseudo-inverse. Let  $\sigma_{\min}(M)$  denote the smallest non-zero singular value of a rank  $R$  matrix  $M$ , and suppose  $\hat{M}$  is a perturbed version of  $M$  which also has rank  $R$ . Then by Wedin (1973), if  $\sigma_{\min}(M) \geq \|\hat{M} - M\|_2$ ,

$$\|\hat{M}^\dagger - M^\dagger\|_2 \leq \left( \frac{1 + \sqrt{5}}{2} \right) \frac{\|\hat{M} - M\|_2}{\sigma_{\min}(M) \{ \sigma_{\min}(M) - \|\hat{M} - M\|_2 \}}.$$

By Lemma 1, we have

$$\left\| \left[ \hat{\Theta}_{\mathcal{D}}^{(1)} - \hat{\Theta}_{\mathcal{D}}^{(2)} \right]_{(d_*)} - (\Theta_{\mathcal{D}}^{(1)} - \Theta_{\mathcal{D}}^{(2)}) \right\|_2 \leq \epsilon_{\mathcal{D}},$$

and by assumption we have

$$\sigma_{\min}(\Theta_{\mathcal{D}}^{(1)} - \Theta_{\mathcal{D}}^{(2)}) \geq s_{\min} \sqrt{(1 - \rho_U)(1 - \rho_V)} \geq 2\epsilon_{\mathcal{D}}.$$

Thus,

$$\begin{aligned} &\left\| \left( \left[ \hat{\Theta}_{\mathcal{D}}^{(1)} - \hat{\Theta}_{\mathcal{D}}^{(2)} \right]_{(d_*)} \right)^\dagger - (\Theta_{\mathcal{D}}^{(1)} - \Theta_{\mathcal{D}}^{(2)})^\dagger \right\|_2 \\ &\leq \frac{(1 + \sqrt{5})\epsilon_{\mathcal{D}}}{2s_{\min} \sqrt{(1 - \rho_U)(1 - \rho_V)} \{ s_{\min} \sqrt{(1 - \rho_U)(1 - \rho_V)} - \epsilon_{\mathcal{D}} \}} \\ &\leq \frac{(1 + \sqrt{5})\epsilon_{\mathcal{D}}}{s_{\min}^2 (1 - \rho_U)(1 - \rho_V)} \end{aligned}$$

is an operator norm perturbation bound for the second factor. Finally, we have

$$\begin{aligned} \left\| \left( \Theta_{\mathcal{D}}^{(1)} - \Theta_{\mathcal{D}}^{(2)} \right)^\dagger \right\|_2 &= \frac{1}{\sigma_{\min}(\Theta_{\mathcal{D}}^{(1)} - \Theta_{\mathcal{D}}^{(2)})} \\ &\leq \frac{1}{s_{\min} \sqrt{(1 - \rho_U)(1 - \rho_V)}}. \end{aligned}$$

We can then establish (45) by plugging these six upper bounds into the general result (46), where the order of the terms  $\epsilon_{\mathbb{T}}^{(1)}, \dots, \epsilon_{\mathbb{T}}^{(7)}$  corresponds to the order in which they appear in (46).

The final result of Proposition 7 follows from a perturbation bound on the singular subspaces of  $\hat{\mathbb{T}}$ . From Qi et al. (2022), Theorem 3.1, we have

$$\min_{O \in \mathcal{O}_{d*}} \|\hat{U} - UO\|_2 + \min_{O \in \mathcal{O}_{d*}} \|\hat{V} - VO\|_2 \leq \frac{4\sqrt{2}\|\hat{\mathbb{T}} - \mathbb{T}\|_2}{\sigma_{\min}(\mathbb{T})}.$$

The proof is complete by plugging in (45), and lower bounding  $\sigma_{\min}(\mathbb{T})$ :

$$\begin{aligned} \sigma_{\min}(\mathbb{T}) &= \sigma_{\min} \left\{ S(V_{[-c]}^\top V_{[-c]})S^{-1}(U_{[-r]}^\top U_{[-r]})S \right\} \\ &\geq \frac{s_{\min}^2(1 - \rho_U)(1 - \rho_V)}{s_{\max}}. \end{aligned}$$

□

## C An application to neuroimaging data

In this section, we apply our projection tests to mesoscale network testing for neuroimaging data (Huang et al., 2022). The data was originally collected and preprocessed by Badea et al. (2017), and consists of functional magnetic resonance imaging (fMRI) brain images for 40 subjects: 20 healthy controls and 20 with Parkinson’s disease. The full sample contains 17 female and 23 male subjects, with mean age around 65 years. Each weighted, undirected edge corresponds to a correlation between activation patterns of two brain regions, mapped to a standard automatic anatomical labeling of 116 regions (AAL116) (Tzourio-Mazoyer et al., 2002). The R package **brainGraph** contains information about the physical location of each of these AAL116 regions, and categorizes the regions by lobe, which we use to formulate mesoscale null hypotheses. In particular, classical research on Parkinson’s disease has identified cognitive impairment in tasks related to the frontal lobe (FL) (Taylor et al., 1986), as well as dysfunction in the cerebellum (CBM) (Wu and Hallett, 2013). Thus, we will test three mesoscale hypotheses: changes in the mean functional connectivity within these two lobes of interest (“FL/FL”, “CBM/CBM”), as well as between them (“FL/CBM”). Of the 116 regions, 28 are part of the frontal lobe, and 26 are part of the cerebellum. We denote these hypothesis sets, as well as the held out node pairs by

$$\left( \begin{array}{cc|c} \text{FL/FL} & \text{FL/CB} & \mathcal{R} \\ \text{FL/CB}^\top & \text{CB/CB} & \\ \hline & & \mathcal{D} \\ \hline \mathcal{R}^\top & & \end{array} \right). \quad (47)$$

Test	$p$ -value			Rej. rate ( $\alpha = 0.05$ )		
	FL/FL	CBM/CBM	FL/CBM	FL/FL	CBM/CBM	FL/CBM
Basic	0.416	<b><math>5.4 \times 10^{-3}</math></b>	<b><math>1.2 \times 10^{-4}</math></b>	0	1	1
Proj ( $d = 2$ )	0.074	<b>0.021</b>	<b><math>8.3 \times 10^{-4}</math></b>	0	1	1
Proj ( $d = 4$ )	<b>0.038</b>	<b>0.022</b>	<b><math>3.1 \times 10^{-3}</math></b>	1	1	1
Proj ( $d = 6$ )	0.053	<b><math>3.4 \times 10^{-3}</math></b>	<b><math>1.2 \times 10^{-4}</math></b>	0	1	1
Proj ( $d = 8$ )	0.081	<b><math>4.4 \times 10^{-3}</math></b>	<b><math>1.7 \times 10^{-4}</math></b>	0	1	1
Proj ( $d = 10$ )	0.087	<b>0.012</b>	<b><math>9.6 \times 10^{-5}</math></b>	0	1	1
RandProj ( $d = 2$ )	0.540	0.488	0.436	0.05	0.08	0.11
RandProj ( $d = 4$ )	0.380	0.347	0.263	0.13	0.18	0.17
RandProj ( $d = 6$ )	0.376	0.223	0.226	0.13	0.21	0.22
RandProj ( $d = 8$ )	0.441	0.196	0.185	0.09	0.24	0.34
RandProj ( $d = 10$ )	0.534	0.161	0.087	0.13	0.33	0.40
BlockProj	0.063	0.297	0.228	0	0	0

Table 3:  $p$ -values for fMRI data mesoscale testing. For uniform random projections, the median adjusted  $p$ -value and rejection rate over 100 replications is reported.  $p$ -values below 0.05 are bolded.

We apply our projection testing approach with learned projections for Gaussian edge networks (“Proj”), as well as the basic  $F$ -test (“Basic”), a projection test using uniform random orthonormal matrices from the Stiefel manifold (“RandProj”), and a projection test which compares the edge mean over the matrix block corresponding to each mesoscale test (“BlockProj”). To learn projections of a given dimension  $d = d_r = d_c$ , we will use submatrices of the eigenvectors of

$$(\hat{\Theta}_{\mathcal{R}}^{(1)} - \hat{\Theta}_{\mathcal{R}}^{(2)}) \left( \left[ \hat{\Theta}_{\mathcal{D}}^{(1)} - \hat{\Theta}_{\mathcal{D}}^{(2)} \right]_{(d)} \right)^{-1} (\hat{\Theta}_{\mathcal{R}}^{(1)} - \hat{\Theta}_{\mathcal{R}}^{(2)})^\top$$

where the subscripts correspond to the blocks in (47), estimated by their sample means. Visual inspection of a scree plot of the singular values of

$$\begin{pmatrix} \hat{\Theta}_{\mathcal{R}}^{(1)} - \hat{\Theta}_{\mathcal{R}}^{(2)} \\ \hat{\Theta}_{\mathcal{D}}^{(1)} - \hat{\Theta}_{\mathcal{D}}^{(2)} \end{pmatrix}$$

leads us to select  $d = 6$  as the dimension of our learned projections. However, for both the learned and uniform random projections, we will also evaluate sensitivity to the projection dimension, varying  $d$  from 2 to 10 in increments of 2. This sensitivity analysis is purely for illustrative purposes—in practice selection of  $d$ , like the choice of projections, must be independent of the edges in the hypothesis set to preserve test validity. The results for each hypothesis test are reported in Table 3. For the uniform random projections, we report the median adjusted  $p$ -value and rejection rate over 100 replications. Table 3 shows that the basic  $F$ -test does not find the connections within the frontal lobe to be significantly different, while the differences in the other two rectangles are found to be significant. The mesoscale projection-based tests generally agree with these rejection decisions. For the FL/FL hypothesis set, the noise reduction from projection leads to  $p$ -values closer to the critical threshold, and for  $d = 4$  the hypothesis is rejected at the  $\alpha = 0.05$  level. The  $p$ -values based on learned projections are much smaller than the corresponding uniform random projections, showing that the learned projections are indeed identifying useful structure at different values of  $d$ . The naive block projection gives a comparable  $p$ -value to the learned projection tests for the FL/FL hypothesis set, but for the other two hypotheses much of the

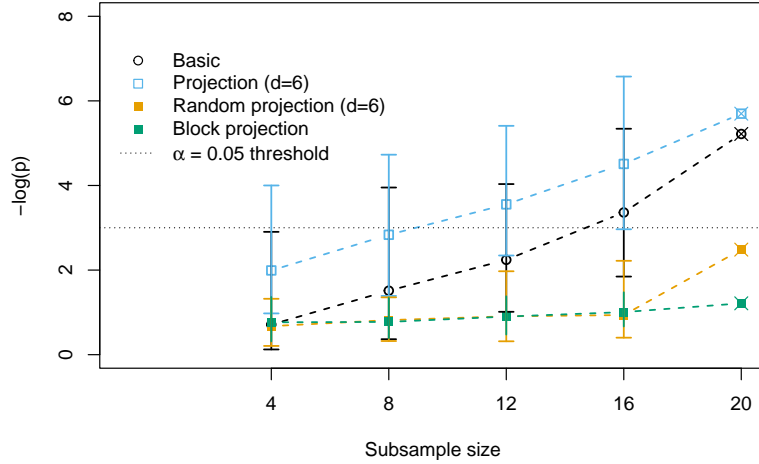


Figure 6: Median  $-\log(p)$  for testing the CBM/CBM hypothesis in fMRI data. varying subsample sizes  $\underline{m}$ . For  $\underline{m} < 20$ , vertical bars span from the 25th to 75th empirical quantiles over 200 replications.

signal appears to be lost in this crude summarization. The rejection of these hypotheses agrees with the existing research that these lobes show damage or dysfunction in subjects with Parkinson’s disease (Taylor et al., 1986; Wu and Hallett, 2013).

We additionally demonstrate the sensitivity of these testing approaches to the number of networks in each sample. For  $\underline{m} = 4, 8, 12, 16$ , we form subsamples by selecting  $\underline{m}$  networks without replacement from each of the two populations. We then test the mesoscale null hypothesis for the CBM/CBM hypothesis set, which was rejected by both the basic and projection tests on the full data. Both the learned and uniform random projection tests use dimension  $d = 6$ . This process was repeated 200 times, and the results are summarized in Figure 6.

We see from Figure 6 that all approaches improve as  $\underline{m}$  increases. For all values of  $\underline{m}$ , the learned projection test leads to a smaller  $p$ -value on average than the competing methods, showing that even with very few networks it is able to find a good projection that summarizes the overall network structure, and reduces the dimension of the test without removing much signal.

For these case-control tests, we would expect to reject the mesoscale hypotheses, and these results show that our projection tests can provide additional evidence against the null. We also apply our tests to compare the edge expectations of the FL/FL hypothesis set between the male and female subgroups of controls. These two samples are made up of 12 male controls and 8 female controls. The basic test ( $p = 0.99$ ) shows little to no difference between these two groups. This is in agreement with the corresponding projection tests, which return  $p > 0.17$  uniformly over all choices of  $d$  from 1 to 28.



## D ADMM algorithm for position-based testing

For the competing position model bootstrap test described in Section 4, we fit  $d$ -dimensional inner product latent position models to each sample of networks, under the mesoscale null hypothesis. Under the Gaussian edge network model the constrained maximum likelihood estimator solves the optimization problem

$$\min_{\Theta^{(1)}, \Theta^{(2)}} \left\{ \|\bar{A}^{(1)} - \Theta^{(1)}\|_F^2 + \|\bar{A}^{(2)} - \Theta^{(2)}\|_F^2 \right\} \quad (48)$$

subject to

$$\text{rank}(\Theta^{(g)}) \leq d, \quad \Theta_S^{(1)} = \Theta_S^{(2)};$$

where

$$\bar{A}^{(g)} = \frac{1}{m} \sum_{k=1}^m A_k^{(g)}$$

for  $g = 1, 2$ .

To solve (48), we derive the following alternating direction method of multipliers (ADMM) steps with step size parameter  $\rho > 0$ . For step  $k \geq 0$ , the iterates  $u_k, z_k, w_k$  are each  $2n^2$ -dimensional vectors, corresponding to the entries of the  $n \times n$  expected adjacency matrices for the two samples.

We set starting values

$$u_0 = \mathbf{0}, \quad [z_0^{(g)}]_S = \frac{1}{2}[\bar{A}^{(1)}]_S + \bar{A}_S^{(2)}, \quad [z_0^{(g)}]_{S^c} = [\bar{A}^{(g)}]_{S^c}.$$

Then the iterations proceed as follows.

1. Update  $w_{k+1}$

$$[w_{k+1}^{(g)}]_S = \frac{2}{4 + 2\rho}([\bar{A}^{(1)}]_S + [\bar{A}^{(2)}]_S) + \frac{\rho}{4 + 2\rho}([z_k^{(1)}]_S + [z_k^{(2)}]_S - [u_k^{(1)}]_S - [u_k^{(2)}]_S)$$

$$[w_{k+1}^{(g)}]_{S^c} = \frac{2}{2 + \rho}[\bar{A}^{(g)}]_{S^c} + \frac{\rho}{2 + \rho}([z_k^{(g)}]_{S^c} - [u_k^{(g)}]_{S^c})$$

2. Update  $z_{k+1}$

$$z_{k+1}^{(g)} = \left[ \text{vec}^{-1}(w_{k+1}^{(g)} + u_k^{(g)}) \right]_{(d)}$$

for  $g = 1, 2$ .

3. Update  $u_{k+1} = u_k + w_{k+1} - z_{k+1}$ .

These iterations continue either a maximum number of iterations  $K$ , or if

$$\max\{\|z_{k+1} - z_k\|_2^2, \|[z_{k+1}^{(1)}]_S - [z_{k+1}^{(2)}]_S\|_1\}$$

is smaller than some prespecified convergence threshold.